UNIVERSIDADE DE BRASÍLIA
INSTITUTO DE GEOCIÊCIAS
PROGRAMA DE PÓS-GRADUAÇÃO EM GEOLOGIA

PROVENIÊNCIA E GEOQUÍMICA ISOTÓPICA DAS FORMAÇÕES FERRÍFERAS DO NORTE DA FAIXA PARAGUAY.

Janaína Almeida de Oliveira

Dissertação de Mestrado N° 417

Área de Concentração: Geologia Regional

Brasília/DF

2018

UNIVERSIDADE DE BRASÍLIA
INSTITUTO DE GEOCIÊCIAS

JANAÍNA ALMEIDA DE OLIVEIRA

PROVENIÊNCIA E GEOQUÍMICA ISOTÓPICA DAS FORMAÇÕES FERRÍFERAS DO NORTE DA FAIXA PARAGUAY.

Dissertação de Mestrado apresentada ao Programa de Pós-Graduação em Geologia do Instituto de Geociências da Universidade de Brasília, como requisito parcial para obtenção do grau Mestre em Geologia, cuja área de concentração é Geologia Regional.

Defesa: 08 de maio de 2018.

Orientador:
Prof. Dr. Elton Luiz Dantas (Presidente – UnB)

Banca Examinadora:
Prof. Dr. Elton Luiz Dantas (Presidente – UnB)
Prof. Dr. Detlef Hans Gert Walde (UnB)
Prof. Dr. Fabrício de Andrade Caxito (UFMG)

Brasília/DF

2018

JANAÍNA ALMEIDA DE OLIVEIRA

PROVENIÊNCIA E GEOQUÍMICA ISOTÓPICA DAS FORMAÇÕES FERRÍFERAS DO NORTE DA FAIXA PARAGUAY.

Dissertação de Mestrado apresentada ao Programa de Pós-Graduação em Geologia do Instituto de Geociências da Universidade de Brasília, como requisito parcial para a obtenção do grau de Mestre em Geologia, cuja área de concentração é Geologia Regional.

08 de maio de 2018

_____

Prof. Dr. Elton Luiz Dantas (Presidente – UnB)

_____

Prof. Dr. Fabrício de Andrade Caxito (UFMG)

_____

Prof. Dr. Detlef Hans-Gert Walde (UnB)

Oliveira, Janaína Almeida
PROVENIÊNCIA E GEOQUÍMICA ISOTÓPICA DAS FORMAÇÕES FERRÍFERAS DO NORTE DA FAIXA PARAGUAI / Janaína Almeida de Oliveira; orientador Elton Luiz Dantas.-- Brasília, 2018. 112 p.
Dissertação (Mestrado - Mestrado em Geologia) -- Universidade de Brasília, 2018.

1. Formações Ferríferas Neoproterozoico. 2. Faixa Paraguai- Brasil central. 3. Isótopos Sm-Nd. 4. Datações U-Pb. 5. , Evento de glaciações sturtiana. Dantas,Elton Luiz , orient. II.

DEDICATÓRIA

"Dedico a Deus, aos meus pais, minha filha, meu companheiro e a todos os familiares e amigos que sempre torceram e acreditaram em mais essa conquista."

AGRADECIMENTOS

A Deus e à toda minha família que sempre me apoiaram e nunca deixaram desistir desse sonho. Em especial, a minha mãe Ilde e meu pai (in memorian), meus irmãos, meu companheiro Saul e a minha filha Alice a quem dedico essa conquista.

Aos professores desta instituição que sempre estiveram disponíveis e abertos à discussões ajudando-nos na evolução de conhecimento e contribuíram para o meu aprendizado, em especial ao meu orientador Elton Dantas pela dedicação, companheirismo, incentivo, confiança, paciência, amizade, assistência e suporte em todos os momentos ao longo do trabalho, incluindo os Sábados, Domingos e feriados a seus alunos dedicados. E aos professores Lucieth e Bernhard Buhn (in memorian).

Aos amigos que estiveram comigo nessa longa jornada: Ilde (minha mãe maravilhosa), Zeza, Naldi, Ednaldo, Benja, Alice, Iêda, Cris, Maza, Mary, Morena, Bebels, Ju, Bola, Carol, César, Thassio, Frankie, Welliton, Joice, Davi, Lila, Carlos Victor, Eduardo, Adila, Luciana, Alan, vocês foram incríveis. Obrigada por acreditarem em mim, pelos incentivos, puxões de orelha, parceria nos estudos, apoio e a amizade. Vocês foram de extrema importância, principalmente na reta final.

Ao Instituto de Geociências e Laboratório de Geocronologia da UnB. Agradecemos a todos aqueles que colaboraram direta ou indiretamente para este estudo, ao CNPq pelos subsídios (Projetos número 308312 / 2014-7 e 454272 / 2014-6) e à Empresa EDEM, por fornecer alguns dados que respaldaram o início da pesquisa.

Muito Obrigada!

RESUMO

As formações ferríferas neoproterozoicas (NIFs) da sequência Serra do Cristalino estão inseridas no contexto geológico da porção Norte da Faixa Paraguai, Brasil Central, estão relacionadas a uma margem passiva do Cráton Amazônico durante o período Criogênico, gerado durante o desmembramento do Rodínia. Formações BIF-jaspilíticas e formações ferríferas clásticas (CIF) na região de Cristalino do Cocalinho-MT, recentemente descoberta, localiza-se cerca de 1500 km a norte do depósito de Urucum no sul do Paraguai. E mostram evidências de camadas originadas em ambientes marinhos profundos e estratificados, influenciada por ciclos glaciais durante o Neoproterozoico. Os BIFs jaspilíticos apresentam camadas alternadas de hematita (amorfa e especular) e jasper de textura criptocristalina. Os CIFs possuem uma matriz criptocristalina que contém micropalhetas de hematita especular cristalizada e goethita, contêm clastos subangulares a angulares de arenito, formações ferríferas, sílex e barita. A geoquímica de BIFs e CIFs mostrou índices composicionais bem semelhantes, bem como as abundâncias de CaO, MgO, MnO, Al_2O_3, Na_2O, e K_2O. Amostras analisadas demonstram um moderado enriquecimento de *HREE* em relação a *LREE* e anomalias negativas verdadeiras em Ce / Ce *(0,7 – 0,95) pouco evidentes, bem como anomalia positiva de Eu / Eu *(0,8 – 1,2) ausentes e anomalia positiva Y / Ho * (1 -1,7). Esses dados sugerem que a formação ferrífera da Serra do Cristalino foi depositada sob a influência de fluidos diluídos e de baixa temperatura em uma bacia que recebeu insumos de material continental. Os padrões de *REE* das CIFs são semelhantes, mas levemente enriquecidos em relação aos BIFs onde as duas rochas refletem a composição da água do mar neoproterozoica, e se depositaram em condições de oceano anóxico de profundidade, influenciado por fluidos hidrotermais de baixas temperaturas (T). Estudos Isotópicos de Nd e de proveniência baseados na geocronologia U-Pb em zircão sugerem que as principais fontes de sedimentos que preencheram a bacia são de idades paleoproterozoicas a mesoproterozoicas, provavelmente derivadas do Cráton Amazônico, o que é consistente com um modelo de margem passiva para a Faixa Paraguai. O zircão mais jovem encontrado na fácies diamictitica da sequência Serra do Cristalino apresenta idade 721 Ma e sugere que seu evento glacial pode estar relacionado ao evento Sturtiano, similar ao Rapitan, podendo também ser correlacionado ao evento de glaciação Marinoana, ambos associados ao segundo grande Evento de Oxigenação Neoproterozoico (NOE).

PALAVRAS-CHAVE: Formação Ferrífera Neoproterozoica (NIF), Faixa Paraguai, Brasil Central, Isótopos Sm-Nd, Datações U-Pb, Evento de glaciações sturtiana.

ABSTRACT

Neoproterozoic Iron Formations (NIFs) of the Serra do Cristalino Sequence, included in the geological context of the Northern Paraguay Belt, Central Brazil, are related to a passive margin of Amazon Craton, during the Cryogenian period, generated during the break-up of Rodinia. Jaspilitic BIF and Clastic Iron Formations (CIF) in the Serra do Cristalino region of the Cocalinho-MT, a new discovery occurrence, 1500 Km northward of well know Urucum deposit at South Paraguay belt, show evidence of a deposition in a deep sub-basin in a stratified sea, influenced by glacial cycles in the Neoproterozoic times. The CIFs present a cryptocrystalline matrix that mainly contains crystallized specular hematite micropellets and goethite. The CIFs contain subangular to angular iron formation, chert, and sandstone clasts. The geochemistry of BIFs and CIFs show similar major elements contents, as well as abundances of CaO, MgO, MnO, Al2O3, Na2O, and K2O. Analyzed samples demonstrate a slight enrichment of HREE relative to LREE, and true negative Ce/Ce*(0,7 – 0,95) anomalies as well as a weakly positive

to absent Eu/Eu* *(0,8 – 1,2) anomaly and positive Y/Ho*(1 -1,7) anomaly. This data suggests that the Serra do Cristalino iron formation have been deposited under the influence of diluted and low-temperature fluids, in a basin that received input from continental material. REE patterns of the CIFs are similar although slightly higher than of the BIFs and reflect the composition of the Neoproterozoic seawater in both sedimentary rocks, in an anoxic deep ocean dominated by low T hydrothermal input. Nd isotopes and provenance studies based on U-Pb zircon geochronology suggest that the main sources of sediments that filled the basin are of Paleoproterozoic to Mesoproterozoic ages and likely derived from the Amazonian Craton, which is consistent with a passive margin model for the Paraguay Belt. In addition, the youngest zircon at around 721 Ma in the diamictites facies from the Serra do Cristalino occurrence, suggest that their glacial event could be related to Sturtian event, similar to Rapitan, being possible also to be correlated to the marinoan glaciation event, and, thus to be associated to the global Neoproterozoic Oxygenation Event (NOE).

KEYWORDS: Neoproterozoic Iron Formation (NIF), Paraguay Belt, Central Brazil, Sm-Nd Isotopes, U-Pb Dates, Sturtian glaciation event.

LISTA DE ILUSTRAÇÕES

CAPÍTULO I

CAPÍTULO II

CAPÍTULO III

LISTA DE TABELAS

CAPÍTULO II

CAPÍTULO III

SUMÁRIO

CAPÍTULO I– INTRODUÇÃO

1. Apresentação e justificativa

O estudo das Formações Ferríferas Bandadas (BIFs, *Banded Iron Formations*) tem dado importante contribuição para o entendimento da evolução tectônica da Terra e das grandes mudanças geoambientais globais, pois são registros desses períodos, incluindo mudanças climáticas, geoquímicas, e também a diversificação da biosfera (Klein & Beukes, 1992; Konhauser *et al.* 2002; Bekker *et al.* 2010; Huston & Logan, 2004; Holland, 2005). Do ponto de vista econômico as BIFs são proto-minérios dos maiores depósitos de ferro do mundo, onde os processos de enriquecimento podem ser hipogênicos ou supergênicos (Walde & Hagemann, 2007; Spier *et al.* 2003; Dalstra & Guedes, 2004; Rosiere & Rios, 2004; Lobato *et al.* 2008; Morris, 1980, Beukes *et al.* 2003; Hensler *et al.* 2014).

A área de estudo corresponde a ocorrência de BIFs na Serra do Cristalino, município de Cocalinho-MT, e está inserida no contexto geológico do norte da Faixa Paraguai (Figura 1), de idade neoproterozoica, do ciclo Brasiliano. A ocorrência, pouco conhecida e não descrita na literatura, dista 1500 Km a norte da bem estudada Serra do Urucum, em similar contexto geológico (Viehmann *et al.* 2016; Angerer *et al.* 2016; Walde & Hagemann, 2007). Almeida (1965) ao descrever a geotectônica do centro-oeste mato-grosse, correlacionou as estruturas desse arco às estruturas encontradas em Goiás, também margeando o Cráton Amazônico, denominando assim faixa de dobramento Paraguai, atribuindo-a ao Ciclo Brasiliano.

A Serra do Cristalino fica isolada em meio à planície recente da bacia do Rio Araguaia e rochas da Bacia do Paraná (Figura 1), onde existem poucos afloramentos e pouco conhecimento geológico da região (Almeida, 1984). As BIFs foram descobertas em 2003 por projetos de pesquisa mineral da EDEM (Empresa de Desenvolvimento em Mineração – *Cristalino Iron Project*).

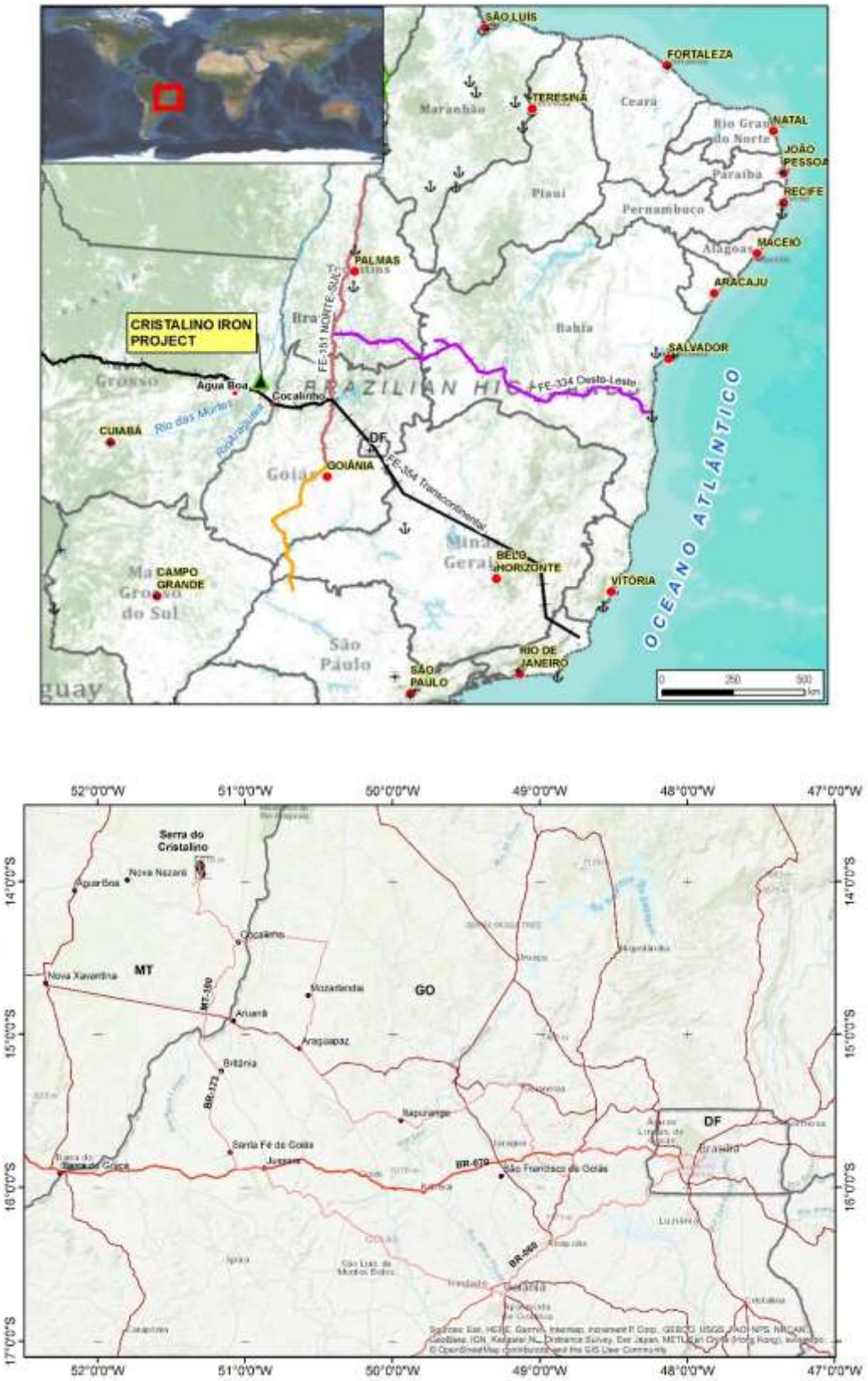

Figura 1. Mapa de localização e vias de acesso à área de estudo Serra do Cristalino- MT-Brasil.

Este estudo é o primeiro a apresentar uma caracterização petrográfica detalhada (pertrografia convencional, MEV e EDS), geoquímica convencional, geologia isotópica (Sm-Nd) e dados geocronológicos (U-Pb em zircão) das formações ferríferas bandadas (BIFs; jaspilitos) e formações ferríferas clásticas (CIF) da Serra do Cristalino, buscando caracterizar o ambiente de deposição, origem, natureza e evolução geológica das BIFs, CIFs e demais rochas da sequência encontrada na Serra do Cristalino e adjacências.

2. Objetivos

O principal objetivo deste trabalho é a integração de dados de geologia isotópica, datações U-Pb, litoquímica e geologia de campo, buscando compreender a evolução geológica que deu origem ao depósito ferrífero da Serra do Cristalino, porção nordeste da Faixa Paraguai, até então nunca descrita na literatura, contribuindo para o avanço do conhecimento geológico da região.

3. Estrutura da Dissertação

Esta dissertação de mestrado encontra-se dividida em quatro capítulos, descritos resumidamente a seguir:

- CAPÍTULO I: Contém conteúdos introdutórios, apresentação, justificativa objetivos e localização da área de pesquisa.
- CAPÍTULO II: Estado da Arte : Caracterização, origem e evolução das Formações Ferríferas Neoproterozoicas.
- CAPÍTULO III: Concentra-se o artigo intitulado como *"Provenance and isotope geochemistry of the Neoproterozoic iron formations of the Northern Paraguay Belt, Central Brazil: A Sturtian missing related event in South America?"* que foi submetido para a revista *Precambrian Research*. Apresenta a discussão dos dados petrológicos, geoquímicos e isotópicos Sm-Nd e U-Pb obtidos.
- APÊNDICES: Ao final do artigo, encontram-se os apêndices com os resultados de análises não apresentados no corpo do artigo.
- CAPÍTULO IV: Expõe a lista das bibliografias consultadas nesta pesquisa, incluindo todas as referências citadas no corpo do texto e no artigo.

CAPÍTULO II – ESTADO DA ARTE

Caracterização, origem e evolução das Formações Ferríferas Neoproterozóica.

1. Introdução

O estudo das formações ferríferas de idade neoproterozoica (NIFs) tem dado importante contribuição para o entendimento da evolução tectônica da Terra e das grandes mudanças geoambientais globais, durante o Criogeniano, entre 720 e 635 Ma, período em que a Terra encontrava-se sob a ação de ciclos glaciogênicos que cobriam o planeta momentaneamente por uma espessa camada de gelo, isolando o mar da atmosfera e tornando-o anóxico.

Partículas de ferro ferroso estavam sendo amplamente transportadas para as bacias, transformando a água do mar em solução rica em metais. Os depósitos de NIFs descritos até o momento sugerem que boa parte se formaram sob forte influência glacial criogeniana (Rapitan, Urucum, Chuos, Nummes, Braemar, Oraparinna e Holowilena).

Contudo as ocorrências egípcias estão associadas com rochas vulcânicas e vulcanoclásticas, demonstrando que as NIFs não são exclusivamente associadas a glaciogênese. Por outro lado todas as NIFs que ocorrem em bacias tipo rifte de alguma forma estão associadas a rochas vulcânicas máficas, sejam elas parte da sequência, substrato dos dépositos (crosta oceânica) e/ou rocha fonte intemperizada que liberou ferro em solução para as bacias. As feições sugerem contribuição hidrotermal, vulcanismo máfico e/ou crosta máfica, que podem ser as principais pré-condições para formação das NIFs (Cox *et al.* 2013). Estudos relativos a NIFs têm contribuído diretamente para o entendimento das condições atmosféricas na superfície do planeta e composição da água do mar durante o Neoproterozoico.

As Formações Ferríferas Bandadas (BIFs, *Banded Iron Formations*) se caracterizam como unidades sedimentares químicas, geralmente bandadas e/ou laminadas, contendo quantidade igual ou superior a 15% de ferro, comumente, mas não obrigatoriamente, contendo camadas de hematita e/ou magnetita, chert e/ou jasper (James, 1954). O estudo das BIFs tem dado importante contribuição para o entendimento da evolução tectônica da Terra e das grandes mudanças geoambientais globais, pois registram mudanças climáticas, geoquímicas e diversificação da biosfera

dos períodos gerados (Klein & Beukes, 1992; Konhauser *et al.* 2005; Bekker *et al.* 2010; Huston e Logan, 2004; Holland, 2006). Do ponto de vista econômico os BIFs são proto-minérios dos maiores depósitos de ferro do mundo, no qual processos de enriquecimento podem ser hipogênicos ou supergênicos (Walde & Hagemann, 2007; Spier *et al.* 2003; Dalstra & Guedes, 2004; Rosiere & Rios, 2004; Lobato *et al.* 2008; Morris, 1980; Beukes *et al.* 2003; Hensler *et al.* 2014).

As BIFs apareceram pela primeira vez no Arqueano, como tipo Algoma e tornaram-se mais abundantes depois do Grande Evento de Oxidação, ca. 2,4 Ga -1,9 Ga (Gross, 1980), dando origem aos maiores depósitos de ferro conhecidos no mundo, do tipo Lago Superior. Após um hiato no registro sedimentar (~1 Ga) as BIFs reaparecem no Neoproterozoico (~ 1000 Ma a 635 Ma) como tipo Rapitan (Isley e Abbott, 1999; Klein, 2005; Cox *et al.* 2013; Hagemann *et al*. 2015) geralmente associadas a sedimentos glaciogênicos e a rochas vulcânicas relacionadas à ruptura do supercontinente Rodínia (Cox *et al.* 2013). A figura 1 mostra a distribuição das formações ferríferas no tempo e volume, já a figura 2 mostra a distribuição espacial no mundo e suas relações.

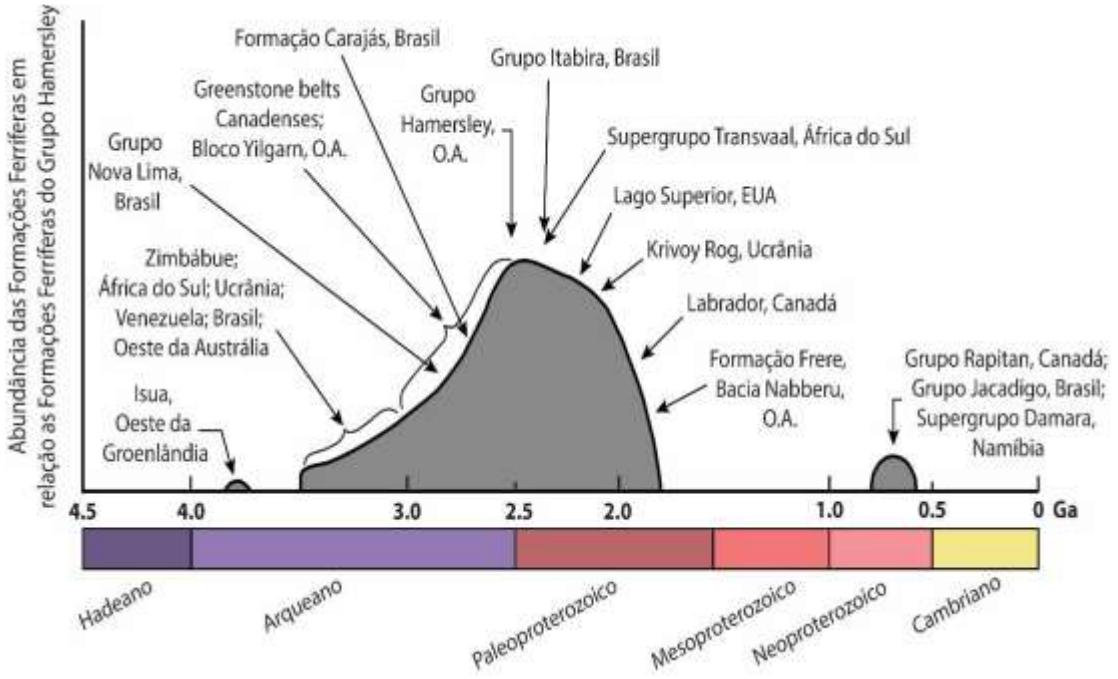

Figura. 1 Abundância e exemplo de formações ferríferas distribuídas segundo o tempo geológico (Extraído e modificado de Saldanha *et al.* 2017 e Klein, 2005).

Figura. 2 Distribuição das principais ocorrências das NIFs mostrando que os eventos ocorreram em escala global: 1 Grupo Bisokpabe; 2 Formação Chuos; 3 Formação Numees; 4 Ironstone Holowilena Yudnamutana/Formação ferrífera Braemar; 5 Grupo Upper Tindir; 6 Formação Rapitan; 7 Formação Kingston Peak; 8 Grupo Jacadigo; Maciço Urucum MS/Boqui-BO e Santa Cruz-MT; 9 Macaúbas; 10 Bodoquena; 11 ANS-Sawawin; 12 Formação Fulu; 13 Formação Maly Khinghan; 14 Formação Yamata; 15 Formação Mugur; 16 Formação Aok 17 Formação Jucurutu; 18 Serra do Cristalino; 19 Formação Yerbel; 20 Formação Lake Khanka. (Modificado de Piacentini et al., 2007, Adaptado de Yeo., 1989).

2. Aspectos genéticos

A deposição das formações ferríferas Neoproterozoicas (NIFs) é associada ao segundo grande evento de oxigenação marinha (NOE; Shields-Zhou e Och, 2011), aliados à grande concentração de massas continentais nas proximidades do paleoequador, que serviram de isolante térmico, capaz de iniciar eventos glaciais, a cerca de 850 Ma, dando origem ao "*Snow Ball Earth*" (Kirschvink, 1992; Hoffman et al. 1998; Hoffman e Schrag, 2002).

A hipótese "Terra bola de neve" sugere que durante o período Criogeniano, entre 720 a 635 Ma, a Terra passou por diversos ciclos glaciogênicos e de degelo, onde grande parte da superfície terrestre e dos oceanos estava coberta por espessa camada de gelo, isolando o mar da atmosfera e tornando-o anóxico. Partículas de ferro ferroso estavam sendo amplamente transportadas para as bacias, transformando a água do mar em uma solução rica em metais (Fe, Mn, Si, Ni, Zn, Pb, L).

Assim, a deposição era dentro e abaixo do *redoxcline* de nível superficial (oceano estratificado) durante a cobertura de gelo (Angerer et al., 2016; Hoffman e Schrag, 2002). Água mais fria e isolamento da luz solar reduziram a atividade microbiana (Angerer et al. 2016; Hoffman e Schrag, 2002; Lyon e Reinhard, 2009, Lyon et al. 2014). Quando a cobertura de gelo nos oceanos começa a derreter, o ferro, residual em solução na água do mar, entra em contato com a água oxigenada que desagua no oceano, se reequilibra, precipitando assim ferro férrico e dando origem aos depósitos das formações ferríferas no Neoproterozoico (Halverson et al. 2011; Stern et.al. 2013).

Existiram três ou quatro idades glaciais significativas no Neoproterozoico tardio (entre c. 750 e c. 580 Ma). Destas, as glaciações do período Criogeniano (Sturtiano (726-660 Ma) e Marinoano (655-635Ma) mostram evidências de geleiras de baixa latitude, susceptíveis a extensão global (Shields-Zhou e Och, 2011), intimamente relacionadas às origens das NIFs (Holland 2006, *Stern et al. 2006*). Hoffman (2005) acredita que as glaciações do período Ediacarano (635-545Ma), por exemplo, os eventos Gaskiers e Kaigas, não levaram a glaciações globais, provavelmente foram eventos glaciogênicos apenas de significância regional (Fairchild e Kennedy, 2007).

As idades dos depósitos associados a essas glaciações consistem em datações indiretas, em que são datadas rochas dos limites de sequências superior e inferior, muitas vezes abrangendo intervalos muito extensos de idade para as glaciações e provavelmente representam vários episódios de deglaciação, principalmente para a glaciação Sturtiana (Babinski, 2012).

A atmosfera neoproterozoica não era completamente anóxica, já que o oxigênio livre era maior em relação à atmosfera primitiva (Bekker *et al*. 2004; Canfield 2005; Frei *et al*. 2009, Lyon e Reinhard, 2009, Lyon *et al*. 2014, Cox *et al.* 2013). Ao passo que, as BIFs neoarqueanas e paleoproterozoicas encontravam-se em condições ambientais de baixo O_2 livre na atmosfera e nos oceanos profundos (Bekker *et al*. 2004; Canfield 2005; Frei *et al.* 2009, Lyon e Reinhard, 2009, Lyon *et al.* 2014).

Posterior a deposição das NIFs, há um aumento nos níveis de oxigênio na atmosfera e nos oceanos ocasionando a ventilação do oceano profundo. Tais condições tornaram os níveis de oxigênio dos oceanos mais próximos das condições atmosféricas e ambientais atuais, possibilitando o surgimento dos primeiros seres multicelulares na Terra (Canfiel e Teske, 1996; Catling e Claire, 2005; Sahoo *et al*. 2012, Frei *et al*. 2009; Lyon e Reinhard, 2009, Lyon *et al*. 2014, Cox *et al*. 2013).

Pesquisas relacionadas a origem e deposição das BIFs têm enfatizado a relação entre o transporte e a precipitação de ferro e sílica nos diferentes ambientes deposicionais dadas as condições físico-químicas, atmosférica e de salinidade no tempo geológico. Tais estudos são baseados, majoritariamente, em geoquímica convencional e isotópica onde a assinatura dos isotópos nos processos diagenéticos e/ou bioquímicos durante a precipitação de Fe e Si em oceanos modernos e antigos (Bekker *et al.* 2004) incluindo a atuação de fontes oriundas de rios, ventos, sedimentos de margem, gelo e atividades vinculadas à fumarolas hidrotermais (Poulton e Raiswell, 2002; Buck *et al.* 2007; Cox *et al*. 2013). Segundo James (1954) e Tagliabue *et al.* (2010), o intemperismo dos continentes e sedimentos de margens continentais são os responsáveis pelo ferro em solução que originou estas rochas.

As NIFs estão intimamente relacionadas à eras glaciais, com ou sem associações a rochas vulcânicas e desenvolvidas em ambientes deposicionais de margens continentais do tipo rifte ou sistemas de grabens extensionais. São associadas a sedimentos glacio-marinhos intercaladas a diamictitos, conglomerados, grauvacas, arenitos e argilitos incluindo dropstones (Klein & Beukes, 1993; Hoffman *et al.* 1998; Gross 1996) e, no topo das sequências, frequentemente são representados por diamictitos e carbonatos de capa do final da glaciação.

Os exemplos glaciogênicos mais bem conhecidos deste tipo de depósito são as formações ferríferas do Grupo Rapitan, no Canadá (Young, 1976; Yeo, 1981; Eisbacher, 1985; Baldwin, 2014) e Formação Santa Cruz do Grupo Jacadigo, no Brasil (Dorr II, 1945; Almeida, 1964; Urban *et al.* 1992; Trompette *et al.* 1998; Klein & Ladeira, 2004; Freitas *et al.* 2011; Alvarenga *et al.* 2011; Angerer *et al*. 2016; Viehmann *et al.* 2016; Frei *et al.* 2017). Ocorrem ainda depósitos relacionados a rochas vulcânicas associados à ruptura do super-continente Rodínia, apresentando atividade hidrotermal localizada (Yeo, 1981; Eyles & Januszczak, 2004; Basta *et al.* 2011; Sial *et*

al. 2015; Stern *et al.* 2013; Cox *et al.* 2013; Gaucher *et al.* 2015; Khalil *et al.* 2015). Esses depósitos são descritos na Formação Jucurutu, da Faixa Seridó (NE do Brasil) (Sial *et al.* 2015) e no depósito de Gebel El Hadid, no Egito (Khalil *et al.* 2015). Há relatos de formações ferríferas associadas a ambientes plataformais como as formações ferríferas do Grupo Shilu, na China (Xu *et al.* 2013).

Os depósitos de NIFs descritos até o momento sugerem que boa parte se forma sob forte influência glacial criogeniana (Rapitan, Urucum, Chuos, Nummes, Braemar, Oraparinna e Holowilena), porém, as ocorrências egípcias estão associadas a rochas vulcânicas e vulcanoclásticas. Por outro lado, todos as NIFs que ocorrem em bacias rifte de alguma forma estão associadas a rochas vulcânicas máficas, seja ela parte da sequência, substrato sobre o qual se depositaram (crosta oceânica) e/ou como rocha fonte que foi intemperizada e liberou ferro em solução para as bacias. As evidências sugerem que há contribuição hidrotermal, vulcanismo máfico e/ou de crosta máfica que podem ser as principais pré-condições para formação das NIFs (Cox *et al*. 2013).

3. Características (petrográficas, litoestratigráficas)

As NIFs geram depósitos geralmente menores, quando comparados aos formados no fim do Arqueano e início do Proterozoico. Petrograficamente, apresentam aspectos texturais como bandamentos pouco desenvolvidos ou ausentes, sendo comum ocorrer como siltitos laminados e ferruginosos ou em matriz de paraconglomerados (Cox *et al*. 2013). A mineralogia das NIFs é, predominantemente, constituída por *chert* ou *jasper* e hematita (como fase principal), enquanto a magnetita ocorre localmente, em regiões de falhas ou como resultado de metamorfismo (Klein & Beukes, 1993; Cox *et al.* 2013). O metamorfismo alcança fácies xisto verde e raramente chega a fácies anfibolito. Quando bandadas, as camadas são compostas por alternâncias de hematita e *jasper* (*chert* rico em Fe). Essas variações composicionais refletem as mudanças sazonais na deposição de Fe *versus* Si (Stern *et al.* 2013).

Os principais depósitos de NIFs conhecidos no mundo (figuras 1 e 2) exibem um fenômeno global, que podem ser correlacionados através da estratigrafia de alguns desses depósitos de ferro denotada na figura 3.

A partir da compilação de todos esses dados, elaborou-se um quadro resumo contendo as principais características das NIFs, levando em consideração a bibliografia

existente e supracitada. Exemplos destas associações de rochas encontram-se no Grupo Rapitan no noroeste canadense (Young, 1976; Yeo, 1981; Eisbacher, 1985), Grupo Umberatana, na Austrália (Trendall, 1973; Preiss e Forbes, 1981; Preiss, 2000; Le Heron *et al.*, 2011a, b), Supergrupo Damara, na Namíbia (Beukes, 1973; Buhn *et al.* 1982; Frimmel, 2011), Grupo Jacadigo, no Maciço de Urucum-Brasil (Dorr II, 1945; Almeida, 1964; Urban *et al.* 1992; Trompette *et al.* 1998; Klein e Ladeira, 2004; Freitas *et al*. 2011; Alvarenga *et al.* 2011; Viehmann *et al.* 2016; Frei *et al.* 2017), Formação Serra do Cristalino, (Oliveira *et al.*, submetido), Formação Jucurutu, nordeste do Brasil (Sial *et al.* 2015), Formação Yerbel, Uruguai (Gaucher *et al*., 2004; Pecoits, 2002), África do Sul - Deserto oriental do Egito - Um Nar - Escudo Árabe - Núbian (Ali *et al.* 2009; Basta *et al.* 2011; Stern *et al.* 2013), Formação Fulu, Sul da China (Tang *et al.* 1987; Zhang *et al*. 2011).

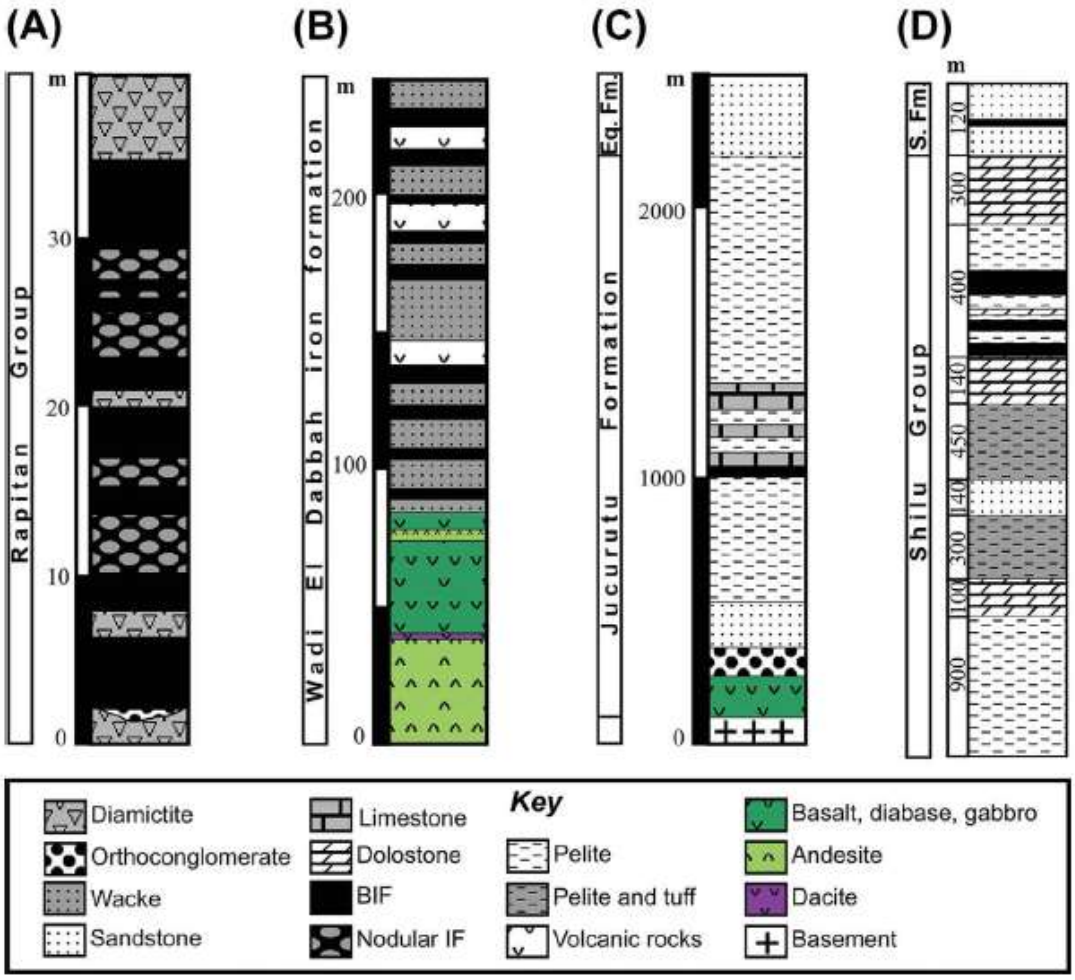

Figura. 3 A Relações litoestratigráficas dos diferentes tipos de depósitos de NIFs (Gaucher *et al.* 2015) baseado na literatura existente do (A) Grupo Rapitan, Canadá, Baldwin *et al.* (2013); (B) Formação ferrífera Wadi El Dabbah, Egito, Ali *et al.* (2009); (C) Formação ferrífera Jucurutu (Sial *et al.* 2015, faixa Seridó, NE Brazil) e Formação ferrífera Equador, Van Schmus *et al.* (2003) e Nascimento *et al.* (2007); (D) Shilu Group, South China, Xu *et al.* (2013b).

Tabela 1. Principais características das NIFs, com base na literatura supracitada.

Formações Ferriferas Neoproterozóicas (NIF)	**Domínio Geotectônico**	**Descrição**
América do sul-Brasil e Bolívia - Gr.Jacadigo - Maciço Urucum, Santa Cruz, Bodoquena, Serra do Cristalino-MT e Boqui	Sistema de grabéns extensionais, da Faixa Paraguai.	O Grupo. Jacadigo corresponde à sucessão de sedimentos glaciogênicos, ocorrem dentro da Formação Santa Cruz, consiste predominantemente por formações ferríferas (Jaspiitos hematitico bem estratificado, por vezes ooidal IF, granular e como matriz de paraconglomerado ferruginosas (matriz ferríca), arenitos ferruginosos e formação mangenesífera, e são recobertas por carbonatos do Gr. Corumbá. Metamorfismo xisto verde, baixo grau. Na porção nordeste da faixa(Serra do Cristalino), apresentam fácies mais distais de granulometria fina onde os diamictitos gradam a microdiamictitos ferruginosos, e não preservam a fácies manganesífera.
América do Norte - Noroeste do Canadá - Gr. Rapitan e Tatonduk	Margem de desenvolvimento Laurentia, seguindo os estágios iniciais de rifiteamento do Rodínia.	Sucessão de sedimentos grosso e bem preservado, depoisitados em sistema de falhas ativas N-NE, Ocorre sobre a forna de laminado de ferro e como um componete da matriz do diamictito, Fácies mais ricas em Fe incluem argilito hematítico (ferrolutito), arenito rico em Fe e diamictito. repousa sobre lavas basálticas MOF e rochas vulcanoclásticas, e são recobertas diamictitos com clastos da formação ferrífera e contato superior por discordâcia angular com carbonatos.
Sul da Austrália - Holowilena e Oraparina	Associadas ao sin-rifte do Gawler em ~827 Ma e outro mais jovem Rifte Pré-Sturtian.	Gr. Umberatana. Como Lamidado IF, intercalados com silitos calcário e como componente da matriz paraconglomerado glaciogênicos, recoberto pela Fm. Wilyerpa (diamictito e ironstone estágios finias glaciais). Metamorfisado fácies Xisto verde alta a anfibolito, composta por Hemtita, magnetita e quartzo e por vezes clorita, muscovita biotita carbonato, apatita e turmalina.
Uruguai - Fm.Yerbal	Abertura estável da margem continental para o leste e sul	Sucessão de sedimentos glaciogenicos, A Fm. Yerbal composta da base para o topo por; Arenitos; siltstones dominar-se a seção, e BIF e intercalações de silex (Gaucher *et al.* 2004) separda das rochas vulcânicas bimodais subjacentes da Fm. Las Ventanas por uma discordância erosiva (Pecoits, 2002). A NIF predominantemente Laminados, na fácies oxido, composta por bandas alternadas de magnetita + hematita e Chert. Estão intercaladas com siltitos, cherts e dolomitos.(Gaucher *et al.* 2004).
Sul da China - Fm. Fulu	Sistema de bacia tipo rifte evoluindo em intima associação com rochas vulcânicas máfica.	Sedimentos glaciogênicos, onde a Fm. Fulu è a principal fonte do minério de Ferro, ocorre entre diamictitos maciços (Fm. Chang´na), arenitos arcoseao a grauvaca com seixos isolados (Membro Liangjiehe), a Fm. Fulu, parece ocorrer como basalto alterado em algumas localidades e, como camadas ricos em ferro dentro de tufos e arcóseos tuffaceous e carbonatos em configurações proximais.
Chuos-Damara-Numees -Namíbia	Sin e pós-rifteamento da margem sudoeste do cráton do Congo. Bacia extensional, evoluindo para uma margem passiva.	As NIFs ocorre dentro dos sedimentos Glaciogênico, muito heterogênea, consiste principalmente diamictitos, arenitos rasos e profundos a formação de ferro é menor, ocorrem localmente associados a fluxos basálticos (Chuos) e a intercalações cíclicas com formações manganesíferas (no cinturão Damara). A Formação ferrífera, com baixo grau metamórfico, forma camadas de magnetita ou silicosas rica em hematita, bem desenvolvida, na maioria das vezes, formam finas bandas.
América do sul-Nordeste do Brasil - Provincia Borborema - Faixa Seridó	Sistema de grabén extensional, bacia Jucurutu	Sequencia metavulcanossedimentar, glaciomarinha, intrudida por granitos calcialcalinos de alto K e repousam sobre o Complexo Caicó (Paleoproterozóico). A formação Jucurutu é constituída por Conglomerados, BIFs e marmores intercalados a gnaisses, mica-xisto, quartzito, calcio-silicáticas e rochas metavulcânicas. Metamorfisado pelo evento orogênico Brasiliano na fácies anfibolito, composta por Itabiritos fácies óxidos e fácies silicáticas (actinolita ou cummingitonita- Itabirito com bandas foliadas de tremolita).
África do Sul-Deserto oriental do Egito- Um Nar-Escudo árabe-Nubian	Ocorre ao longo da costa do Mar Vermelho do Egito, no Escucdo Arábico-Nubiano	As NIFs Foi depositadas em sistema de bacia marinha do tipo *back arc*, associados a rochas vulcânicas e a sedimentos clásticos imaturos, são laminado depositados intercalados com piroclásticos relacionados com fluxos de lava. Composta principalmente por hematita, magnetita e quarto com ankerita em menor quantidade e em algumas camadas, metamorfismo é variado chegando a fácies anfibolito, evidenciada pela presença de Granada e Actinolita

4. Características Geoquímicas

A geoquímica de elementos maiores, traços e terras raras é a ferramenta que ajuda a obter valiosas informações sobre o contexto de deposição das formações ferríferas, mostrando as principais áreas fontes que contribuiam com sedimentos para a bacia, assim como as assinaturas das águas ou de fumarolas que estavam presentes (Bau & Dulski, 1996).

4.1 Elementos Maiores e Traços

As NIFs são constituídas essencialmente por Fe e Si, podendo ser enriquecidas em até ~40% durante os estágios finais de deposição das formações ferríferas, onde o manganês geralmente encontram-se em teores >1%. Em alguns casos, podem ocorrer camadas de formações manganesíferas associadas às formações ferríferas, onde os depósitos de Mn representam ambientes mais rasos e mais oxidantes que os de Fe. O Mn e a Si também podem indicar mobilização diagenética, com as NIFs sendo enriquecidas nesse processo. Ca e Mg, quando mostram uma correlação positiva forte, sugerem a presença de minerais carbonáticos hospedados nas NIFs.

Correlações positivas de Al, Ti, K e Na sugerem que, provavelmente, houveram contribuições detríticas ou misturas de fontes (Cox *et al.* 2013). Quando os teores de Zr, Hf, Ti e Al estão relativamente altos, atribui-se às formações ferríferas uma contribuição de sedimentos continentais pois esses elementos possuem maior afinidade química com rochas félsicas. Normalmente, as BIFs mais puras são oriundas de fluídos hidrotermais onde o Zr e Hf ocorrem em concentrações baixas (< 8 ppm) e sem grande contaminação continental (Wang, 2006a; Wang, 2006b). A relação entre Fe/Ti *versus* Al/Al+Fe+Mn) expressa por Bostrom (1973) e Peter *et al*. (2003) (Figura 4) é útil para estimar a proporção de componentes clásticos *versus* hidrotermais nas NIFs, sendo que o produto sugere que houve uma contribuição hidrotermal nas formações ferríferas e uma mistura acentuada dos dois componentes para as formações ferríferas mais impuras.

O enriquecimento em fosfato, geralmente, representa um teor elevado de P dissolvido na água do mar, possivelmente relacionado a Terra pós-glacial (Swanson-Hysell *et al.* 2010).

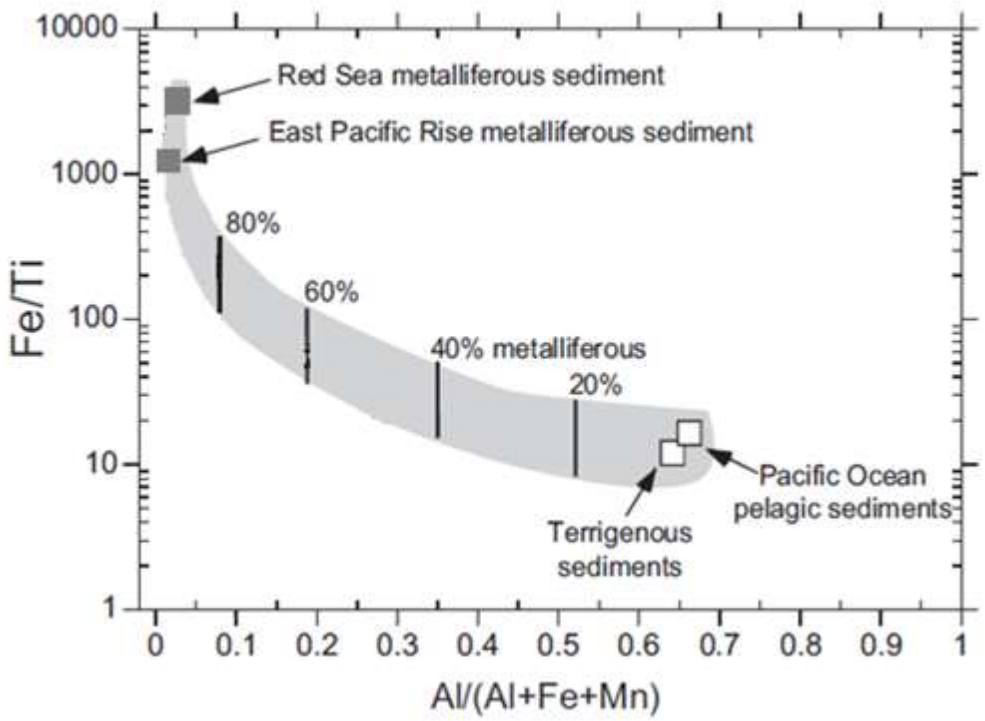

Figura. 4 Diagrama de Fe / Ti vs. Al / (Al + Fe + Mn) (% em peso) (modificado de Bostrom, 1973; Peter *et al.* 2003), estimando a contribuição relativa da entrada hidrotermal no sistema deposicional das NIFs.

As correlações positivas de elementos traços (Co + Cu + Ni) geralmente representam contribuição de fluidos hidrotermais e/ou magmatismo e são comumente associados a enriquecimentos em elementos terras raras (REE) (Klein, 2005).

4.2 Geoquímica REEY

A geoquímica dos elementos terras raras e ítrio (REEY) permite identificar as condições do ambiente de deposição, temperatura e profundidade da lâmina d'água, bem como rastrear as fontes geradoras de ferro, situação paleogeográfica, ambiente tectônico, condições de EH e pH da água do mar, compreendendo assim os caminhos de deposição das BIFs (Lascelles, 2007; Bau, 1993; Alexander *et al.* 2008; Cox *et al.* 2013 e entre outros), bem como determinar situações de deposição das BIF em relação às fontes hidrotermais, ou seja, se as mesmas são distais ou proximais (Kato *et al.* 1998).

Os sedimentos químicos (BIF) são os materiais mais adequados para traçar mudanças temporais no comportamento dos REEY em ambientes sedimentares devido à pouca presença de material clástico e a ampla distribuição espacial e temporal (Fryer, 1977).

Os REEY apresentam diferentes comportamentos na água do mar durante a evolução do tempo geológico produzindo alguns padrões de anomalias nos elementos Ce, Eu e Y/Ho, indicando as condições ambientais de deposição da BIF. Além disso, padrões de REEY da água do mar mostram fracionamento à medida em que a deposição se afasta da fonte, sendo diluídos na água do mar e gerando decréscimo gradual do empobrecimento em LREE em relação aos HREE (Bau *et al.* 1997; Alexander e Bau 2009; Cox *et al*. 2013). Isso ocorre porque os HREE formam complexos que permanecem livres na água do mar. Por outro lado, os LREE são adsorvidos e precipitam junto com os sedimentos marinhos e/ou em margens continentais. Para água dos oceanos modernos, o empobrecimento em LREE é mais acentuado e pode ser resultado da interação da água do mar, que resulta na eliminação preferencial dos LREE (Cox *et al.* 2013), ou ainda, refletem fontes de cargas detríticas ou alguma combinação desses dois processos (diluição dos fluidos hidrotermais + detritos) para a empobrecimento dos REEY (Cox *et al*. 2013).

Estudos realizados a partir de soluções hidrotermais da Dorsal Meso-Atlântica e do Pacífico leste (fluidos quentes >300°C) foram caracterizados como padrões enriquecidos em LREE, com fortes anomalias positivas de Eu (Michard *et al.* 1983, Michard e Albarède 1986, Bau e Dulski, 1999; Douville *et al.* 1999). Já a água do mar nos oceanos modernos (fluidos relativamente mais frios < 200°C) e as soluções hidrotermais são mais diluídas na água dos grandes oceanos apresentando padrões de enriquecimento em HREE; anomalias negativas em Ce; anomalias positivas em Y (Elderfield e Greaves, 1982; Bau *et al*. 1996; Alibo e Nozaki, 1999) e, considerando que nos fluidos produzidos por alteração hidrotermal, a temperatura é baixa, com fraca ou ausência de anomalia de Eu (Michard *et al.* 1993).

O comportamento desses elementos nas NIFs ocorre em atmosfera bem mais oxigenada e bem próxima das águas dos oceanos modernos, apresentando anomalias negativas em Ce, anomalias positivas em Y/Ho* e fracas ou ausentes anomalias de Eu (<1). Nos oceanos arqueanos, estudos de REE nas BIFs mostram anomalia fortemente

negativa em Ce e anomalia positiva em Eu (>2) representando as condições da água do mar, com altas temperaturas, influência dos fluidos hidrotermais que eram emitidos pelas fumarolas negras em bacias restritas e profundas, com intensa atividade vulcânica relacionada (James, 1954; Gross, 1993; Klein, 2005). Nos BIFs paleoproterozoicos, essas anomalias são menos constantes pois, dadas as proporções das bacias serem mais amplas e os fluidos hidrotermais serem mais diluídos, geraram anomalias negativas em Ce e positivas em Eu (>1 e < 2).

Os padrões REEY normalizados pelo PAAS (enriquecimento de HREE e suave a ausente anomalia positiva de Eu) (Figuras 5 e 6) de vários NIFs em todo o mundo são interpretados com intuito de retratar a mistura da água do mar com soluções hidrotermais de baixa temperatura.

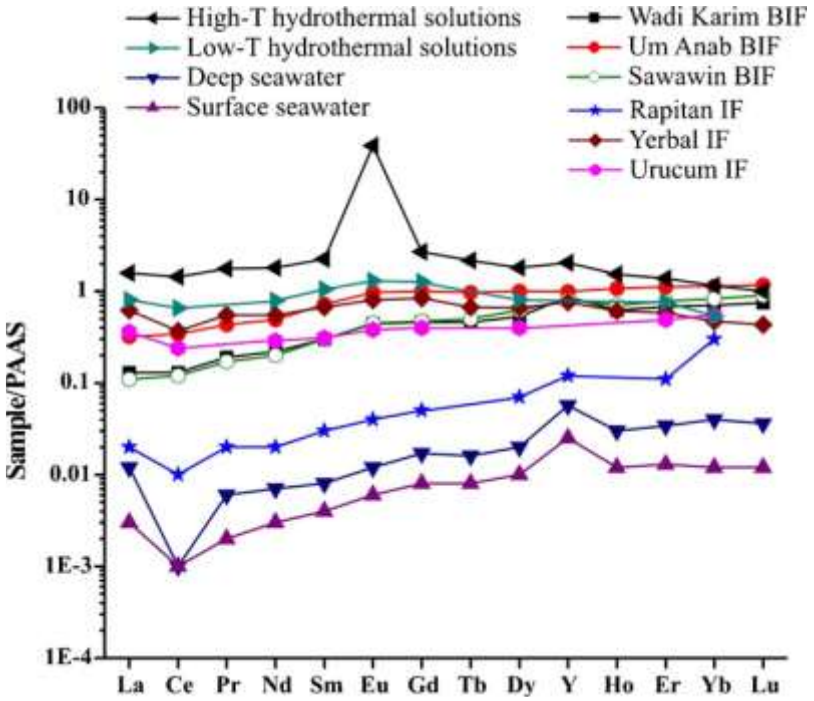

Figura. 5 Gráfico de Basta *et al.* (2011) - Padrões REEY normalizados PAAS para fluidos hidrotermais médios (× 105), água do mar (× 105), formações de ferro do Nepal e do Neoproterozóico do Leste Oriental (Wadi Karim e Um Anab). Fontes de dados: média de soluções hidrotermais de alto T de TAG e EPR, 13◦N e 17-19 ° S (Douville *et al.* 1999); Soluções hidrotermais de baixo T (Michard *et al.* 1993); média de águas profundas de EPR (~ 2500 m, Klinkhammer et al.1983; Bau *et al.* 1995; e 1000-2000 m, Bau *et al.* 1996); água do mar de superfície do Oceano Pacífico norte (Alibo e Nozaki, 1999); Urucum IF, Brasil (Derry e Jacobsen, 1990); Rapitan IF, Canadá (Fryer, 1977a); Yerbal IF, Uruguai (Pecoits, 2010); Sawawin BIF, Arábia Saudita (Mukherjee, 2008). Basta *et al.* (2011)e Bau e Dulski (1996) sugeriram enriquecimento em ETRP e anomalias positivas Y (PAAS) em BIF pré-cambriano são sinais herdados de águas superficiais marinhas, enquanto anomalias positivas Eu (PAAS) são sinais herdados da água de fundo marinho através da contribuição de soluções hidrotermais. Barrett *et al.* (1988), por outro lado, propuseram enriquecimento em padrões ETRP- normalizada pelo PAAS, para algumas formações de ferro associadas a rochas vulcânicas, é possivelmente herdado de uma fonte vulcânica máfica, na sequência de interação água do mar/ rocha em baixa temperatura.

As fracas ou ausentes anomalias em Eu nas NIFs não representam fontes hidrotermais proximais, mas provavelmente, foram geradas por soluções hidrotermais relativamente frias e diluídas na água do mar, distantes das fumarolas fontes (Stern *et al*. 2013; Basta *et al.* 2011). O comportamento do Ce e Pr nos mostram razões (Ce/Ce*, Pr/Pr*) com valores médios <1 (Figura 05, 06 e 07) sendo que, as verdadeiras anomalias negativas em Ce indicam que as formações das BIFs ocorreram em associação com águas mais superficiais, suficientemente capazes de oxidar o Ce semelhantes as massas de água óxicas e subóxicas dos oceanos modernos.

A abundância em La pode mascarar as anomalias em Ce. As anomalias negativas de Ce refletem as condições de oxidação do ambiente marinho, quanto mais oxidante mais negativas são as anomalias. Na tentativa de investigar as condições de oxidação dos oceanos, Bau e Dulski (1996a) sugerem o diagrama Ce/Ce* *versus* Pr/Pr* para verificar as verdadeiras anomalias negativas em Ce (Figura 6).

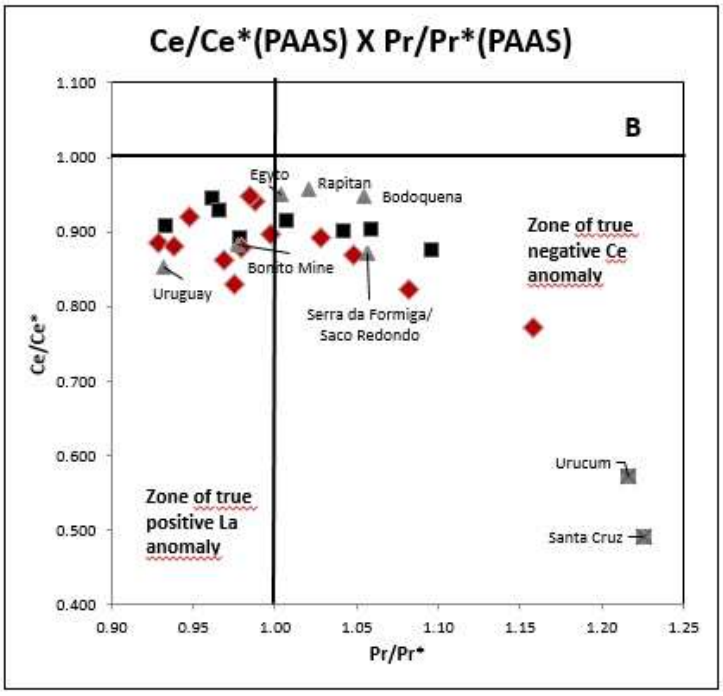

Figura. 6 Diagrama Ce/Ce* versus Pr/Pr* normalizado pelo PAAS, para amostras de NIFs, Santa Cruz (Angerer *et al.* 2016), Urucum (Viehmann *et al.* 2016), Egito (Khalil *et al.* 2015), Rapitan (Halverson *et al.* 2011), Bodoquena (Piacentini *et al*. 2013), Uruguai (Pecoits, 2010), mina Bonito Jucurutu e Serra da Formiga/Morro Redondo (Sial *et al.* 2015) e Serra do Cristalino (Oliveira *et al.*, submetido) mostrando o comportamento de NIFs, onde se observa que, em algumas das amostras no campo das verdadeiras anomalias negativas em Ce/Ce*, e outras no campo de anomalias positivas em La.

O comportamento de Ce mostra que as anomalias negativas em Ce não são muito acentuadas e refletem águas mais profundas e distais. As anomalias negativas de Ce são mais acentuadas nas águas mais rasas, onde os ambientes geralmente são mais oxidantes com mais abundância de Ce vindo do continente.

5. Geoquímica Isótopica Sm/Nd e U-Pb em Zircão

A geoquímica isotópica Sm/Nd, fornece informações importantes de quantificação das fontes e proveniência do Fe para os oceanos. Até o momento, não foi desenvolvido um método de datação direta para as formações ferríferas, as isócronas de Sm/Nd não fornecem dados concisos pois as fontes são mistas (fluidos hidrotermais juvenis e fluidos continentais), porém, foi utilizado dados de U–Pb em zircão das encaixantes onde é possível traçar os limites de deposição das sequências, associando os dados isotópicos de Sm/Nd à proveniência das principais fontes dos sedimentos que preencheram a bacia (Frei e Polat, 2007; Frei *et al.* 2008; Alexander e Bau, 2009). Quando associadas com elementos traços podem sugerir o ambiente de deposição e gênese (Frei *et al.* 2008).

O método Sm/Nd é confiável pois, somente se modifica se houver uma eventual diferenciação manto–crosta, preservando suas assinaturas iniciais independente dos processos geológicos que a rocha tenha sofrido, permitindo assim datar em qualquer rocha a época em que seu magma parental (protólito crustal) se diferenciou do manto.

Viehmann *et. al*. (2016) realizaram datações de U-Pb em zircão do granito do embasamento do Urucum (1826,3 ± 4,2 Ma) e de um *dropstone* granítico (1847,1 ± 3.4Ma), encontrados nos sedimentos químicos do Urucum. Esses dados sugerem que o embasamento cristalino foi erodido durante o intervalo glacial e eventualmente depositado como *dropstone.*

A associação do método Sm-Nd ao método U-Pb resulta na determinação das idades de deposição de sequências químio-sedimentares, como BIFs intercaladas com vulcânicas de idades pré-cambrianas (Alibert e McCulloch, 1993).

6. Modelos deposicionais

As NIFs são subdivididas em três modelos principais: Glaciogênicos (Rapitan, Urucum, Chuos, Nummes, Braemar, Oraparinna e Holowilena, figura 7A), em sistemas de rifte e/ou falhas extensionais; modelos vulcanogênicos (Jucurutu, Egito e Arábia Saudita, figura 7B), relacionados à ruptura do supercontinente Rodínia e, por fim, em ambientes plataformais, como as formações ferríferas do Grupo Shilu, na China, e Yerbal, no Uruguai (figura 7C).

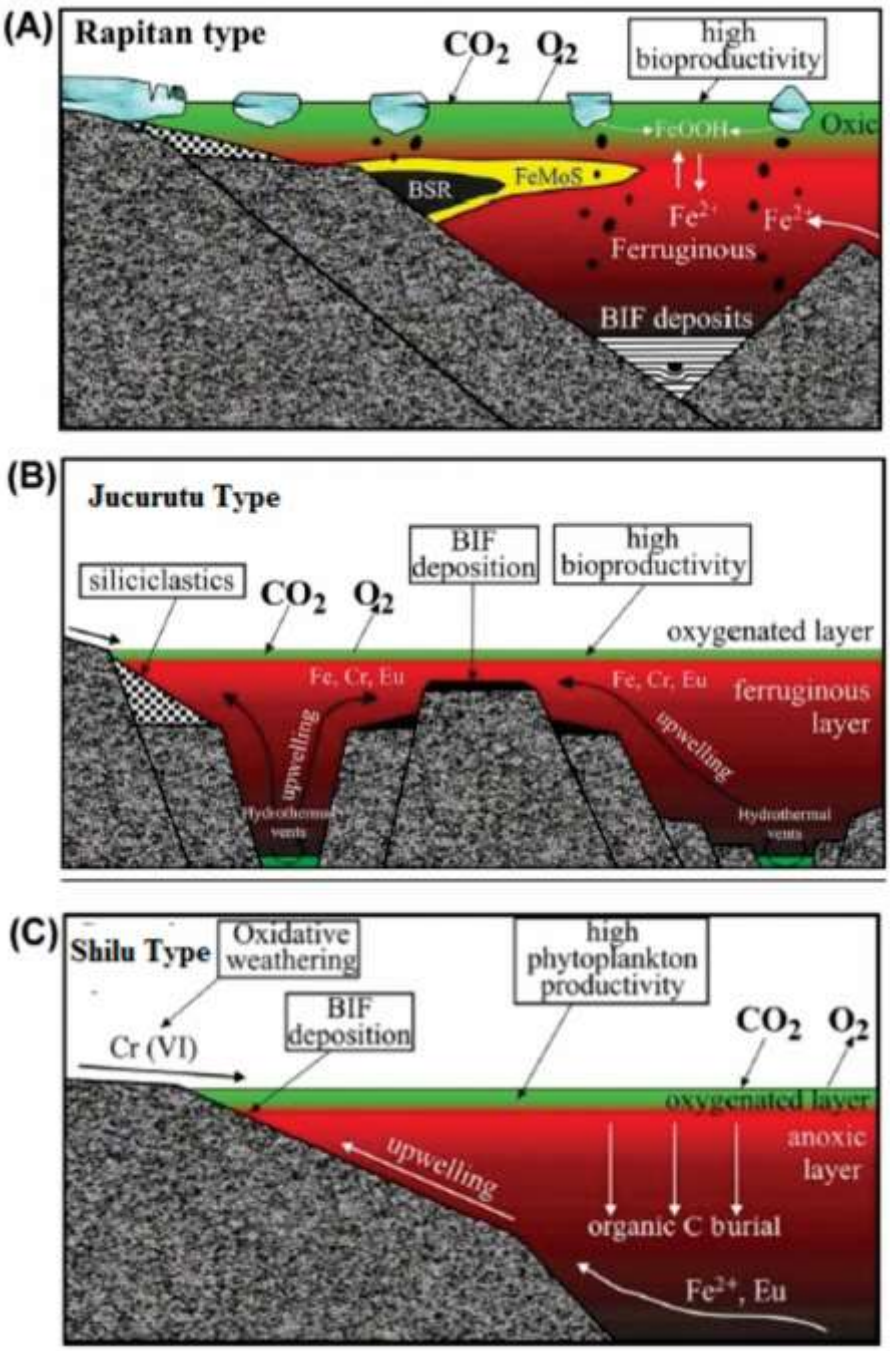

Figura. 7 Modelos deposicionais para os diferentes tipos de NIF´s discutidos na literatura por Gaucher *et al.* (2015), baseado nas literaturas existentes do grupo Rapitan, Canada (modificado de Baldwin *et al.* (2012); (B) modelo Vulcanogênico ("Algoma Type") Formação ferrífera Jucurutu –Faixa Seridó, NE Brazil (Sial *et al*. 2015) e Formações Arabia-Nubian Shield (Stern *et al*. 2013); (C) modelo em ambiente plataformal ("Lago Superior") aplicáveis à formação Yerbal (Frei *et al.* 2013) e Shilu Group, South China (Xu *et al.* 2013b).

CAPÍTULO III

Provenance and isotope geochemistry of the Neoproterozoic iron formations of the Northern Paraguay Belt, Central Brazil: A Sturtian missing related event in South America?

Janaína Almeida de Oliveira[1]; Elton Luiz Dantas[1], Bernhard Buhn (in memorian)[1], Michael Bau[2] and Lucieth Cruz Vieira[1]

[1] Institute of Geosciences, University of Brasília (UnB), Brasília, Brazil;

[2] University of Bremen, Germany

ABSTRACT

Neoproterozoic Iron Formations (NIFs) of the Serra do Cristalino Sequence, included in the geological context of the Northern Paraguay Belt, Central Brazil, are related to a passive margin of Amazon Craton, during the Cryogenian period, generated during the break-up of Rodinia. Jaspilitic BIF and Clastic Iron Formations (CIF) in the Serra do Cristalino region of the Cocalinho-MT, a new discovery occurrence, 1500 Km northward of well know Urucum deposit at South Paraguay belt, show evidence of a deposition in a deep sub-basin in a stratified sea, influenced by glacial cycles in the Neoproterozoic times. The CIFs present a cryptocrystalline matrix that mainly contains crystallized specular hematite micropellets and goethite. The CIFs contain subangular to angular iron formation, chert, and sandstone clasts. The geochemistry of BIFs and CIFs show similar major elements contents, as well as abundances of CaO, MgO, MnO, Al2O3, Na2O, and K2O. Analyzed samples demonstrate a slight enrichment of HREE relative to LREE, and true negative Ce/Ce*(0,7 – 0,95) anomalies as well as a weakly positive to absent Eu/Eu* *(0,8 – 1,2) anomaly and positive Y/Ho*(1 -1,7) anomaly. This data suggests that the Serra do Cristalino iron formation have been deposited under the influence of diluted and low-temperature fluids, in a basin that received input from continental material. REE patterns of the CIFs are similar although slightly higher than of the BIFs and reflect the composition of the Neoproterozoic seawater in both sedimentary rocks, in an anoxic deep ocean dominated by low T hydrothermal input. Nd isotopes and provenance studies based on U-Pb zircon geochronology suggest that the main sources of sediments that filled the basin are of Paleoproterozoic to Mesoproterozoic ages and likely derived from the Amazonian Craton, which is consistent with a passive margin model for the Paraguay Belt. In addition, the youngest zircon at around 721 Ma in the diamictites facies from the Serra do Cristalino occurrence, suggest that their glacial event could be related to Sturtian event, similar to Rapitan, being possible also to be correlated to the marinoan glaciation event, and, thus to be associated to the global Neoproterozoic Oxygenation Event (NOE).

KEY WORDS: Neoproterozoic Iron Formation (NIF), Paraguay Belt, central Brazil, Sm-Nd Isotopes, U-Pb Dates, Sturtian glaciation event.

1. INTRODUCTION

The deposition of Neoproterozoic Iron Formations (NIFs) is associated with the second largest marine oxygenation event (NOE) in Earth's history (Shields-Zhou and Och, 2011; Och and Shields-Zhou, 2012). During this period large concentration of continental masses in the vicinity of the paleoequador served as a thermal insulation, capable of initiating glacial events, about 750-580 Ma, and was correlated with the Snow Ball Earth hypothesis (Kirschvink 1992, Hoffman et al. , Hoffman and Schrag, 2002).

The "Snowball Earth" hypothesis suggests that during the cryogenic period (726 and 635 Ma) the earth was covered by a thick layer of ice, which often went through cyclic glaciogenic and deglaciogenic episodes of the earth. Many events changes cyclically the atmospheric and oceanic conditions allowing the deposition of NIFs. The ice layer that covered the surface of the earth and the oceans, isolating the sea from the atmosphere making it anoxic. Ferrous iron particles were widely transported to the basins, transforming seawater into a metal rich solution (Fe, Mn, Si, Ni, Zn, Pb, L). Thus, deposition was within and below redoxicline at the surface level (stratified ocean) during ice coverage (Angerer et al., 2016; Hoffman and Schrag, 2002). Cooler water and the isolation of sunlight reduced microbial activity (Angerer et al., 2016, Hoffman and Schrag, 2002, Lyon and Reinhard, 2009, Lyon et al., 2014). When the ice cover in the oceans began to melt, iron, which remains in solution in seawater, comes into contact with the hydrogen peroxide that flows into the ocean and rebalances, precipitating ferric iron, generating deposits of iron formations . or Neoproterozoic (Halverson et al., 2011, Stern et al., 2013).

NIFs are closely relate to ice ages, with or without influence of volcanism. In the first case, they were mainly formed in continental depositional environments, rift-type, extensional grabens systems, associated with glacial-marine sediments, intercalated with diamictites, conglomerates, greywacke sandstones and argillites, including dropstones (Klein and Beukes, 1993; Hoffman et al., 1998; Gross 1996), with the top of the sequences frequently being represented by cap carbonates from the late glaciation and diamictites. The non-glaciogenic models, on the other hand, report that NIFs are associated with volcanic rocks, presenting intense hydrothermal activity and related to the rupture of the supercontinent of Rodinia in a passive margin formation or

either in an island arc volcanism at 750 Ma (Yeo, 1981; Eyles and Januszczak, 2004; Basta et al., 2011 and Stern et al., 2013). NIF when banded commonly form deposits composed of layers of hematite and jasper. However, NIFs generally consist only of poorly developed or absent bands and are often reported as ferruginous rolled siltstones or as a ferruginous paraconglomerate matrix (Klein and Beukes, 1993, Cox et al., 2013).

Studies related to the origin deposition of BIFs have emphasized the iron and silica transport and precipitation in different depositional environments, in relation to the physical-chemical conditions and the composition of seawater and Earth's atmosphere evolution. These studies are based mainly on conventional isotopic geochemistry, involving the isotopic signature in diagenetic and/or biochemical processes in the precipitation of Fe and Si in modern and ancient oceans (Bekker et al., 2004, Poulton and Raiswell, 2002; Buck et al., 2007; Cox et al., 2013). The geochemistry of the Rare Earth Elements + Ytrio (REEY) has been one of the most important tools in the studies and characterization of the global Iron formations, and allowed to model the depositional conditions, temperature and depth of the water sheet, as well as to trace the iron oxide sources, paleographic situation, tectonic environment, Eh and pH of seawater (Lascelles, 2007; Bau, 1993; Alexander et al., 2008; Cox et al., 2013 and others). BIFs are the most suitable materials to trace temporal changes in the behavior of REEY in marine environments, due to the low of clastic material and their wide spatial and temporal distribution (Fryer, 1977). Variations in the REEY patterns are also used to determine the deposition of BIF in relation to the hydrothermal sources, that is, distal or proximal sources from the vents (Kato et al., 1998). In addition, the Sm/Nd isotopic geochemistry of BIFs provides important information on the provenance of detrital and mantelic sources into depositional basin (Alexander et al., 2008; Viehmann et al., 2016).

The REE patterns of seawater commonly show a LREE depletion relative to HREE in PAAS normalized spider graphs (Bau et al., 1997b; Alexander et al. Cox et al., 2013). This is due to the faet that HREE form complexes that remain free in the seawater, whereas, LREE are adsorbed to and thus enter the composition of solid particles and precipitate together with marine sediments (James 1954). In modern oceans waters, this depletion in LREE is more pronounced, and may be the result of seawater interaction, which results in the preferential elimination of LREE (Cox et al.,

2013), or reflects sources of detrital loads or some combination of these two processes (dilution of hydrothermal fluids + debris) for the impoverishment of the REE.

Hydrothermal solutions of the mid Atlantic and East Pacific Dorsal (hot fluids> 300°C, and low diluted) are characterized by LREE-enriched patterns with strongly positive Eu anomalies (Michard et al., 1983, Michard And Albarède 1986, Bau and Dulski, 1999 and Douville et al., 1999), while seawater in the modern oceans, with relatively cooler fluids <200°C and diluted in the water of the great oceans, present (PAAS-normalized) enrichment patterns in HREE, with negative Ce and positive Y anomalies (Elderfield and Greaves, 1982; Bau et al., 1996 and Alibo and Nozaki, 1999). Thus, we consider that the fluids produced by hydrothermal alteration are of low temperature, present a weak or absent Eu anomaly (Michard et al., 1993).

The elements behavior in the NIFs occurs in a much more oxygenated ocean and very is close to the waters of the modern oceans, presenting negative anomalies in Ce, positive anomalies in Y / Ho *, and weak positive or absent anomalies and Eu (<1). In the Archaean oceans, REE studies in BIFs show strongly negative anomalies in Ce and a positive anomaly in Eu (> 2), representing seawater conditions, with high temperatures, influence of the hydrothermal fluids that were emitted by the black fumaroles in basins (Danielson et al., 1992, Bau and Moller, 1993, Douville et al., 1999, Cox et al., 2013). In the Paleoproterozoic BIFs, these anomalies are less pronounced, the basins are wider and the hydrothermal fluids slightly more diluted, generating a negative anomaly in Ce and the positive anomaly in Eu (> 1 and <2) (Danielson et al., 1992, Bau and Moller, 1993, Douville et al., 1999, Cox et al., 2013).

The most well-known glaciogenic NIFs of this type of deposit are the iron formations of the Rapitan Group in Canada (Young 1976, Yeo 1981, Eisbacher 1985, Baldwin 2014) and the Urucum deposit, in the Santa Cruz Formation of the Jacadigo Group in Brazil. (Dorr II 1945, Almeida 1964, Urban et al., 1992, Trompette et al., 1998, Klein and Ladeira, 2004, Freitas et al.2011, Angerer et al., 2011, Viehmann et al. Frei et al., 2017). In addition to the Gebel El Hadid deposit in Egypt (Khalil et al.2015) where the BIFs are associated to volcanism in an island arc tectonic setting. There are also reports of ferrous formations associated with platform environments, such as the Shilu Group iron formations in China (Xu et al. 2013).

The study area corresponds to the occurrence of BIFs in Serra do Cristalino, municipality of Cocalinho-MT. Serra do Cristalino is an isolated mountain chain, with a high topographic relief in the middle of the Araguaia River flat land, and the alluvional deposits from the Bananal Basin. There little geological knowledge about the geology of this region and the few outcrops of BIFs from Serra do Cristalino occurrence is not yet describe in the regional literature (Almeida 1984a). The occurrence is located 1500 km north of the well-studied Serra de Urucum Iron deposit, and 100 Km northward from the Nova Xavantina occurrence, which has a similar geological context of the Paraguay belt (Viehmann et al., 2016, Angerer 2016, Walde 2007, Pinho et al.,1990, Martinelli et al. (1997) and Martinelli (1998)). BIFs in the Serra do Cristalino area were discovery in 2003 by mineral research projects of EDEM (Mineral Development Company - Cristalino Iron Project).

This study is the first to present a detailed petrographic and mineralogical characterization of BIFs and CIFs of Serra do Cristalino via, comparing their chemical and mineralogical compositions with other Neoproterozoic BIFs, in order to interpret the conditions of the Neoproterozoic ocean at the Northeastern portion of the Paraguay belt.

2. GEOLOGICAL SETTING

The Paraguay Belt ’s a thick Neoproterozoic sedimentary sequence, deposited in the passive margin at the edge of the Amazon Craton and has been deformed and elongated during the Brasiliano Orogeny (Almeida 1984a, Alvarenga 1985, Dantas et al., 2009).The Paraguay belt had be studied since Almeida (1965), when the presence of banded iron formations was first identified, but only after the discovery of Urucum deposit, it is that was give more attention of geologic community. The occurrences of BIFs in the Paraguay Belt are well knowledge in the southern part of the belt, represented by the Jacadigo group (Urucum-Corumbá district, Santa Cruz hill, Puga Formation in the Bodoquena region. Also, there are occurrence in the north part in the Nova Xavantina area (Pinho, 1990; Martinelli et al., 1998). Finally, in the Boqui

formation, an extension of the belt in the Bolivian territory; Trompette et al., 1998 , Piacentini et al., 2013; Angerer et al., 2016; Cox et al., 2013).

Alvarenga et al. (2000) propose a lithostratigraphic division based on the sedimentary, tectonic and metamorphic zonation along the north Paraguay Belt, suggesting a depositional model where the lower unit is composed by turbidític-glaciogenic influenced rocks, one intermediate unit of carbonate nature, and a superior unit, consisting of siliciclastic sediments. Alvarenga (1985) and Alvarenga and Trompette (1989) interpreted the Cuiabá Group as glacial-marine deposits, which were deposited in a deep and reducing marine environment, possibly in an inclined position and distal to the platform margins, filling extensive faults of the graben systems of the Paraguay belt (Almeida, 1964a, Trompete et al., 1998). The Cuiabá Group, dominant unit in the north part of Paraguay belt, represents lithologies and characteristics of a passive margin, with sediment environment transitional from a shallow platform to deep sea (Alvarenga 1984- Alvarenga and Trompette 1984, Alvarenga 2001, Almeida 1984a and 1945). Another occurrence of glacial sediments associated with BIF was describe by Pinho (1990) and Martinelli et al. (2000) in the Nova Xavantina region, considered by first author as part of Cuiabá Group and by the other as an independent unit, the Nova Xavantina Sequence.

In the Corumbá region, south part of Paraguay belt, sedimentological study conducted by Freitas et al.,(2011), based on the paleocurrent analysis and tectono-sedimentary evolution of the basin, suggest the absence of glaciation for Jacadigo group deposition. It justifies the presence of dropstones in the sedimentary sequence, originating from debris and turbidite flows in underwater currents or subareas of rocks in steep terrain of high slope in extensive fault movements (Freitas et al., 2011). However, almost all the other authors that study in the region, agree on a glacial deposition environment for the Jacadigo Group (Urban et al., 1992, Graf et al., 1994, Walde and Hagemann, 2007, Alvarenga et al., 2011, Gaucher et al., 2015, Viehmann et al., 2016, Angerer et al., 2016 and Frei et al., 2017). In this case, geochemical stratigraphic data of Fe and C stable isotopes from Santa Cruz iron deposits (Angerer et al., 2016), suggest that the deposition of the sequence occurred in the sub-basin environment, whereas the BIF layers interspersed with in up to three diamictites layers. Theses evidence suggest thay they are marked by transgressive and regressive tracts depositional systems related to variation of the glacioeustatic level, with seasonal influx

of continental river waters and resurgence of sea water enriched in deeper anoxic zones (Almeida 1964; Alvarenga, 1985; Alvarenga and Trompette, 1989 and Alvarenga 2011, and Angerer 2016). Thus, available data characterize the Jacadigo group as glacio-marine sediments (Graf et al.,1994, Walde and Hagemann, 2007, Alvarenga et al., 1990, Gaucher et al., 2015, Viehmann et al., 2016, Angerer et al., 2016 and Frei et al., 2017).

Possibly there are records of two or more glacial events in the Paraguay belt, as we do not have an accurate dating for these rocks. Thus, we can infer the limits of deposition by dating detrital zircons, limiting the deposition around 700 -590 ma for the rocks of these sequences (Babinski et.al. 2006 and Piacentini et al., 2013). For the marine sedimentation attributed to the Araras Group, that consist of a carbonate unit, that marks the end of the glacial influence in the basin, with a presence of cap carbonates, which is related to a period of relative sea level rise, an age of about 600 Ma is suggested (Alvarenga, 1990; Rodrigues et al., 1994). Nogueira et al. (2007) corroborate the Marinoan age suggested by Babinski et al. (2006) for the lower Araras Group, on the basis of C and Sr chemostratigraphy. Thus, the IF deposition age is considered as end of Cyrogenian, Marinoan glaciation event, (at about 635 Ma; Babinski et al., 2013; Piacentini et al. 2013, Viehmann et al., 2016).

Similar Marinoan age is consider for the Jacadigo Group and Puga Formation in the south part of Paraguay belt, based on another line of evidence, where Ar/Ar dating of Mn minerals of the Jacadigo Group suggested a depositional age of the Iron Formation and Mn formation between ca. 700 Ma and 590 Ma.

However, McGee et al. (2015) present U-Pb detrital zircon ages, which suggest a Gaskiers age for the Serra Azul Formation and open the possibility of a Gaskiers age for the Jacadigo Group is also possible, once that the diamictites and BIFs of the Puga Formation are probable time-equivalents of BIFs of the Jacadigo Group (Piacentini et al., 2013, Gaucher et al., 2015, Angerer el al., 2016 and Frei et al., 2017). considering that correlation between the Puga and Serra Azul and Jagadigo formations, these youngest zircons at around 590 Ma, marks the maximum depositional age for all (Babinski et.al., 2013 and Piacentini et al., 2013).

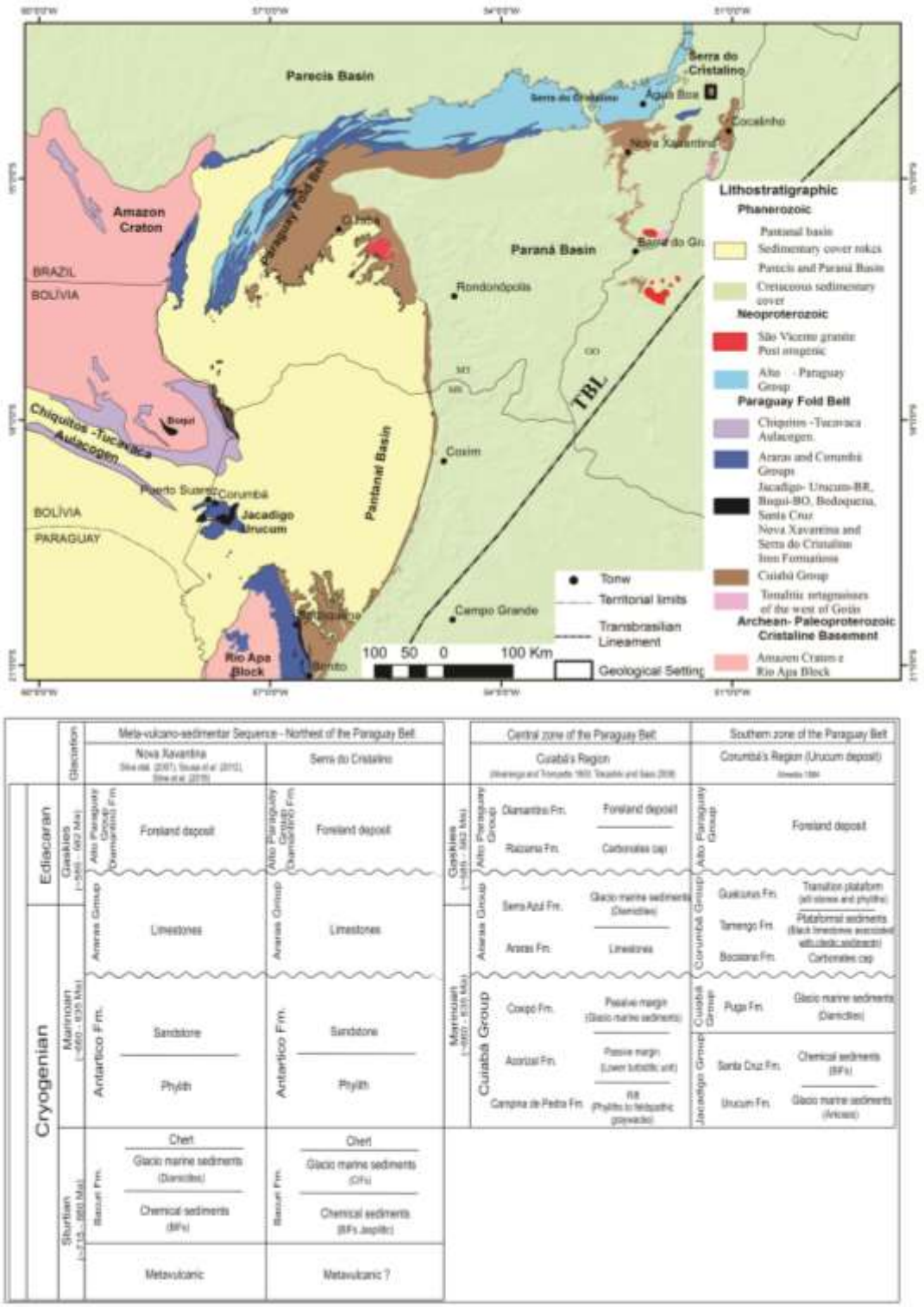

Figure 1. Simplified Geological Map of the Paraguay Belt, modified after Almeida 1968; Schobbenhaus et al., 1981; Alvarenga and Trompette, 1993; Trompette and Alvarega 1998; Angerer et al., 2016; Tokashiki and Saes 2008, Silva 2007 and Sousa et al., 2012, Map modified from geological survey of Brazil-CPRM and photointerpretation of satellite images available in Esri's database evidencing the occurrences of iron formations along the Paraguay belt. Table with the stratigraphic correlations between the different geological units of the Paraguay belt and the rocks found in the Serra do Cristalino-MT study area.

A Sm-Nd isochron obtain for Urucum BIF of 566±110 Ma (Viehmann et al. , 2016) present once again allowing a Marinoan or a Gaskiers age for the unit. Nd isotopes in the all rocks that constitute the Paraguay belt, suggest a dominant sediment source is typically continental and their provenance is relate to the Paleoproterozoic rocks derived from erosion of the Amazonian Craton. Dantas et al. (2009) and Mc Gee et al. (2015) also stated that there is an inversion of the initial passive margin basin, to a foreland basin type, for the top units of the Paraguay Belt, in the Diamantino Formation, which presents reworked molasses type sediments.

The post orogenic São Vicente granite with an age of 518 ± 4 Ma (Mc Gee et al., 2012) intruded the deformed and metamorphic basal unit of the Cuiabá group at the north of the Paraguay Belt (Mc Gee et al., 2012) marking the orogenic phase and the formation of the supercontinent Gondwana in the region.

The Serra do Cristalino is located on the flat terrain of the Cristalino River and represents a small range, ranging from 300 to 500 m above sea level, and has an extension of approximately 10 km and a width of about 1.5 to 2, 5 km. The Serra do Cristalino contains meta-sedimentary rocks of low metamorphic degree, and was mentioned in the literature only by few authors (Lacerda Filho et al., 2006), in this case interpreted as part of the Cuiabá Group.

3. MATERIALS AND METHODS

The Serra do Cristalino deposit was mapped using satellite images of the Esri Database, LandSat 7 images and geological evidence obtained in two field campaigns, where samples were taken, associated with a structural and descriptive systematic profile data. The mapping involve about seven E-W profiles, perpendicular to the layers strike of the hill, which presents a main NS structural trend of strike and dipping 45 degres to E. We selected 35 samples of the rocks from the sequence of the Serra do Cristalino and adjacent areas, including 19 samples of BIFs, 7 of Clastic Iron Formations and 9 samples of sedimentary clastic rocks. The petrographic sections were made in the laboratory of the Institute of Geosciences of the Universidade de Brasília (UnB-Brazil) and the petrographic analyzes were carried out using Polarizing microscope and double illumination (transmitted and incident) of the brand Olympus, model BX-41. The petrographic characterization were determined in the Microscopy

and Geochronology laboratories of UnB. The slides were also metallized for subsequent scanning electron microscopy (SEM) analyzes.

All samples were prepared in the Geochronology Laboratory of the Institute of Geosciences at University of Brasília. The material was firstly fragmented, crushed and pulverized to be done the chemistry analysis.

The rock samples were analyzed at the ACME- ANALYTICAL LABORATORIES LTD in Canada. The total abundance of the major oxides and various trace elements is determined from the melting of 0.2 g of sample with lithium metaborate / tetraborte, diluted nitric acid digestion and analyzed by ICP-OES. After melting at 1000 ° C, the LOI is calculated by the weight difference of the sample. Base and precious metal grades were determined by digestion in Aqua Regia followed by ICP-MS (Inductively Coupled Plasma - Mass Spectrometry) analysis. The abundances of the major element oxides were obtained by X-ray Fluorescence after sample melting with lithium tetraborate.

U-Pb isotopic analyses were performed on zircon grains using a Thermo-Fisher Neptune HR-MC-ICP-MS coupled with a Nd: YAG UP213 New Wave laser ablation system, also at the Laboratory of Geochronology of the University of Brasilia. The U-Pb analyses on zircon grains were carried out by the standard-sample bracketing method (Albarède et al., 2004) using the GJ-1 standard zircon (Jackson et al., 2004) in order to quantify the amount of ICP-MS fractionation. The tuned masses were 238, 207, 206, 204 and 202. The integration time was 1 second and the ablation time was 40 second. A 30 μm spot size was used and the laser setting was 10 Hz and 2-3 J/cm2. Two to four unknown grains were analyzed between GJ-1 analyses. 206Pb/207Pb and 206Pb/238U ratios were time corrected. On smaller zircon grains (about 50 μm), single-spot laser-induced fractionation of the 206Pb/238U ratio was corrected using the linear regression method (Košler et al., 2002). The raw data were processed off-line and reduced using an Excel worksheet (Buhn et al., 2009). During the analytical sessions the zircon standard 91500 (Jackson et al., 2004) was also analyzed as an external standard.

Common 204Pb was monitored using the 202Hg and (204Hg+204Pb) masses. Common Pb corrections were not done due to very low signals for 204Pb (< 30 cps) and high 206Pb/204Pb ratios. Reported errors are propagated by quadratic addition [(2SD2+2SE2)1/2] (SD = standard deviation; SE = standard error) of external

reproducibility and within-run precision. External reproducibility is represented by the standard deviation obtained from repeated analyses (n=20, ~1.1 % for 207Pb/206Pb and up to ~2 % for 206Pb/238U) of the GJ-1 zircon standard during the analytical sessions, and the within-run precision is the standard error calculated for each analysis. Concordia diagrams (2σ error ellipses), probability density plots and weighted average ages were calculated using the Isoplot-3/Ex software (Ludwig, 2003).

Sm-Nd isotopic data were measured at Geochronology Laboratory, in the University of Brasília, on a multi-collector Finnigan TRITON mass spectrometer in static mode and methodology executed as described by Gioia & Pimentel (2000). Whole-rock samples (ca. 50 mg powdered) were mixed with 149Sm-150Nd spike solution and dissolved in HF, HNO3 and HCl in Savillex capsules. Cation exchange techniques were implanted for Sm and Nd extraction of whole-rock samples using Teflon columns containing LN-Spec resin (HDEHP-di-ethylhexil phosphoric acid supported on PTFE powder). Sm and Nd samples were loaded onto Re evaporation filaments in a double filament assembly. Uncertainties for Sm/Nd and 143Nd/144Nd ratios are better than ±0.5% (2sigma) and ±0.005% (2sigma), respectively, based on repeated analyses of intern rock standards BHVO-1 and BCR-1. 143Nd/144Nd ratios were normalized to 146Nd/144Nd of 0.7219. De Paolo (1981) model was used to calculate TDM ages. Sm-Nd isochrones were calculated using the Isoplot-3/Ex software (Ludwig, 2003).

RESULTS

4. LITHOSTRATIGRAPHY OF THE SERRA DO CRISTALINO

The Serra do Cristalino sequence is composited by several types of rocks, which stratigraphic sequences is describe bellow. In the base occur Iron Formations, including laminate Jaspilitic intercaled with Clastic Iron Formations (CIF), represented by microdiamictitic with matrix iron- rich, presented average thickness of 200m. On the top, occur subordinate cherts of light gray, red (Jasper) and yellowish colors, as well as argilites and greenish siltites. Sometimes ferruginous and subarkosean and sandstone are present, but the relationships with other lithologies is unclear. All area, present covered by a thin layer of debris flow (~ 1.5m) of fluvial sediments (Figure 2).

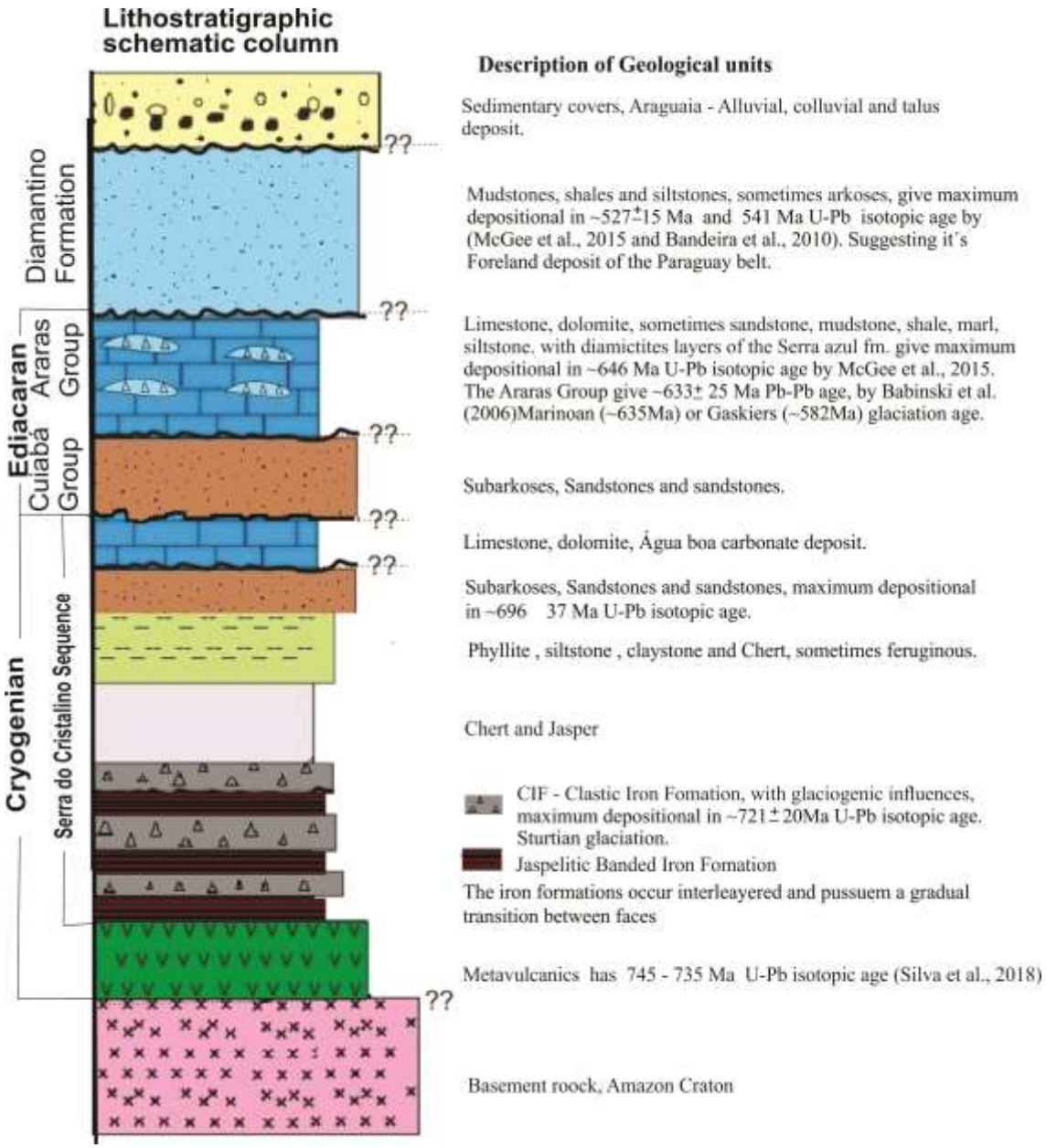

Figure 2. Schematic stratigraphic column of the "Serra do Cristalino" and adjacent areas.

The Serra do Cristalino rocks were deformed and present major folding phases, given by open to close folds, oriented in NNW to NS tredding, with foliation or layering plunging 30° to 45° for ENE (Figure 3).

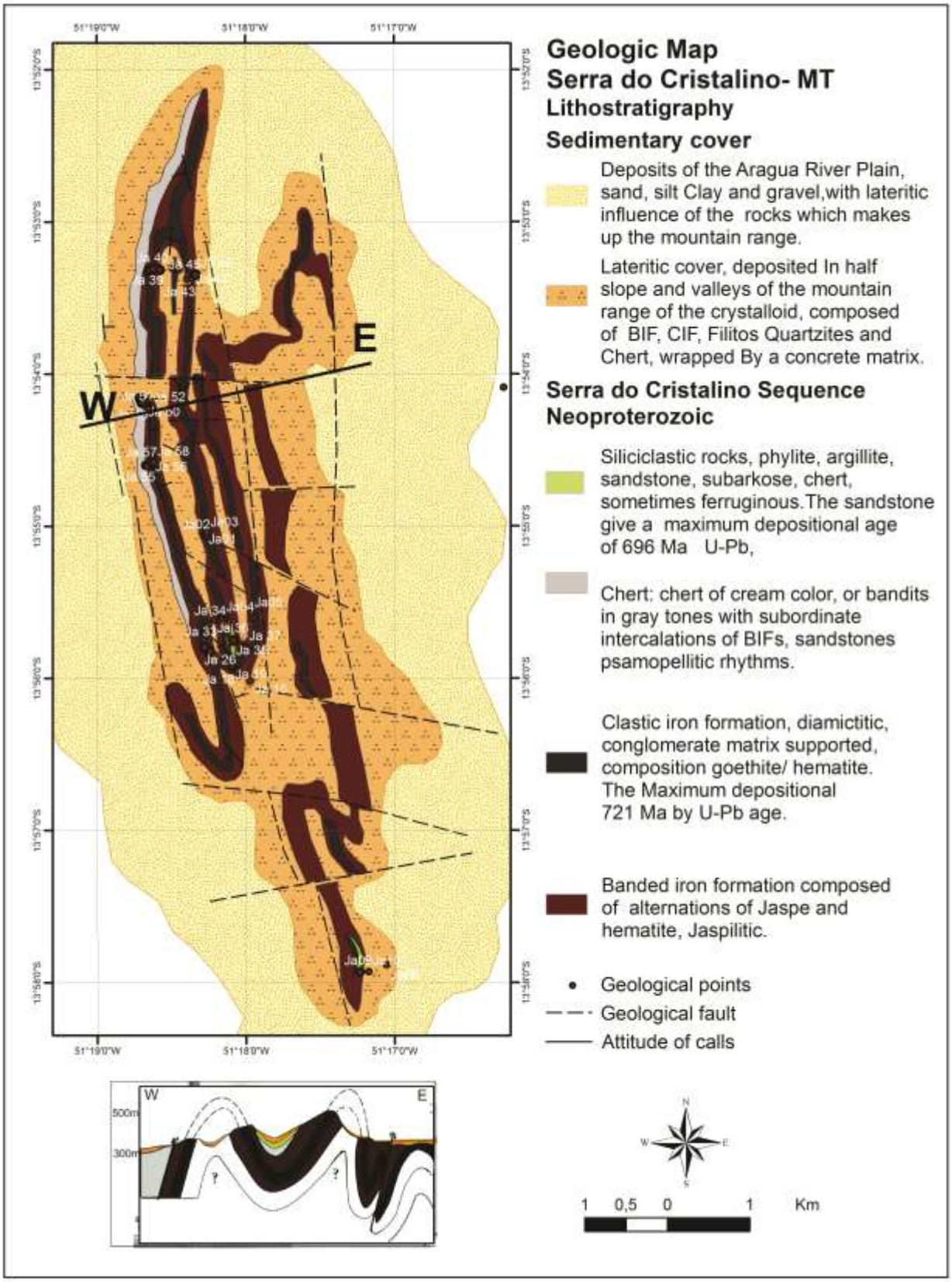

Figure 3. Geological map of the "Serra do Cristalino" sequence, modified of the Cristalino iron project (EDEM- Mining Development Company).

4.1 Serra do Cristalino Iron Formations

The iron formations could be classified, according to the mineralization, the texture and the depositional setting (Trendall and Morris, 1983, Klein and Beukes, 1993 Cox et al., 2013). The “Serra do Cristalino” iron formation deposit has two distinct lithofacies : 1. Jaspilitic banded iron formation (figure 04 A and B) (Jaspilitic BIFs) and 2. Clastic Iron Formation (CIFs)(figure 4 C and D). BIFs and CIFs occur interlayered and have transitional or angular discordant contacts. The BIFs of the Serra do Cristalino occur as jaspilitics, finely banded or laminated rocks, alternating of hematite and jasper layers with hematite matrix texture from fine to cryptocrystalline. The clastic iron formations (CIF) are not banded rocks, and present a homogenous texture, with clasts of varied composition, represented by some detrital contribution, in a chemical sedimentation environment, are interpreted as microconglomerate composed by ferruginous matrix (Figure 04 C and D) and jasper and chert (Figure 04 E and F).

Jaspilitic Banded Iron Formations (Jaspilitic BIFs)

The Jaspilitic BIFs are laminated to banded.

In general, the banding is composed of millimeter layers of jasper (red chert) and iron oxide (hematite). Sometimes they form thicker layers varying from 1mm to 10mm for the layers of jasper, and the hematite occurs as micropellets disseminated in the bands of jasper to layers of up to 5mm thickness. They are laminated, can be diluted or thinned and form pods, where jasper pods wrapped by iron oxide and / or iron oxide pods involved in jasper. The BIF layers often contain micro-fractures, which are filly up with quartz and / or iron oxides and / or goethite, in addition to small folds (Figure 04A and B). The BIF layers locally are brecciated (Figure 04). The Jaspilitic BIFs occur essentially interdigitated with the classic iron formations CIF.

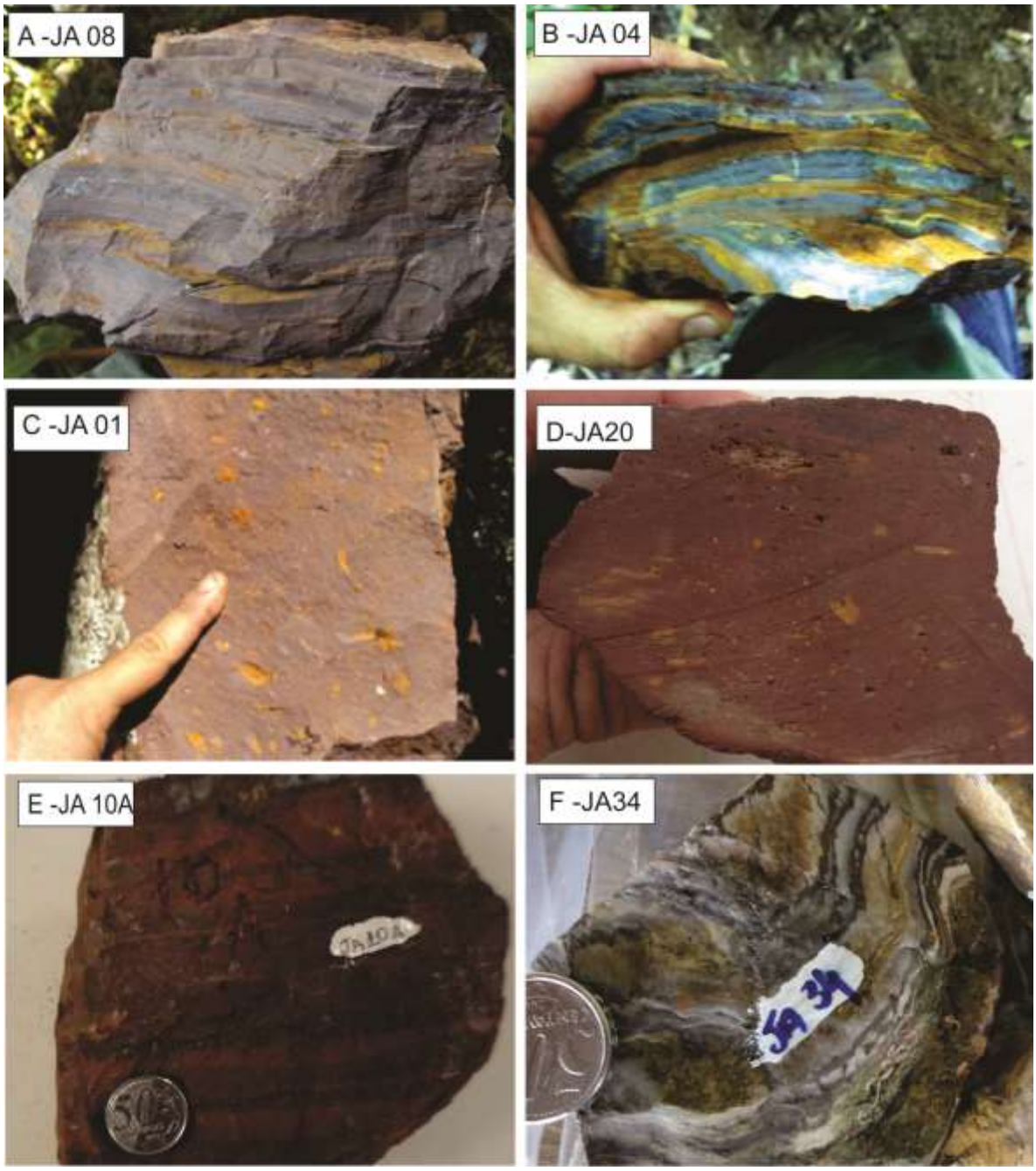

Figure 4. Pictures A - Jaspilitic BIF with very thin layers B- sample JA-04 folded siliceous layers of yellowish to reddish Jaspilitic BIF, contend very thin layers, of hematite with a fine granulometry. C and D- CIF Showing the clastic texture of the rock, and a a microcrystalline, ferruginous red-brownish coloration matrix, with angular to subangular clasts. The matrix of ferruginous composition (goetite hematite) has fragments of varying sizes and roundness degree; E- Jasper and F- Compositional banding is observed with the most prominent Chert layers, with an impoverishment in Iron.

The banding of the iron formation are usually horizontal and parallel to the layering and may be regular or discontinuous and preserve diagenetic features. It further more, iron formation locally display a secondary porosity that likely results from leaching, especially of silica, and the removal of iron from the layers. Such processes is

presumably related to the weathering conditions and supergenic processes which further may have been responsible for the enrichment of iron, which locally accounts to 80% of the rock weight.

The japilitic iron formation mainly contain hematite and are easily distinguishable by its gray color, metallic luster, red trace and the absence of magnetism. The iron formation are banded, laminated with alternating between jasper and hematite.

Hematite iron oxides are microcrystalline to very fine, usually anhedral, in massive layers, and in the form of micropellets generally disseminated in the layers of chert and / or Jasper of the rock (Figure 06 A and B). Hematite presenting a radial acicular habit, and they suggest the existence of two phases of mineral crystallization (Figure 06, C), which may be derived from amorphous oxide layers and another that generate partially specular hematite microchips of late crystallization, possibly derived from low-grade diagenetic and / or metamorphic recrystallization processes. The most silicic bands present also dolomite pseudomorphs that were replaced by iron oxide and hydroxide and silica respectively (Figure 06 D and E), a supergene alteration process with goethite bordering the Hematite crystals and Hematite layers (Figure 06 F).

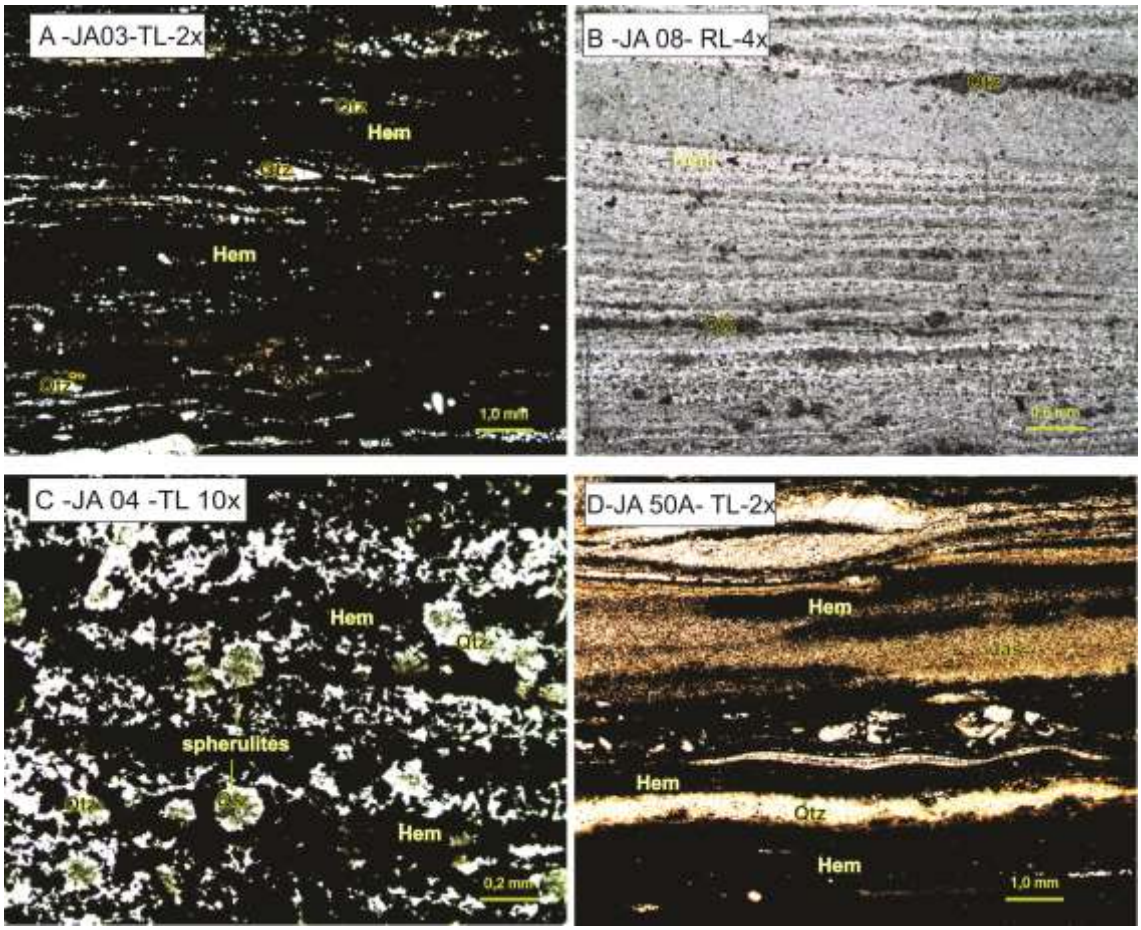

Figure 5. Petrography of Jaspilitic BIF, A - photograph in transmitted light (TL) and 2x objective, of JA03 blade showing a very thin, lamellar texture from where the chert/Quartz layers are thinned to form lenses and silica pods, B - Reflected Light (RL) photograph of sample JA08, with a magnification of 4x, showing the thin intercalated layers of Hematite and chert, similar to sample JA03; C - Photograph in TL, showing spheroidal structure where the center and quartz composition is surrounded by Hematite, It also presents spheroidal habit of hematite nuclei; such structures (spherulites) are evidences of bacterial activity, in the deposition of BIFs; D - Showing the most jaspilitic layers of BIFs and compositional frames and banding.

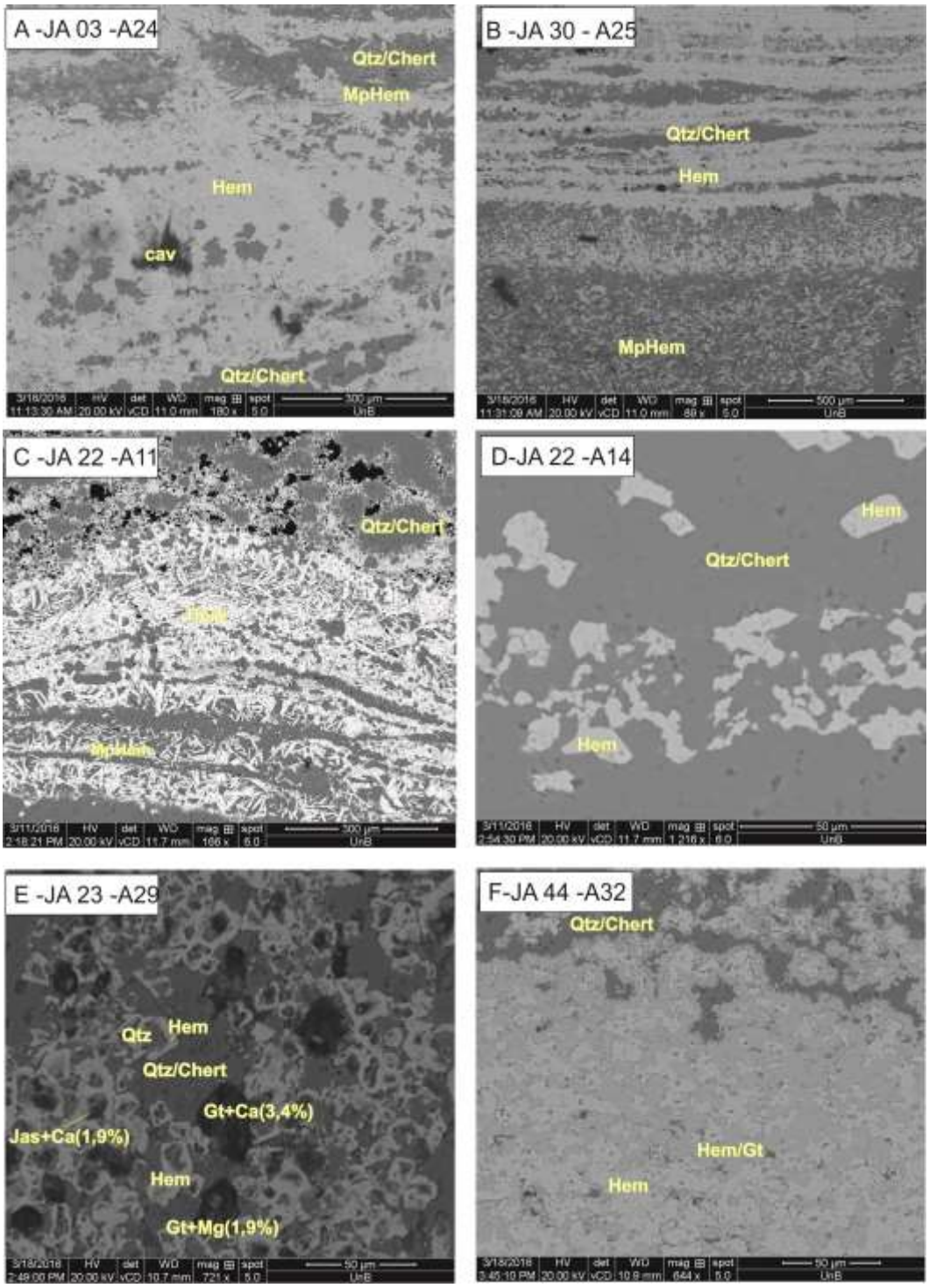

Figure 6. Micrographs obtained in MEV, type BKS, with the use of EDS (chemical quantitative of minerals), showing the different characteristics found in Jaspilitic Facies Rocks, A- Showing the practically massive layer of amorphous Hematite, with preserved Chert and Jasper nuclei, and in the upper portion of the photo, partially oriented hematite micropellets, there are still cavities in the lower part of the photograph; B- shows that the rock is banded, layers rich in amorphous Hematite and another one more siliceous with specular, disseminated, non or partially oriented hematite micropellets, pods of silica encased by iron oxide, C- Photograph of detail showing the habit of garnular (amorphous) and specular hematite minerals (micropellets);D- E Pseudomorphs of carbonates being substituted by iron oxide and silica; where D- Band rich in silica, chert, showing hematite replacing carbonate minerals; E - The substitution of carbonate for silica occurs in the nucleus and hematite in the border; F- Shows the amorphous Hematite, autereretion to goethite.

4.2 Clastic Iron Formations

Clastic Iron Formation (CIF) is composed by a paraconglomerate or ferruginous paraconglomerate diamictitic, microcrystalline iron matrix supported, including hematite, goethite and jasper micropellets, and large amount of clasts, which sizes vary and composition, and generally have angular to subangular shapes (Figure 04 C and D and Figure 7A to F). The large clast (< 5 cm) are composed of millimetric fragments, often including fragments of rocks reworked of the Cristalino sequence, cryptocrystalline quartz, chert, sandstones and own BIF (Figure 07A to B). We recognize clasts of barite(Figure 07 A and B) and plagioclase, and crystal rock fragments (Figure 07-E) in this microconglomerate unit contend a matrix with high grade iron.

The CIF occur closely related to the jaspilitic layers intercalated, on the top of the the Cristalino sequence, as gradual and transitional contact. Another hand, they present an angular disagreement occurring at the base contact with jaspilitic BIF , that is supported by the presence of BIF clastics into CIF formation.

The matrix of CIF has hematite/ goethitic -limonitic composition, cryptocrystalline to microcrystalline with amorphous silica, in addition to hematite micropellets. The hematite exhibit a radial acicular habit, disseminated in the middle of the amorphous mass of goethite, with or without partial orientation. The micropellets and the cryptocrystalline quartz pockets, that exist in the CIF, were possibly formed by a low-grade diagenetic and/or metamorphic recrystallization process (Figure 07 C and D).

Texturally this group of rocks represents a shift in the environment from low energy chemical sedimentation to a regime of higher energy in places where there was limited contribution of fine clastic sediments during the prevailing chemical sedimentation. Also suggests, a probable shift from the chemical sedimentation conditions to a higher energy environment, with a little more siliciclastic contribution than the deposition of BIFs, and possibly related to glaciogenic contributions.

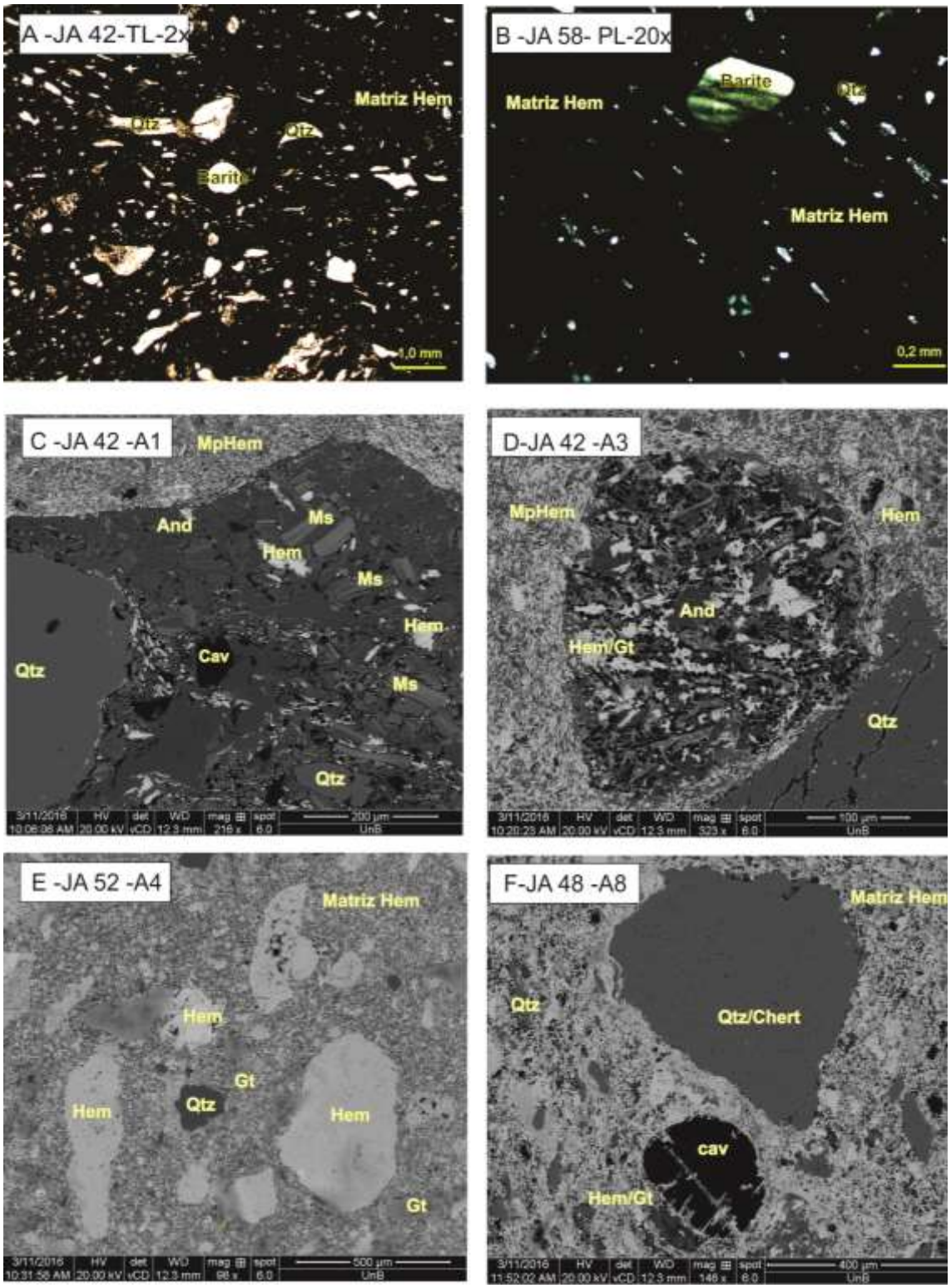

Figure 7. Petrography of CIFs, A- photograph in a 2x magnification, showing that the fine-grained matrix rock of ferruginous composition (goetite hematite) with fragments of varying sizes, roundness degree and composition is generally quartz cryptocrystalline (chert); B- Photo in LP showing rounded barite grain with parallel extinction; C-F: Micrographs obtained in MEV, showing the different characteristics found in the Clastic Iron Formations - CIFs, E- Rock fragment composed of granular quartz, muscovite slats with no orientation, the fragment is enveloped by a jasper matrix with micropellets (Mp) of Hematite with no orientation; D - Rounded clast with hematite minerals, calcium plagioclase, immersed in matrix of the upper side composed of Mp hematite and jasper, and on the other side, chert/quartz; E and F- Show rock

fragments of the quartz and ematite sequence, sometimes undergoing oxidation to subanglar to angular goethite, it seems to be the reworking of the rocks in the sequence.

4.3 Grey, yellowish and ferruginous cherts

These rocks present an enrichment of up 90% in silica, show cryptocrystalline texture, and are banded (Figure 04 E and F). Chert and/or ferruginous chert occur in much of the western portion of the Serra do Cristalino hill and intercalated with the BIFs jaspilitic facies. The rock with siliceous/chert composition has a color ranging from white, light grey, and yellowish to red, when vary to a jasper facies. The silicon layer inserted with millimeter scale iron oxides layers, with gradual impoverishment in iron. Sometimes, the rock becomes a virtually pure chert, and suggest that there was a gradual change in the environment during chemical sedimentation, and change in the fluids composition, causing the seawater impoverished in iron. This way layers representing the late facies of the chemical precipitation of Fe/Si solution. Layers of jasper - Figure 08 A and chert show finely chrystallized spherulites and hematite with bothoidal habit (Figure 08 B). The presence of spherulites evidence bacterial activity during chert deposition. Figure 08 C and D- with hematite levels replacing the carbonate pseudomorphs and hematite venules in the microphotograph D.

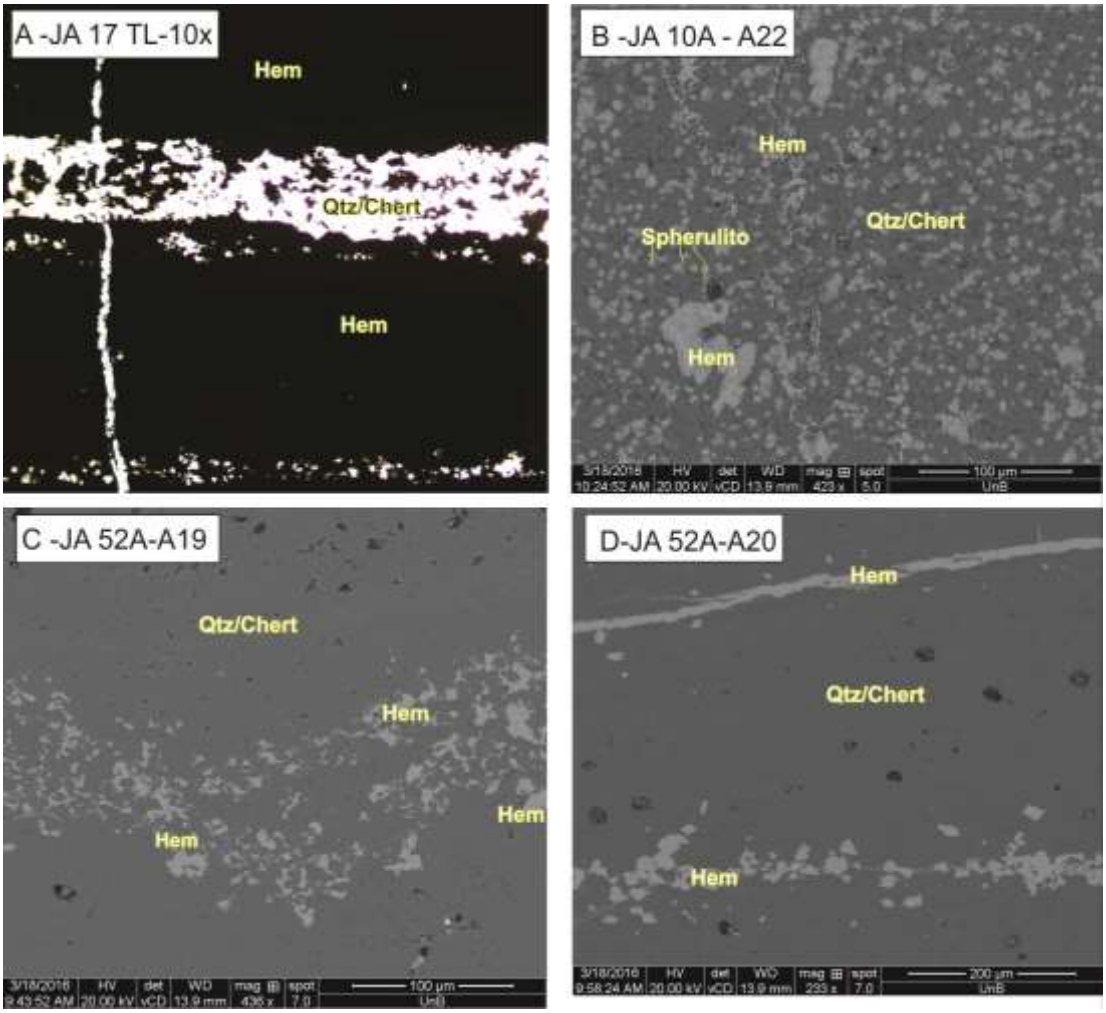

Figure 8. Petrographic and SEM analysis using EDS shows in A- rock composed mainly by Jasper, with opaque cryptocrystalline texture, in B- detail photo of jasper layer showing the morphology of hematite with botoidral habit and spherulites (Evidence of bacterial activity for chert deposition); C and D – Pure chert, with 94% of the silica composition, with hematite levels replacing the carbonate pseudomorphs and hematite venules in the microphotograph D.

4.4 Phylite, shales and siltstones

The rocks that marks the end of the chemical sedimentation, and overline the iron formations and chert formations of the Serra do Cristalino sequence. The pelitic sediments are fine, shales and siltstones. They occur on the top of the hill, as fragments in situ associated with CIF layers. Shales and siltstones occur as a very fine granular rock, silica-rich, with small layers of clay minerals and iron oxide/hidroxide (Figure 9 A). These rocks are strongly deformed by brittle condictions, showing a brecciated texture, characterized by a net of microfractures and faults filled by quartz and iron oxide. These features are interpreted as post-depositional, and the brecchia was formed

by epigenic fluids derived from ferruginous source that occurs below the clastic sequence (Figure 9 E).

We interpret the pelitic sequence as representative of a change in the sedimentation environment that stops being chemical and becomes more siliciclastic, but still deep environment, with pelitic sedimentation.

Figure 9. A: Outcropping of the siltites rocks on the right bank of the road that gives access to "Serra do Cristalino" Deposit, near the cocalinho is about 40km from the study area samples with varying iron content B - JA07 - outcrop of quartzite cut by vertical quartz veins. It occurs in an outcrop surrounding the Serra do Cristaino.C and D, Sandstone arkose sample of the Serra do Cristalino sequence, by U-Pb age. E. Phyllite showing post-depositional veins and brecchias, which epigenic fluids are derived from a

ferruginous source. The veins cross cut perpendicular the sediment layering. F. Photomicrographs of the JA53 obtained in flat polarized light a 4x magnification, showing that the arenites consist mainly of rounded quartz grains

4.5 Subarkoses and Sandstones

The siliciclastic rocks present in the study area, represent the top of the sequence Serra do Cristalino. The best exposure and outcrops occur 47 km southeast from the deposit, on the road from Cocalinho city, but sandstone in situ blocks are found within the Serra do Cristalino hill, in their central portion, in four distinct localities, and was not possible individualize these occurrences on a map. However, it´s clear that rocks are occurring on the top of the sequence and mark a siliciclastic environment into that. The impure sandstone consists essentially of more than 90% of quartz, varying to some arkosean composition, given by some muscovite and feldspar grains (Figure 9 B, C, D e F) . Deformational brittle process are evidence by quartz veins cutting cross the rocks in different directions N10, N60 and N345 (Figure 09B).

We interpret the arenite rocks as they may have deposited into small layers of seasonal flows that increase the energy of the system, forming of lenses that represent the proximal portion from continental sources, influenced by shallower waters conditions.

5. GEOCHEMISTRY

We analyze all rocks from the entire stratigraphic section of chemical sediments from the Serra do Cristalino sequence. Was identified three different groups of, including samples of BIF jaspilitic, CIF and chert facies and two siliciclastic facies. Geochemistry studies in iron formations has been widely used as a representative of the chemical composition of seawater, because they are the purest precipitated sediments (Bekker et al., 2010, Angerer et al., 2016, Viehmman et al.2016, Kallil et al 2015, Cox et al 2013).

The geochemistry of the major and traces elements are presented in Tables 01 and 02. The samples of the jaspilitic (BIF) and the clastic iron formations (CIF) present similar Fe_2O_3 and SiO_2 contend. The Fe_2O_3 values ranging from 40% to 82% (mean = 53% by weight), whereas SiO_2 raging between 14% and 58% (mean = 42%). However, CIFs are more enriched relatively compared to BIF samples in Al_2O_3 (1,2-

2,6% by weight), CaO (0,05-0,2%), P_2O_5 (1,0-3,5%). The pure chert is ~ 95% by weight SiO2 and 4.2% by weight Fe_2O_3, leaving less than 1% for the other main elements. Binary diagram for BIF-jaspilitic, Clastic Iron Formations (CIF) and Pure Chert of the Serra do Cristalino allow to evaluate the contribution of the debris between the chemical sedimentary facies (Figure 10 A to D).

Table 1. Geochemical data of pure BIF of the Serra do Cristalino deposit.

Lithology	**JAPILITIC - BANDED IRON FORMATION**															
Sample ID	**JA 03**	**JA 04**	**JA 08**	**JA-17**	**JA-18**	**JA-19**	**JA-21**	**JA-22**	**JA-30**	**JA-34**	**JA-39**	**JA-44**	**JA-45**	**JA-50A**	**JA-51**	**JA-56**
SiO_2 (%)	39,37	35,66	44,12	43,02	33,7	34,63	53,2	43,68	46	50,35	54,36	13,79	25,04	39,22	42,64	58,31
Al_2O_3 (%)	0,17	0,28	0,13	0,09	0,07	0,31	0,38	0,34	0,18	0,11	0,1	0,16	0,29	0,17	0,17	0,18
Fe_2O_3 (%)	56,71	58,55	50,88	53,43	62,18	61,31	42,89	51,82	50,73	44,16	39,63	81,58	70,81	55,82	54,42	40,09
MgO (%)	0,06	0,08	0,12	<0.01	0,02	0,04	0,05	0,03	0,08	0,02	0,06	0,05	0,04	0,05	0,02	0,02
CaO (%)	0,05	0,09	0,04	0,03	0,03	0,07	0,08	0,06	0,12	<0.01	0,04	0,03	0,03	0,05	0,03	0,02
Na_2O (%)	0,04	<0.01	0,01	<0.01	<0.01	<0.01	0,01	<0.01	<0.01	<0.01	<0.01	<0.01	<0.01	<0.01	<0.01	<0.01
K_2O (%)	0,02	0,02	0,01	<0.01	<0.01	<0.01	<0.01	<0.01	<0.01	<0.01	<0.01	<0.01	<0.01	<0.01	<0.01	<0.01
TiO_2 (%)	0,02	0,02	0,02	0,02	0,02	0,03	0,07	0,06	0,03	0,03	0,02	0,04	0,03	0,03	0,02	0,02
P_2O_5 (%)	0,66	0,92	0,48	0,31	0,64	0,72	0,58	0,68	0,35	0,28	0,3	0,45	0,71	0,47	0,33	0,24
MnO (%)	0,02	0,1	0,03	0,01	<0.01	0,04	0,06	0,02	0,02	<0.01	<0.01	0,02	0,02	0,02	0,01	<0.01
Cr_2O_3 (%)	0	<0.002	<0.002	<0.002	0	<0.002	0,01	0	<0.002	0	<0.002	0	0	<0.002	<0.002	0
LOI (%)	2,8	4,2	4,1	3,1	3,3	2,8	2,6	3,3	2,4	5	5,5	3,8	3	4,2	2,3	1
TOTAL(%)	99,92	99,92	99,94	100,01	99,96	99,95	99,93	99,99	99,91	99,95	100,01	99,92	99,97	100,03	99,94	99,88
U (ppm)	<0.1	<0.1	<0.1	<0.1	<0.1	<0.1	<0.1	<0.1	<0.1	0,3	<0.1	<0.1	<0.1	<0.1	0,5	<0.1
V	33	28	26	24	69	33	61	50	21	22	16	70	45	19	76	15
Zr	5,4	6,4	7,3	6,7	5,3	7,9	15,8	11,1	31,5	7,4	5,7	6,7	8,4	7,7	5,3	7,7
Ag	0	0	0	<0.1	<0.1	<0.1	<0.1	<0.1	<0.1	<0.1	<0.1	<0.1	<0.1	<0.1	<0.1	<0.1
As_	0	0	0	1,2	0,9	1	1,6	1,4	1	0,7	1,1	<0.5	1,2	0,7	4,3	0,8
Au	0	0	0	0,7	<0.5	1,1	1,4	<0.5	1,7	<0.5	2	1,3	0,5	1,6	<0.5	<0.5
Bi	0	0	0	<0.1	<0.1	<0.1	<0.1	<0.1	<0.1	<0.1	<0.1	<0.1	<0.1	<0.1	<0.1	<0.1
Cd	0	0	0	<0.1	<0.1	0,1	0,2	0,2	<0.1	<0.1	<0.1	<0.1	<0.1	<0.1	<0.1	<0.1
Cu	0	0	0	1,9	1,3	3,7	4,5	2,7	1,7	0,5	2,4	0,9	2,3	2,4	2	1,6
Hg	0	0	0	<0.01	<0.01	<0.01	0,02	<0.01	<0.01	<0.01	<0.01	<0.01	<0.01	<0.01	<0.01	<0.01
Mo	0	0	0	0,1	<0.1	0,1	0,4	0,3	0,1	0,5	0,7	<0.1	<0.1	0,9	3,1	0,1
Ni	0	0	0	<0.1	0,9	6,1	5,2	3,3	1,5	0,6	1,6	0,8	1,2	1,4	11,1	1,2
Pb	0	0	0	0,7	0,6	0,6	0,3	0,2	186	<0.1	183,7	113,1	0,4	1,1	1,6	0,1
Sb	0	0	0	<0.1	<0.1	<0.1	<0.1	<0.1	<0.1	<0.1	<0.1	<0.1	<0.1	<0.1	<0.1	<0.1
Se	0	0	0	<0.5	<0.5	<0.5	<0.5	<0.5	<0.5	<0.5	<0.5	<0.5	<0.5	<0.5	<0.5	<0.5
Tl	0	0	0	<0.1	<0.1	0,1	0,3	<0.1	<0.1	<0.1	<0.1	<0.1	<0.1	<0.1	<0.1	<0.1
Zn	0	0	0	4	3	10	13	11	9	3	8	3	4	5	10	5
Nb	0,7	0,7	0,8	0,5	1,5	0,2	1,1	0,8	0,9	0,5	0,2	0,5	0,9	0,6	0,7	0,5
Rb	0,4	0,7	0,3	0,1	0,1	0,2	0,5	0,3	0,2	<0.1	<0.1	0,1	0,2	<0.1	0,2	<0.1
Sc	2	2	2	3	2	3	6	5	4	3	2	4	3	3	2	2
Sn	<1	<1	<1	<1	<1	<1	<1	<1	<1	<1	<1	<1	<1	<1	<1	<1
Sr	22,4	33,9	13,2	12,1	29,2	36,8	64,9	40,3	61	5,1	8,1	32,6	16	49,5	48,8	28,9
Ta	0,1	0,1	0,1	<0.1	0,1	<0.1	<0.1	<0.1	0,2	<0.1	<0.1	<0.1	<0.1	<0.1	<0.1	0,1
Th	0,2	0,3	0,2	<0.2	0,3	0,5	1	0,9	0,5	0,3	<0.2	0,4	0,2	0,3	<0.2	<0.2
Ba	112	262	60	87	155	147	260	102	101	25	23	120	56	82	117	251
Be	<1	3	<1	<1	<1	<1	<1	<1	<1	<1	2	<1	6	2	3	<1
Co	13,6	19,1	12,8	36,5	27,8	16,4	21,5	21,9	60,9	37	28,5	17,7	20,7	34,4	48,5	88,1
Cs	<0.1	<0.1	<0.1	<0.1	<0.1	<0.1	<0.1	<0.1	<0.1	<0.1	<0.1	<0.1	<0.1	<0.1	<0.1	<0.1
Ga	0,6	0,6	<0.5	<0.5	<0.5	<0.5	0,9	0,8	2,2	<0.5	<0.5	<0.5	<0.5	<0.5	2,5	<0.5
Hf	0,1	<0.1	0,1	0,1	0,2	<0.1	0,2	0,2	0,2	<0.1	<0.1	<0.1	0,2	<0.1	0,1	0,2
La	1,8	2,7	3	4,8	1,5	7,5	21,5	17,3	10,2	6,5	1,8	7,8	2,3	5	1,2	1,5
Ce	3,4	5	6,4	9,1	2,7	15	43,9	37	19,3	11,9	3,7	13,9	4,3	9,4	2,6	3
Pr	0,5	0,64	0,91	1,14	0,43	1,8	5,9	4,93	2,44	1,56	0,52	1,92	0,58	1,21	0,33	0,42
Nd	2,1	3,6	4,8	5,9	1,7	7,6	26,7	24,2	10	7,3	2,5	9,2	3,2	5,9	2,4	1,8
Sm	0,6	0,65	1,02	1,03	0,47	1,68	5,96	5,21	2,17	1,54	0,53	1,98	0,59	1,25	0,31	0,49
Eu	0,15	0,17	0,26	0,31	0,11	0,44	1,48	1,23	0,49	0,36	0,14	0,5	0,17	0,27	0,1	0,12
Gd	0,74	1,01	1,64	1,8	0,74	2,6	8,47	7,13	2,75	2,14	0,94	2,94	1,08	1,59	0,48	0,81
Tb	0,2	0,25	0,35	0,33	0,16	0,47	1,45	1,17	0,44	0,38	0,21	0,53	0,22	0,27	0,11	0,15
Dy	1,72	1,97	3,13	2,67	1,58	3,7	9,83	8	3	2,88	1,92	4,31	2,37	1,89	0,97	1,3
Y	18,1	23,4	25,7	21,3	16,7	28,1	62,1	49,7	18,7	19,7	18,6	31,7	23,8	11,8	9,6	11,7
Ho	0,47	0,55	0,8	0,58	0,4	0,88	2,14	1,79	0,68	0,65	0,5	0,9	0,58	0,41	0,27	0,33
Er	1,6	1,94	2,26	1,96	1,47	2,61	6,15	4,82	2,03	1,84	1,69	3,03	2,39	1,18	0,87	1,02
Tm	0,27	0,33	0,37	0,29	0,24	0,41	0,86	0,7	0,3	0,27	0,25	0,46	0,35	0,18	0,15	0,15
Yb	1,95	2,11	2,52	1,93	1,78	2,61	5,21	4,44	1,96	1,75	1,72	3,15	2,57	1,27	0,94	1,12
Lu	0,28	0,34	0,4	0,32	0,28	0,43	0,82	0,72	0,31	0,29	0,28	0,41	0,39	0,2	0,15	0,19
Σ REEY	33,88	44,66	53,56	53,46	30,26	75,83	202,47	168,34	74,77	59,06	35,3	82,73	44,89	41,82	20,48	24,1
Co+Cu+Ni	13,6	19,1	12,8	38,4	30	26,2	31,2	27,9	64,1	38,1	32,5	19,4	24,2	38,2	61,6	90,9
Ce/Ce*(PAAS)	0,82	0,88	0,89	0,9	0,77	0,94	0,9	0,92	0,89	0,86	0,88	0,83	0,86	0,88	0,95	0,87
Eu /Eu*	1,04	0,94	0,9	1	0,84	0,95	0,95	0,92	0,92	0,9	0,87	0,94	0,93	0,88	1,17	0,85
Eu/Sm*	1,28	1,34	1,31	1,55	1,2	1,35	1,28	1,21	1,16	1,2	1,36	1,3	1,48	1,11	1,66	1,26
Pr/Pr*	1,08	0,86	0,93	0,9	1,16	0,99	1	0,95	1,03	0,97	0,98	0,98	0,89	0,94	0,72	1,05

Sm/Yb*	0,16	0,16	0,21	0,27	0,13	0,33	0,58	0,6	0,56	0,45	0,16	0,32	0,12	0,5	0,17	0,22
La/Sm*	0,44	0,6	0,43	0,68	0,46	0,65	0,52	0,48	0,68	0,61	0,49	0,57	0,57	0,58	0,56	0,44
La/Yb*	0,18	0,22	0,17	0,29	0,19	0,32	0,3	0,3	0,47	0,35	0,17	0,3	0,21	0,38	0,22	0,2
Y/Ho*	1,41	1,56	1,18	1,35	1,53	1,17	1,07	1,02	1,01	1,11	1,37	1,29	1,51	1,06	1,31	1,3
Y/Ho	38,51	42,55	32,13	36,72	41,75	31,93	29,02	27,77	27,5	30,31	37,2	35,22	41,03	28,78	35,56	35,45

Table 2. Geochemical data of CIFs, Chert, Argilites and arenite of the Serra do Cristalino deposit.

Lithology	**CLASTIC IRON FOMATION**								**CHERT**	**PHILITE**			**SANDSTONE**				
Sample ID	**JA 01**	**JA 02**	**JA 05**	**JA-20**	**JA-42**	**JA-50B**	**JA-52B**	**JA-58**	**JA-52A**	**JA 09 A**	**JA 09 B**	**JA-49**	**JA 06**	**JA 07**	**JA-36**	**JA-38**	**JA-53**
SiO2(%)	43,36	30,9	42,9	33,23	49,99	3,3	10,65	48,06	94,52	91,52	84,6	61,85	96,04	98,97	91,56	38,66	95
Al2O3 (%)	1,16	2,49	1,87	1,39	1,32	1,69	1,38	2,61	0,02	0,13	0,1	0,15	1,84	0,05	0,68	20,14	2,06
Fe2O3 (%)	49,11	57,18	49,75	59,77	44,44	83,5	68,24	44,01	4,24	6,78	13,26	32,91	0,42	0,37	5,75	14,57	0,7
MgO (%)	0,05	0,06	0,06	0,03	0,03	0,09	<0.01	0,03	<0.01	0,03	0,08	0,03	0,02	<0.01	0,02	5,16	0,02
CaO (%)	0,06	0,05	0,07	0,17	0,12	0,08	0,06	0,06	0,06	0,07	0,07	0,05	0,04	<0.01	0,02	15,71	<0.01
Na2O (%)	0,04	0,02	0,02	<0.01	<0.01	<0.01	<0.01	<0.01	<0.01	<0.01	<0.01	<0.01	0,02	<0.01	<0.01	0,92	<0.01
K2O (%)	0,03	0,02	0,03	0,02	<0.01	<0.01	<0.01	0,03	0,02	0,01	0,01	<0.01	0,08	<0.01	<0.01	0,53	0,03
TiO2 (%)	0,11	0,14	0,11	0,12	0,14	0,11	0,09	0,13	<0.01	<0.01	<0.01	0,02	0,03	<0.01	0,02	2,63	0,11
P2O5 (%)	1,49	3,49	0,86	1,44	1,14	2,13	2,59	0,95	0,13	0,13	0,18	0,5	0,19	<0.01	0,18	0,17	0,03
MnO (%)	0,02	0,01	0,06	0,02	<0.01	0,03	0,01	0,02	<0.01	0,01	0,02	0,01	<0.01	<0.01	0,01	0,15	0,01
Cr2O3 (%)	0	0	0	0,01	<0.002	0,01	0	0	0	0,01	<0.002	<0.002	0,01	0,02	<0.002	0,04	0,01
LOI (%)	4,5	5,4	3,9	3,6	2,7	8,9	10,3	3,9	0,9	1,3	1,7	4,5	1,3	0,5	1,7	0,9	1,9
TOTAL(%)	99,93	99,76	99,63	99,8	99,88	99,84	93,32	99,8	99,89	99,99	100,02	100,02	99,99	99,91	99,94	99,58	99,87
U (ppm)	0,2	0,5	0,4	0,1	0,2	2	1,4	0,3	<0.1	<0.1	<0.1	<0.1	0,3	<0.1	0,1	1,7	0,3
V	49	54	62	82	45	278	72	35	10	<8	11	10	11	<8	19	218	10
Zr	30,8	38,1	30,2	37,5	43	18,7	28,5	62,3	13,7	9,5	5,8	9,4	38,2	0,3	14,6	140,5	59,4
Ag	0	0	0	<0.1	<0.1	<0.1	<0.1	<0.1	<0.1	0	0	<0.1	0	0	<0.1	<0.1	<0.1
As_	0	0	0	1,1	1,3	12	3,6	1,2	<0.5	0	0	0,8	0	0	1,6	<0.5	0,7
Au	0	0	0	<0.5	2,5	2	<0.5	<0.5	<0.5	0	0	1,4	0	0	1,2	1,9	<0.5
Bi	0	0	0	<0.1	<0.1	<0.1	<0.1	<0.1	<0.1	0	0	<0.1	0	0	<0.1	<0.1	<0.1
Cd	0	0	0	0,5	0,3	0,6	0,3	0,1	<0.1	0	0	<0.1	0	0	<0.1	<0.1	<0.1
Cu	0	0	0	10,4	7,3	92,1	18,4	11,7	1,1	0	0	5,5	0	0	6,8	0,3	1,7
Hg	0	0	0	<0.01	<0.01	0,02	0,02	0,02	<0.01	0	0	<0.01	0	0	<0.01	<0.01	<0.01
Mo	0	0	0	0,2	0,1	2,1	0,6	0,2	0,3	0	0	0,9	0	0	0,4	0,2	0,2
Ni	0	0	0	10,8	14,3	35,2	12	8,4	1	0	0	1,5	0	0	3,4	28,3	2,2
Pb	0	0	0	2,2	90,8	0,8	2,3	3,5	4,1	0	0	1	0	0	1,9	6,1	1,3
Sb	0	0	0	<0.1	<0.1	<0.1	<0.1	<0.1	<0.1	0	0	<0.1	0	0	<0.1	<0.1	<0.1
Se	0	0	0	<0.5	<0.5	0,6	<0.5	<0.5	<0.5	0	0	<0.5	0	0	<0.5	<0.5	<0.5
Tl	0	0	0	<0.1	<0.1	<0.1	<0.1	<0.1	<0.1	0	0	<0.1	0	0	0,1	<0.1	<0.1
Zn	0	0	0	23	12	67	27	14	8	0	0	8	0	0	6	35	5
Nb	3,5	4,1	2,9	4	4,5	0,6	2,2	5,6	0,9	2	4,4	0,3	1,1	<0.1	2,8	16,1	2,6
Rb	1	0,6	1,4	0,7	1,3	<0.1	0,1	1,3	<0.1	0,5	0,4	0,1	2,9	0,3	0,6	8,7	1
Sc	4	6	4	4	5	10	5	4	<1	<1	<1	2	1	<1	2	47	2
Sn	<1	<1	<1	<1	<1	<1	<1	<1	<1	<1	<1	<1	<1	<1	<1	2	<1
Sr	162,1	247,2	233,1	374,4	139,2	248,9	75,3	295,6	19	30,6	23,5	27,3	59,3	0,6	37,5	1683,5	3,2
Ta	0,3	0,3	0,3	0,3	0,3	<0.1	<0.1	0,4	0,3	0,2	<0.1	<0.1	0,2	0,1	0,3	0,8	0,4
Th	1,4	2	1,5	1,6	1,7	2,5	1,4	2,3	<0.2	<0.2	0,3	0,3	1,3	<0.2	0,3	0,6	2
Ba	225	1286	2358	658	292	337	152	1208	22	37	61	48	104	3	303	112	30
Be	<1	2	2	<1	1	13	5	3	<1	3	<1	1	1	<1	<1	3	<1
Co	13,7	10,4	5,9	20,5	18,3	25,5	13	10,6	84,4	25,5	37,6	27,9	23,1	46,3	73,3	63,1	77,4
Cs	<0.1	<0.1	<0.1	<0.1	<0.1	<0.1	<0.1	<0.1	<0.1	<0.1	<0.1	<0.1	<0.1	<0.1	<0.1	0,3	<0.1
Ga	1,8	2,3	2,1	2,6	2,7	1,4	3,7	3,3	0,6	0,7	<0.5	<0.5	1,7	<0.5	1,1	25,7	1,9
Hf	0,8	0,9	0,6	0,7	0,9	0,5	0,6	1,4	<0.1	0,3	<0.1	<0.1	0,8	<0.1	0,6	3,7	1,5
La	7,1	7,7	9,5	7,8	10,7	26,5	7,4	10,7	0,8	0,5	4,8	3	7,8	0,2	2,9	10,9	5,9
Ce	13,7	14,6	18,5	15,1	19,3	63,9	14,1	19,8	1,6	0,8	9,2	5,9	18,9	0,2	6,3	27,4	10,3
Pr	1,73	1,93	2,42	1,92	2,22	8,9	1,74	2,27	0,19	0,1	1,13	0,7	2,24	0,02	0,76	3,97	1,09
Nd	6,7	7,3	11,1	7,7	8,7	43,8	8,3	9,6	0,8	<0.3	5,4	3,3	8,9	<0.3	2,8	19,7	4,5
Sm	1,31	1,57	2,27	2,02	1,84	10,35	1,38	1,53	0,11	0,14	1,11	0,69	1,76	0,06	0,61	5,4	0,5
Eu	0,31	0,36	0,54	0,46	0,44	2,33	0,31	0,29	0,04	<0.02	0,24	0,17	0,44	<0.02	0,16	1,9	0,11
Gd	1,5	1,97	2,81	2,69	2,44	13,36	2,24	1,55	0,24	0,09	1,23	1,05	1,57	<0.05	0,63	6,97	0,57
Tb	0,28	0,39	0,53	0,41	0,43	2,09	0,41	0,23	0,04	0,02	0,19	0,17	0,22	<0.01	0,11	1,2	0,09
Dy	1,98	2,73	3,85	3,37	3,2	14,76	3,45	1,69	0,25	0,14	1,14	1,19	1,22	<0.05	0,67	7,93	0,51
Y	16,7	34,7	28,7	30,3	26,2	111	35	14,7	1,8	0,7	4,8	7,9	5,7	<0.1	4,7	44,4	2,9
Ho	0,49	0,75	0,86	0,77	0,73	3,2	0,82	0,37	0,06	<0.02	0,2	0,24	0,17	<0.02	0,13	1,61	0,11
Er	1,58	2,67	2,62	2,45	1,99	9,37	2,81	1,28	0,17	0,07	0,49	0,84	0,53	0,04	0,45	4,77	0,3
Tm	0,25	0,47	0,37	0,35	0,27	1,52	0,47	0,18	0,03	0,01	0,07	0,11	0,08	<0.01	0,08	0,71	0,04
Yb	1,51	3,48	2,56	2,29	1,53	10,94	2,98	1,16	0,17	0,13	0,41	0,76	0,41	<0.05	0,45	4,33	0,38
Lu	0,25	0,62	0,34	0,33	0,25	1,96	0,52	0,18	0,03	0,01	0,06	0,13	0,07	<0.01	0,09	0,66	0,06
Σ REEY	55,39	81,24	86,97	77,96	80,24	323,98	81,93	65,53	6,33	2,71	30,47	26,15	50,01	0,52	20,84	141,85	27,36
Co+Cu+Ni	13,7	10,4	5,9	41,7	39,9	152,8	43,4	30,7	86,5	25,5	37,6	34,9	23,1	46,3	83,5	91,7	81,3
Ce/Ce*(PAAS)	0,9	0,87	0,89	0,9	0,91	0,94	0,91	0,93	0,95								
Eu /Eu*	1,03	0,94	0,99	0,91	0,95	0,91	0,79	0,88	1,04								
Eu/Sm*	1,22	1,18	1,22	1,17	1,23	1,16	1,15	0,97	1,87								
Pr/Pr*	1,06	1,1	0,98	1,04	1,01	0,96	0,93	0,97	0,98								
Sm/Yb*	0,44	0,23	0,45	0,45	0,61	0,48	0,24	0,67	0,33								
La/Sm*	0,79	0,71	0,61	0,56	0,84	0,37	0,78	1,02	1,06								

La/Yb*	0,51	0,4	0,36	0,39	0,5	0,26	0,37	0,94	0,41		
Y/Ho*	1,25	1,7	1,22	1,44	1,32	1,27	1,57	1,46	1,1		
Y/Ho	34,08	46,27	33,37	39,35	35,89	34,69	42,68	39,73	30		

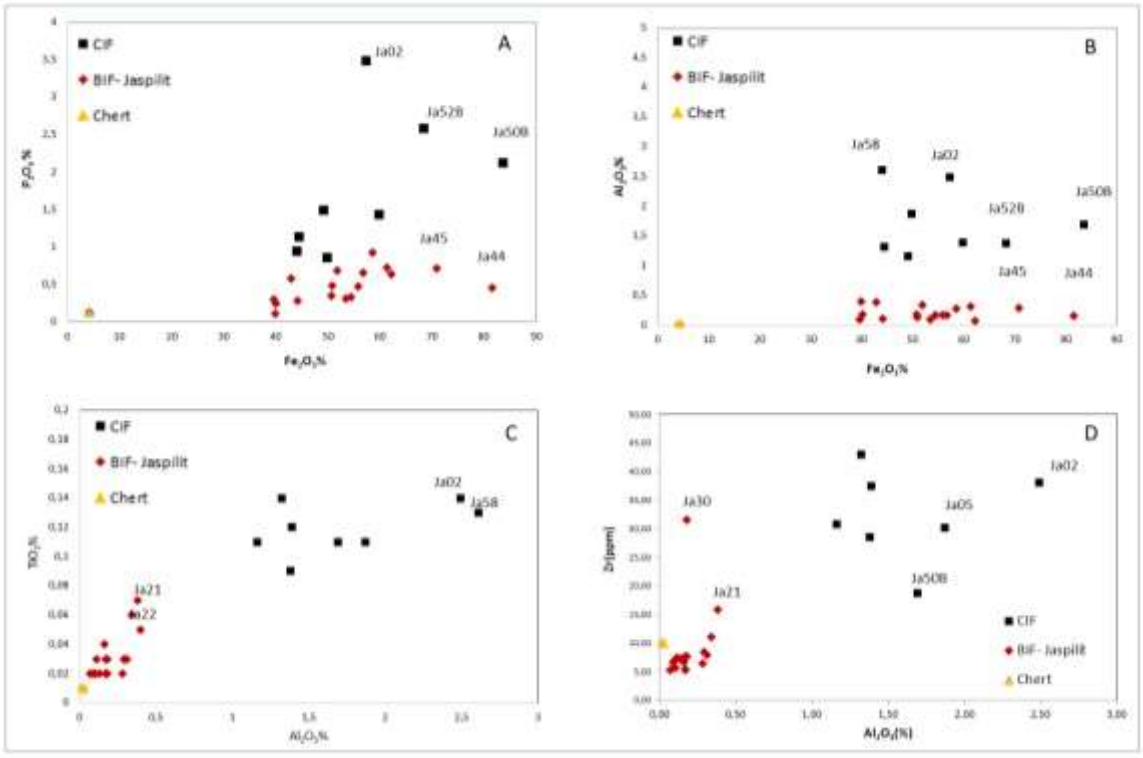

Figure 10. Binary diagram for BIF-jaspilitic, Clastic Iron Formations (CIF) and Pure Chert of the Serra do Cristalino. (A) Bivalent diagram P_2O_5 versus Fe_2O_3; (B) Bivalent diagram Al_2O_3 versus Fe_2O_3, (C) Bivalent TiO_2 versus Al_2O_3 diagram (D) Bivalent diagram Zr versus Al_2O_3 ;. The graphs show that there are well-defined groups, almost pure chert, essentially siliceous, with no detritic contaminants, with values Al_2O_3, P_2O_5 and MgO very close to zero, jaspilitic BIF and CIFs, clastic rocks are a little more enriched in Al_2O_3, P_2O_5 and TiO_2 in relation to the BIFs, clearly showing the contribution of detritus to the CIFs.

Trace elements in the CIF facies show a strong enrichment when compared to the BIF facies rocks and present high levels of Ba, Nd, Zr, V, Zn, and Cu. Sometimes the enrichment are more than 10 times the average (Figure 11 A to D). The CIF also have high P_2O_5 content. The rocks present low levels of metal components (Cu, Mo, V, Cr, Co, and Zn). Chert shows mostly very pure geochemistry, similar to BIFs, without significant compositional variations in terms of trace elements.

The geochemical relationships plotted in the binary diagrams (Figure 11A - D) show that CIF rocks has enrichment in Al_2O_3 ,TiO_2, and Zr related to BIFs and indicate a major detrital contribution in their source. Also the increase of P_2O_5 are related to a glaciogenic influence or volcanogenic processes involved in the deposition of Iron formations from Serra do Cristalino. Our results suggest a a higher contribution of

debris flows to the CIF compared to BIF and pure cherts, but also show that chemical input of volcanic material was the main source to the formation of these rocks, not the continental clastic source.

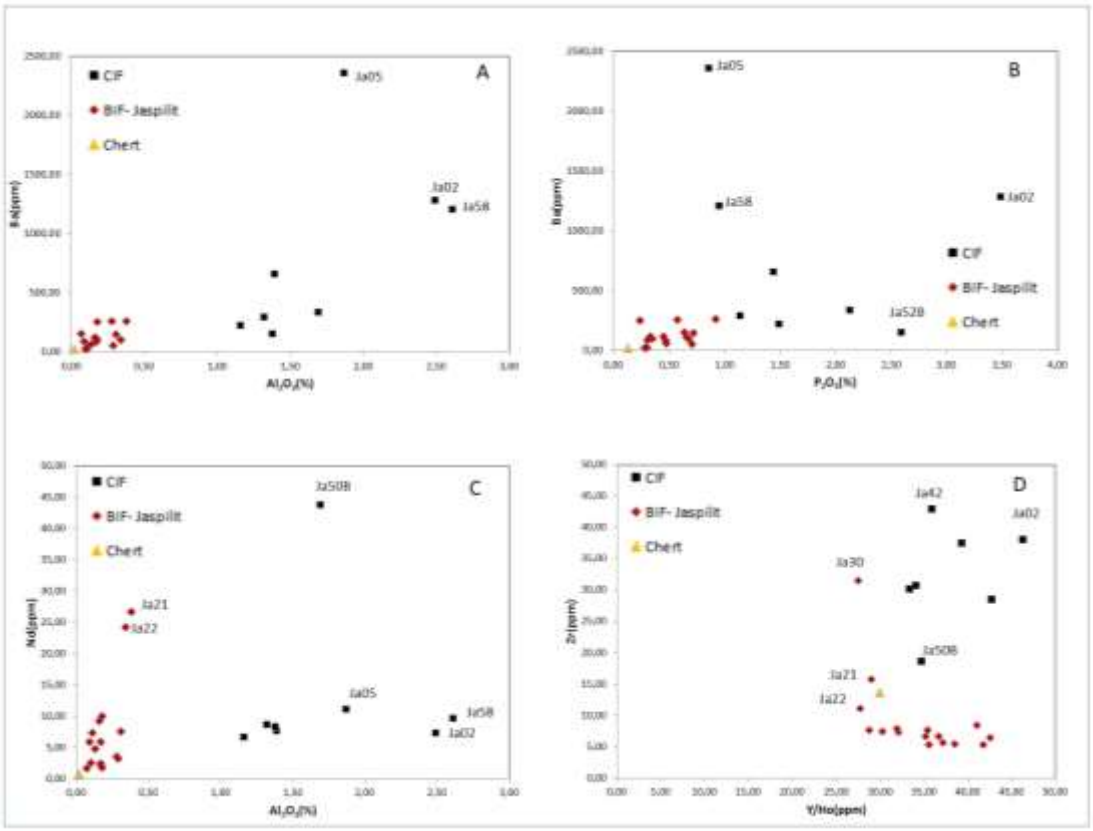

Figure 11. Binary diagrams for BIFs, chert and CIFs samples of Serra do Cristalino, A- Binary diagram Ba (ppm) versus Al_2O_3 (%); B Binary diagram Ba (ppm) versus P_2O_5; C- Bivariate diagram Nd (ppm) versus Al_2O_3 (%); D- Bivariate diagram Zr (ppm) versus Y/Ho(ppm).

Normalized to the post-archaean Australian shale signatures (Figures 12A and 12B-b), BIF and CIF show a depletion in LREE over HREE (BIF A / Yb = 0.2, n = 19, 1 σ = 0,1) and (CIF - mean La / Yb = 0,3, n = 7, 1 σ = 0,2), and a no positive Eu anomaly (BIFs - Eu / Eu * = 0,8 – 1,17ppm, mean = 0,9ppm, n = 19, 1 σ = 0,05) and (CIF Eu / Eu * = 0,8-1 ppm = 0.9 ppm, n = 7, 1 = 0,05). REE shows the sum REEY * (3 ppm - 23 ppm, n = 19, 1 σ = 4) for the BIFs and REEY * Clastic iron formations (5 ppm - 39 ppm, n = 7,1 σ = 8). REE show sum REEY * (3 ppm - 23 ppm, n = 19, 1 σ = 4) for the BIFs and for the REEY * Iron Formations (5 ppm - 39 ppm, n = 7,1 σ = 8).

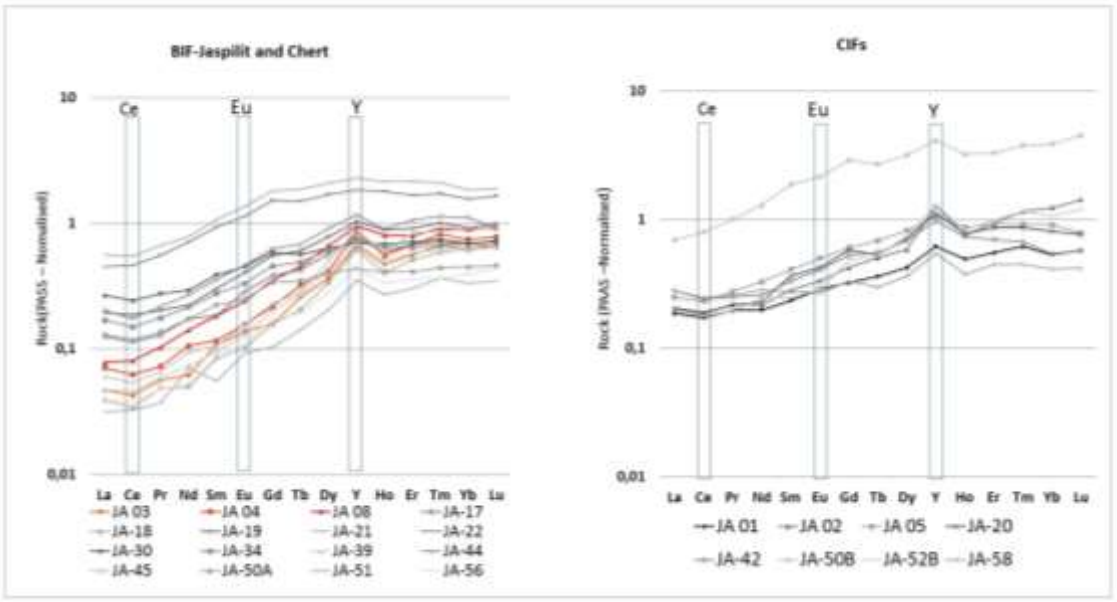

Figure 12. REEY signatures of the BIFs and Clastic Iron Formations present an enrichment in heavy rare earth elements (HREE), in relation to the light ones (LREE), Eu with absent anomalies and a anomaly in Y. They also show that the two groups of rocks are subdivided and two, specifically, that can be explained by a variation in the chemical composition of these rocks generally more enriched in metals. The samples (JA 21, JA22 (Group1) and JA50B (group 2) that are more enriched in REEY , JA 21, JA22 (Group1) coincide with the samples that present asymmetric pelitic sediments, , and for JA50B (Group 2) coincide with the samples that present higher iron contents.

Most of the BIF samples not have negative Ce anomaly (BIFs-Ce/Ce*=0,8 - 1ppm, mean = 0,9 ppm, n = 19, 1 σ = 0,02) and for the CIFs - Ce/Ce*=0,8 – 0,9 ppm, mean =0,9 ppm, n=7, 1 σ = 0,01), and some have similar positive anomalies in La (Fig. 13; Bau and Dulski, 1996). The CIFs have similar positive anomalies in La (Fig. 12B). , the BIFs have a strong PAAS-normalized positive anomaly Y (Y/Ho = 1,2 -1,6ppm, mean = 1,3ppm, n = 19; 1σ = 0,1), and the CIFs show a Y anomaly similar to the BIFs (Y/Ho = 1,2 -1,7ppm, mean = 1,4ppm, n = 7, 1 σ = 0,1).

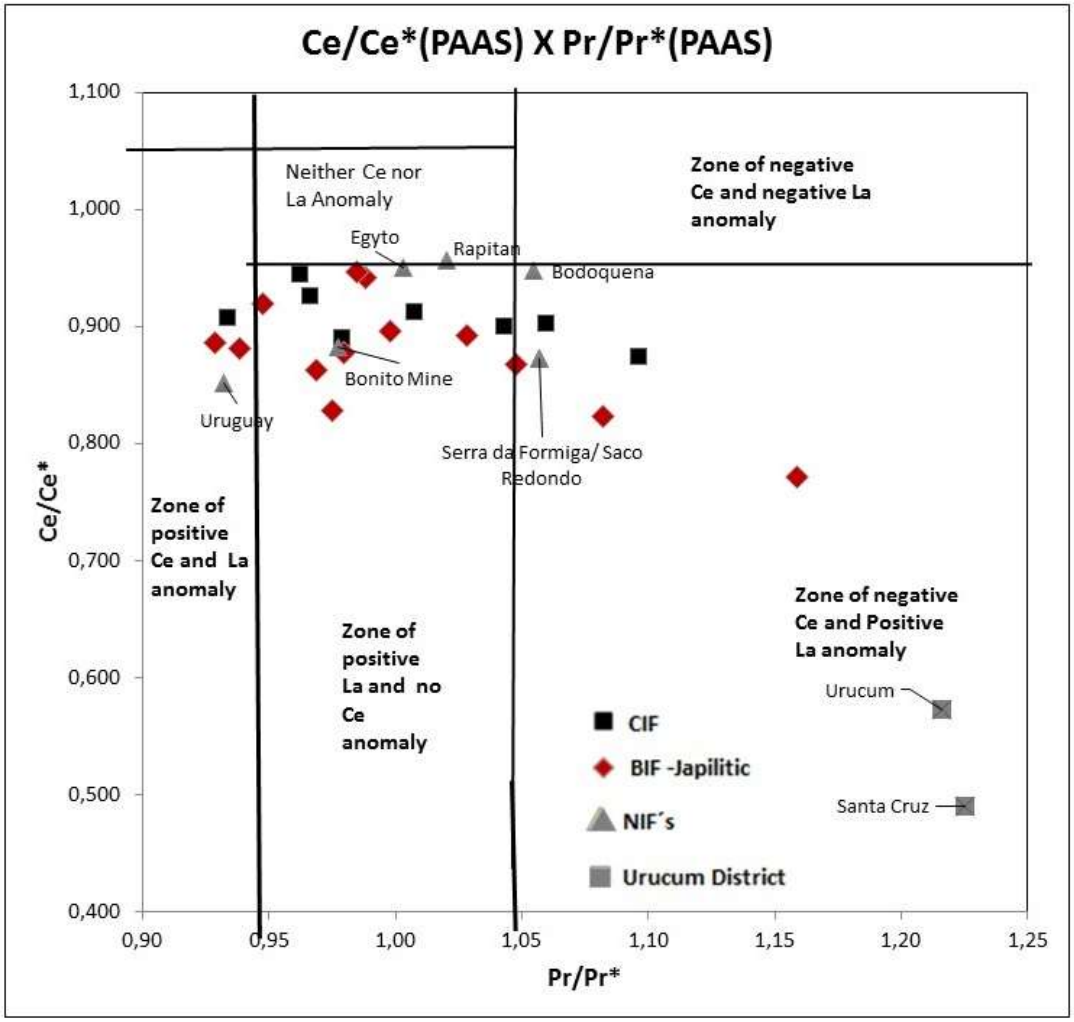

Figure 13. A: Data were plotted on binary diagram Ce/Ce* versus Pr/Pr* normalized by the PAAS, Bau and Dulski, 1996,showing the behavior for the jaspilitic and clastic IF facies, compared for NIF samples, Santa Cruz (Angerer et al., 2016), Urucum (Viehmann et al., 2016), Egypt (Piacentini et al.2013), Uruguay (Pecoits 2010), Bonito Jucurutu and Serra da Formiga / Morro Redondo Mine (Sial et al., 2010) and Serra of the Crystals showing the behavior of NIFs, where it is observed that, most of the samples present a positive anomaly in Lanthanum and absence of anomaly in cerium, some of the samples in the field of true negative anomalies in Ce / Ce *, where we also observe the NIFs of Urucum districts are much more negative in Ce than the other NIFs in the world, and others in the field of positive anomalies in La and Ce.

BIFs have similar geochemical data compared to the chert and the geochemistry data from of the CIFs is much more enriched in comparison to the BIFs, and their elevated contents of Zr, Al, Ba, P, Nd, Ti, Y/Ho, Fe may be the result of a larger detrital input.

6. U/Pb AND Nd ISOTOPES

The different samples collected from sedimentary rocks of the Serra do Cristalino sequence to provenance U-Pb zircon geochronologic studies. The ages help us to determine the origin of the sediments that filled the basin, the sources of the detrital zircon grains, allowing to suggest the limits of deposition of BIFs and other rocks of the Serra do Cristalino sedimentary sequence in the northern portion of the Paraguayan belt.

Sample JA01 corresponds to a clastic facies (CIF) of the Serra do Cristalino sequence. We found only 35 zircon grains, which are small, translucent and almost colourless and brown, sub-rounded, sometimes preserving their prismatic habit, and some broken grains (angular grains) are microscopically zoned. The analyzes were performed as close as possible to the nucleus. Analytical data with dated zircon isotope ratios are available in Annex 01.

The detrital zircon of the CIF sample shows grains that the main sources show ages of provenance, varying between 1800 and 2200 Ma, and subordinately an Archaean source at 2758 Ma (Figure 14A). In addition, Mesoproterozoic sources are present. We interpret because sediment sources are derived from the Amazonian Cratonic area. The youngest analysed zircon give 721 Ma age, considered the maximum depositional age of this facies in the Serra do Cristalino sequence.

The sandstone samples presented a large number of zircons and were analyzed for a total of 94 zircon grains for the JA 06 sample and 64 zircon grains for the JA 53 sandstone sample. It had small crystals, most of which are colourless and some of the brown colour are both translucent, rounded, sub-rounded, preserve their prismatic habit and some broken grains. The analytical data with the isotopic ratios of the dated zircons are available in Appendices 02 and 03. The JA53 sample, collect within in the Serra do Cristalino, displays a large variety of its zircon populations, with peaks of 900 Ma,

1200, 1500, 1770 a 2180 Ma, and the earliest provenance has about 2560 to 2750 Ma (Figure 14B and C).

The sample of sandstones (JA06), has a main zircon population with a peak around 918 Ma, a Mesoproterozoic source, however, the youngest zircon was dated at 696 Ma (Figure 14B), which we interpret as the maximum depositional age in the basin. Old provenance Paleo and Mesoproterozoic sources are also present in this rock.

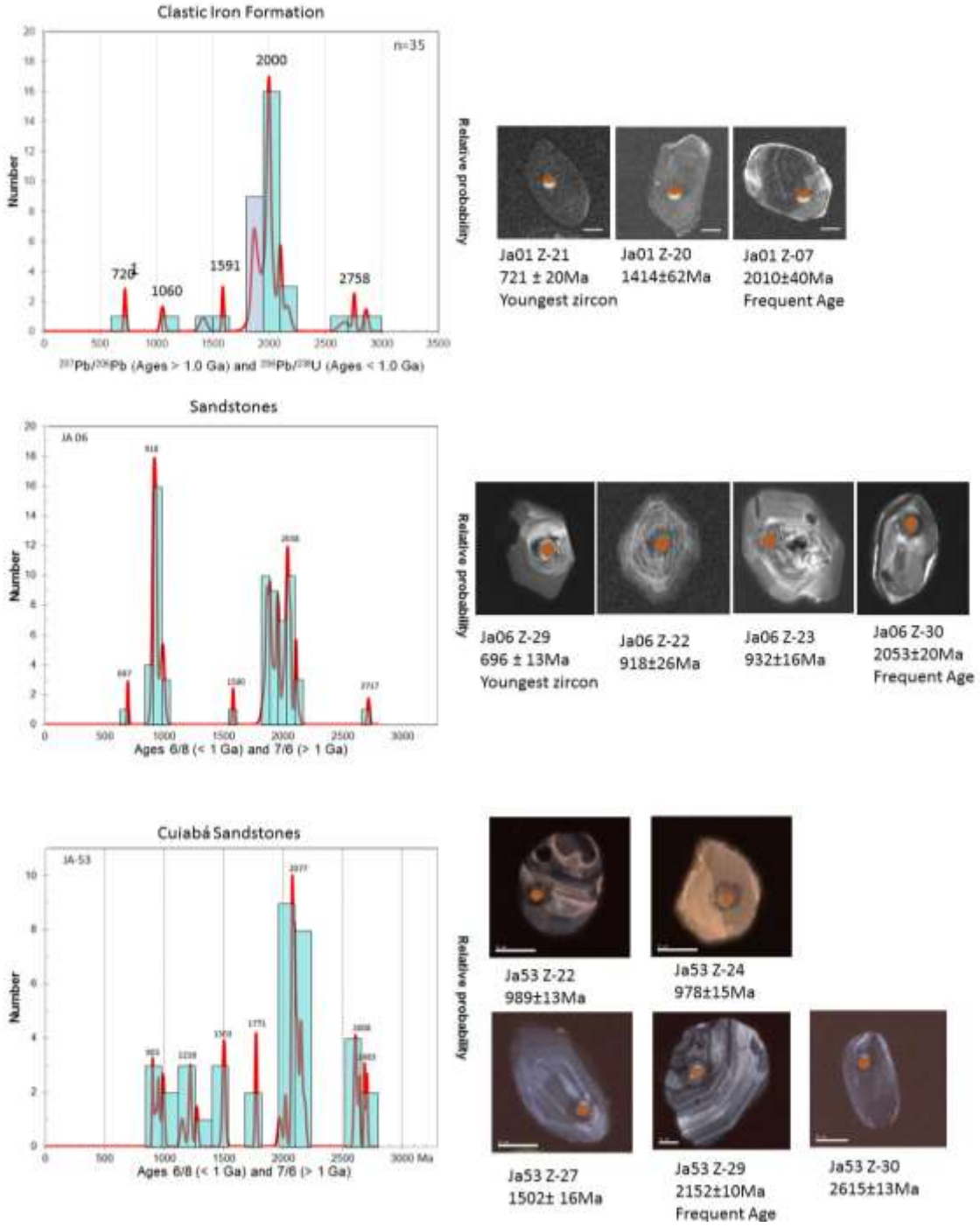

Figure 14. The histogran shows the populations of zircons over geological time CIFs, the curve shows the populations of zircons over geological time. The Graph A (JA01) shows two major populations, one around 1800Ma and another around 2200Ma, and zirconia of 721, 1440 and 2900Ma. The histogran shows the populations of zircons over geological time for arenite composition rocks; The graph B (JA06) shows two major populations, one around 890 to 950Ma and another around 1820 to 2020Ma; C The histogran of the (JA53) shows ages ranging from 900 to 2750Ma with most representative group of zircon showing ages from close 2000 Ma.

Nd Isotopes

Were carried a systematic isotopic studies over all stratigraphic units of the Serra do Cristalino sequence. Several samples of sedimentary rocks was analyze on the different position level on the stratigraphic, from the base to the top. Thus we include the I) Japilitic BIFs ; II) Clastic Iron Formations ; III) siliciclastic rocks: Shales and siltstone (3 samples) and subarkoses and sandstone (5 Samples). The time of depositional sequence around 700 Ma was chose to use in the End (t) value, based on the U/Pb data indicating that our young ages of detrital zircons of provenance up to 721 Ma, and the fact that the sequence is inserted in a geotectonic context of the Neoproterozoic age passive margin of the Paraguay Belt (Figure15).

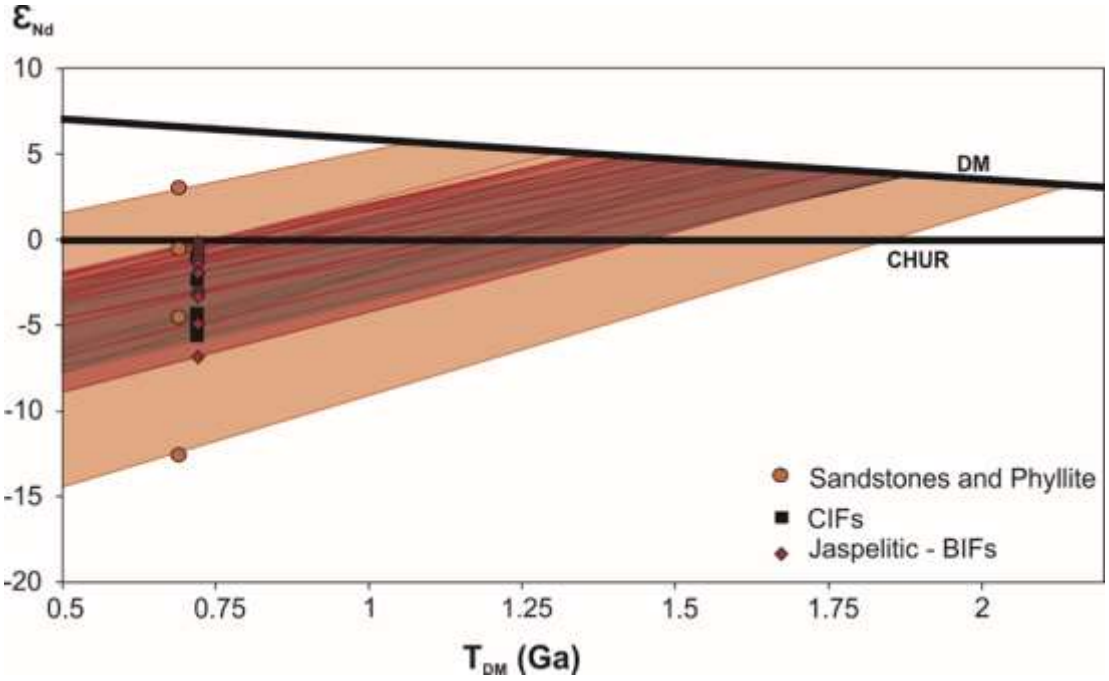

Figure 15. T_{DM} model ages plotted through the view of the stratigraphic column with several peaks of old T_{DM} model ages (about 2.2-1.03 Ga) and E_{Nd} (T) calculated at 700 Ma exhibit values of -0,9 to -13,7 for the rocks of the Metassedimentary Sequence of the CS.

The BIFs present T_{DM} Model ages ranging from 1,35 to 1,5 Ga and present slightly negative E_{Nd} (t) to close to zero, ranging from -1,6 to -0,4 in average. Some samples has a probable continental detrital component and the source has more negative E_{Nd} (t) values at -3 and T_{DM} at 1.7 Ga.

The CIF exhibit narrow and homogeneous range of T_{DM} Model ages and negative E_{Nd} (t) values between 1,6 to 1,87 Ga and -4,4 to -5,4, respectively.

Table 3. Sm and Nd Isotope Data of Serra do Cristalino deposit.

Sample	Litology	Sm(ppm)	Nd(ppm)	$^{147}Sm/^{144}Nd$	$^{143}Nd/^{144}Nd$ (ε 2SE)	ε Nd (0)	ε Nd (700Ma)	T_{DM} (Ga)
JA- 01	CIF	1,447	7,3	0,1261	0,512078+/-15	-10,93	-4,62	1.67
JA-02	CIF	1,571	7,726	0,1229	0,512074+/-9	-11	-4,41	1.61
JA-20	CIF	1,776	7,81	0,1374	0,512069+/-11	-11,11	-5,8	1.93
JA-42	CIF	1,802	8,803	0,1237	0,512050+/-6	-11,47	-4,95	1.67
JA-50B	CIF	9,217	38,171	0,146	0,512277+/-12	-7,04	-2,52	1.7
JA-52B	CIF	1,457	6,653	0,1324	0,512287+/-53	-6,84	-1,11	1.4
JA-58	CIF	1,423	8,107	0,1061	0,511946+/-11	-13,49	-5,41	1.54
JA 03	JASPILITC/BIF	0,57	2,375	0,1451	0,512295+/-3	-6,68	-2,08	1.64
JA 04	JASPILITC/BIF	0,687	3,105	0,1338	0,512085+/-13	-10,78	-5,17	1.81
JA 08	JASPILITC/BIF	1,015	4,342	0,1413	0,512316+/-5	-6,27	-1,33	1.51
JA-17	JASPILITC/BIF	1,173	5,379	0,1318	0,512257+/-8	-7,43	-1,64	1.45
JA-18	JASPILITC/BIF	0,526	2,207	0,1442	0,512313+/-7	-6,35	-1,65	1.58
JA-19	JASPILITC/BIF	1,688	7,631	0,1337	0,512330+/-18	-6	-0,38	1.34
JA-21	JASPILITC/BIF	5,919	27,53	0,13	0,512260+/-7	-7,37	-1,42	1.41
JA-22	JASPILITC/BIF	5,276	22,83	0,1397	0,512308+/-5	-6,44	-1,35	1.5
JA-30	JASPILITC/BIF	2,246	10,589	0,1282	0,512282+/-3	-6,94	-0,83	1.34
JA-34	JASPILITC/BIF	1,464	6,832	0,1295	0,512283+/-12	-6,92	-0,92	1.36
JA-39	JASPILITC/BIF	0,547	2,351	0,1405	0,512349+/-19	-5,64	-0,62	1.43
JA-44	JASPILITC/BIF	1,884	8,584	0,1327	0,5123203+/-8	-6,53	-0,48	1.38
JA-45	JASPILITC/BIF	0,572	2,432	0,142	0,512222+/-14	-8,12	-3,23	1.73
JA-50A	JASPILITC/BIF	1,185	5,254	0,1363	0,512254+/-27	-7,49	-2,1	1.54
JA-51	JASPILITC/BIF	0,3	1,346	0,1346	0,512181+/-6	-8,91	-3,37	1.64
JA-56	JASPILITC/BIF	0,427	1,934	0,1477	0,512244+/-9	-7,69	-3,31	1.83
JA 05	JASPILITC/BIF	2,146	10,187	0,1274	0,511960+/-22	-13,22	-7,04	1.9
JA-52A	CHERT	0,181	0,836	0,131	0,512249+/-10	-7,59	-1,72	1.45
JA-09A	PHYLLITE	0,105	0,472	0,1347	0,512122+/-13	-10,06	-4,53	1.76
JA-09B	PHYLLITE	1,099	5,246	0,1266	0,512296+/-17	-6,66	-0,41	1.3
JA-49	PHYLLITE	0,778	3,412	0,1378	0512221+/-3	-8,13	-2,88	1.63
JA-06	SANDSTONE	1,912	9,773	0,1182	0,511645+/-11	-19,37	-12,36	2.2
JA-07	SANDSTONE	0,013	0,059	0,1353	0,512513+/-10	-2,44	3,04	1.03
JA-53	SANDSTONE	0,6	3,662	0,099	0,511530+/-5	-21,61	-12,89	2
JA-36	SANDSTONE	0,716	3,458	0,1252	0,512144+/-10	-9,65	-3,25	1.54

The clastic rocks of the sedimentary Serra do Cristalino sequence shows a larger ages variation in the E_{Nd} members, with T_{DM} model since paleoproterozoic to

Mesoproterozoic sources (varying from 2.14 to 1.5 Ga), witch E_{Nd} (t) values raging between -12.34 to - 3.43. The sample JA07 present the youngest T_{DM} model ages at 1.0 Ga (Figure 16).

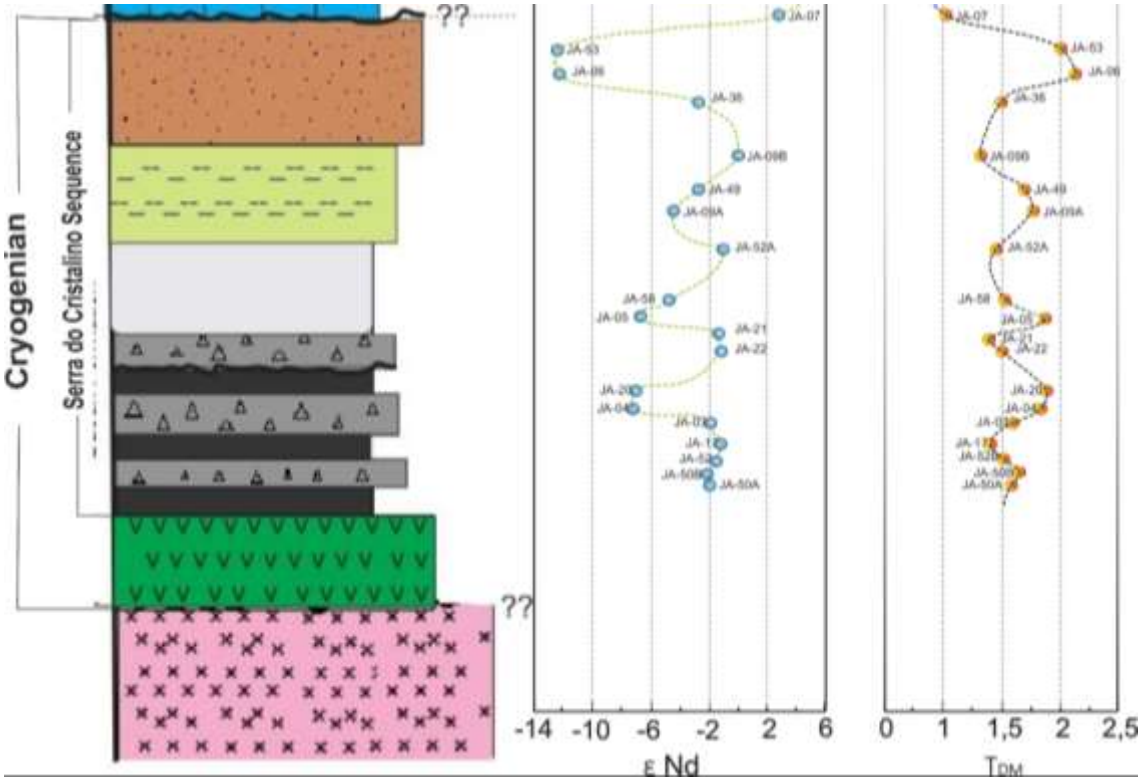

Figure 16. The T_{DM} model ages plotted through the view of the stratigraphic column with several peaks of old T_{DM} model ages (about 2.2-1.03 Ga) and E_{Nd} (T) calculated at 700 Ma exhibit values of -0,9 to -13,7 for the rocks of the Serra do Cristalino Metassedimentary Sequence.

7. DISCUSSION

Geological, geochronological and geochemical data of rocks from the Serra do Cristalino deposit shows that the BIFs and CIF formations have a Neoproterozoic age, during the Cryogenian period of Earth evolution. Thus, we will discuss the common characteristics of our BIFs data in the Paraguay belt with other evidence of the NOE – Sturtian event around the world. Here we will make a comparison with the existing data in the literature and show the similarities and differences between them for seeking to elucidate their environment of deposition and genetic evolution for the Sequence of the Serra do Critalino occurrence.

7.1 Iron Sources (detrital contribution)

Our results show that the CIFs are slightly more enriched in Fe_2O_3, Al_2O_3, CaO, TiO_2 and P_2O_5 in relation to the jaspilitic BIFs (Figure 10 A-D). This suggests that are a

major detrital contribution in the CIFs unit, or these rocks were subject to a more effective reworking process, mixing rocks that already were deposited in the basin, due increase in the energy during transport of sediments, forming the conglomerate facies of CIFs. Positive correlations of Al, Ti, K and Na suggest that probably material contributed by detrital origin, or mixtures of sources (Cox et al., 2013). When the Zr, Hf, Ti and Al contents are relatively high, they suggest that iron formations contribute to continental sediments, since they are elements more common in felsic rock. Also, the enrichment in phosphorus (P_2O_5), suggest the high content of P dissolved in seawater, generally represents a contribution or glacial influence in the genesis of the CIFs. (Figure 10).

The data from the Serra do Cristalino BIFs (Figure 17) show an 80% sedimentation environment suggesting hydrothermal contribution, and that they represent almost pure chemical precipitates, with low detrital component (low Ti and Al). Evidence of hydrothermal sources can be observed in the binary diagrams Fe/Ti versus Al/(Al+Fe+Mn) (Figure 17) and Al_2O_3 x Zr (Figure 10D). When we compared our results with other Neoproterozoi BIFs as Urucum (Viehmann et al., 2016), Santa Cruz (Angerer et al., 2016) and Egypt (Khalil al., 2015), they shows similar hydrothermal chemical sedimentation as the main source of iron.

Similar conclusion is given by analyze of trace elements, where the CIFs have Ba, Zr and Cu contends more enriched than BIFs, and shows relatively high Zr, Hf, Ti and Al contents that its. This relationship suggest that the CIFs have a contribution from continental sediments. Commonly, the most pure BIFs derived from hydrothermal fluids Zr and Hf occur at low concentrations (<8 ppm), without major continental contamination (Wang et al., 2016), without and/or less detrital contribution than the CIFs.

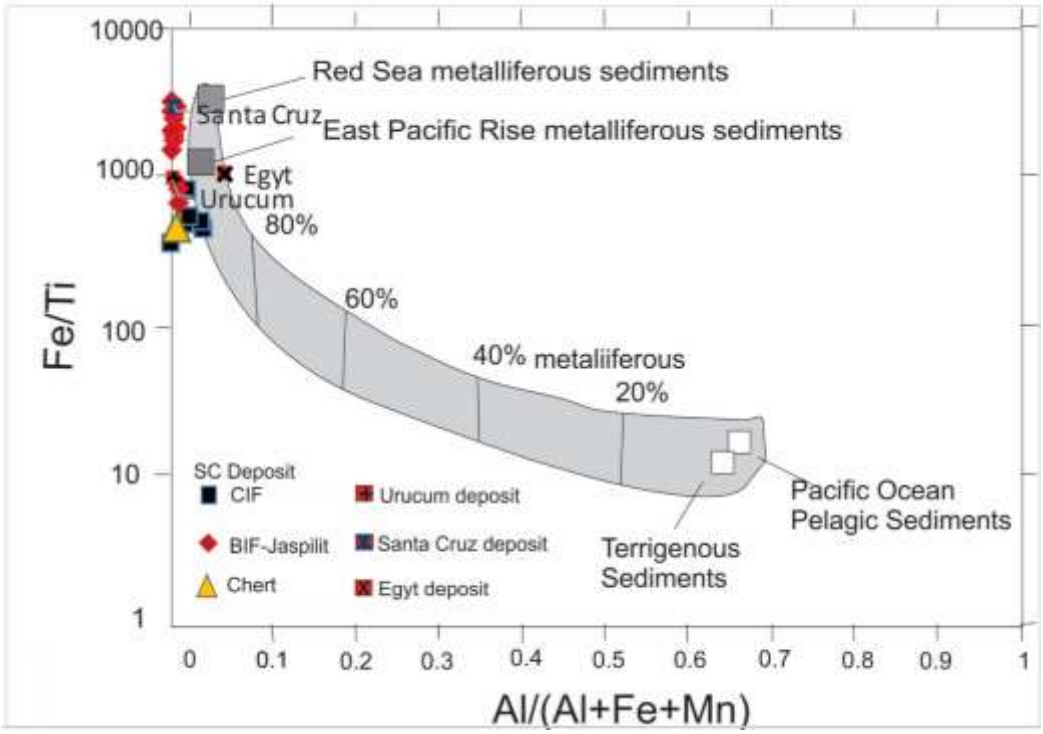

Figure 17. Samples fell in the field where the environment 80% hydrothermal sediments when compared to the graphs of Bostrom 1973 and Peter et al., 2003. (of the Urucum (Viehmann et al., 2016), Santa Cruz (Angerer et al., 2016) and Egyto (Khalil et al., 2015).

7.2 Fluid temperature, ocean condictions and distance from the source

The BIFs and CIFs of the Serra do Cristalino (CS), have a small or absent anomaly in Eu (Table 01 and 02; Figure 12 A and B.) and Eu/Eu * <1 ratios and a positive anomaly in Y. In this sense, the presence or absence of Eu anomaly is especially sensitive to hydrothermal vents because Eu is abundant in hydrothermal fluids as a function of solution temperature (Danielson et al., 1992). The chemical behaviour of rocks in the Serra do Cristalino is similar to the signature of all worldwide Neoproterozoic Iron Formations (NIF), indicating that they do not represent proximal hydrothermal sources. Thus, we suggest that they were generated by relatively cold hydrothermal solutions diluted in seawater, at some distance from the original source and possibly with some contribution of a continental component, already evidenced by the Al_2O_3 ratios. The iron formation of the Serra do Cristalino samples had influences from mixed sources.

The high Y/Ho indexes in the Serra do Cristalino samples, as ratios between 34 to 47 for CIF and 27 to 43 for BIF, and around 30 in cherts. When comparing the

typical Y/Ho ratios of seawater (60 - 90), and the ratios presented for continental waters (26 - 27) (Planavsky et al., 2010), our data suggest that we can consider the BIFs and cherts from Serra do Cristalino as pure chemical sediments, and they could represent the seawater Neoproterozoic environmental conditions (Figure 18 A and D).

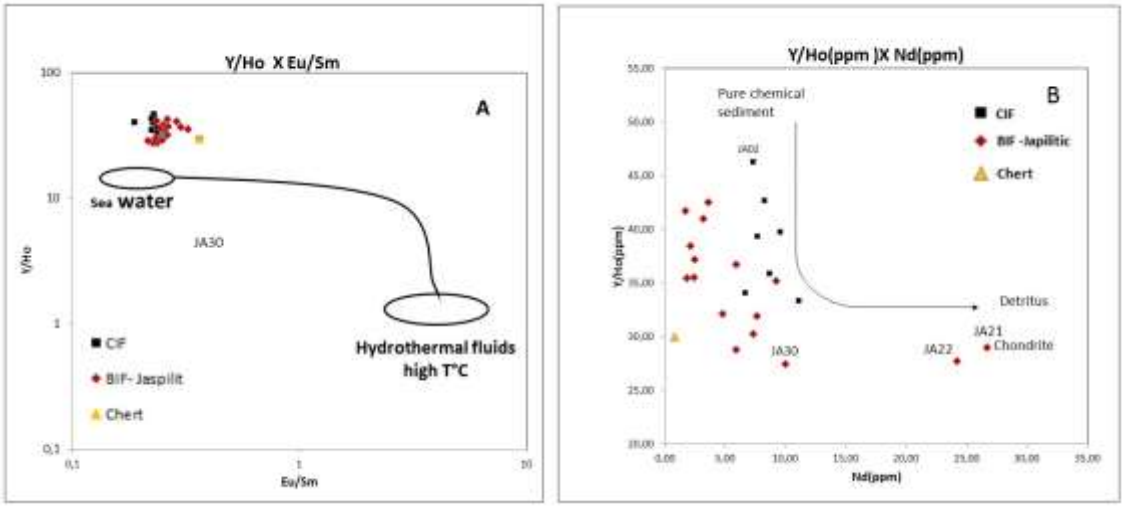

Figure 18. A: Data were plotted on binary diagrams of Y/Ho x Eu/Sm (Bau and Dulski 1999), to characterize temperature of hydrothermal fluids, where the reasons approximate to those presented for seawater with some hydrothermal component of cold fluid evidenced by the low ratio Eu/Sm <1; B: a majority of the samples are plotted of the pure chemical sediments field, with the exception of the samples JA 21 and JA22, where in laminas they present texture of Phylite rich in iron. The samples are plotted of with the exception of the samples JA 21, JA22 and JA50B, where in laminas they present texture of Phylite rich in Zr, clastic contribuition.

The Ce and Pr behavior presented a ratio (Ce / Ce *, Pr / Pr *) with mean values <1 (Figure 13) and a true negative Ce* anomalies, indicating that BIF formations occurred in association with (surface) waters sufficiently to oxidize the Ce, similar to the oxy and suboxic water masses of the concentrations of the modern oceans.

The behaviour of Ce anomalies in the Serra do Cristalino rocks shows that the negative anomalies in Ce are not very pronounced, and reflect deeper and distal waters. Ce negative anomalies are more pronounce in shallower waters, where environments are generally more oxidizing with more abundance of cerium coming from the continent. When we compare the Serra do Cristalino sequence with other deposit in the Paraguay belt, as Urucum (Viehmann et al., 2016) and Santa Cruz (Angerer et al., 2016), it's clear that Serra do Cristalino has a different origin. Their genesis reflects more anoxic, deep and distal environments in relation to their other Iron Formations deposited in the south of the Paraguay Belt (Figure 19 e Figure13). The petrographic and geochemical

characteristics reflect the deeper, less oxygenated and more distal environment conditions of the Serra do Cristalino occurrence. It is also observed that they present patterns similar to those of other deposits of NIFs, such as Rapitan (Halverson et al., 2011), Bodoquena (Piecetini et al., 2013), Egito (Khalil et al., 2015), Bonito mine and Jucurutu (Sial et al., 2015).

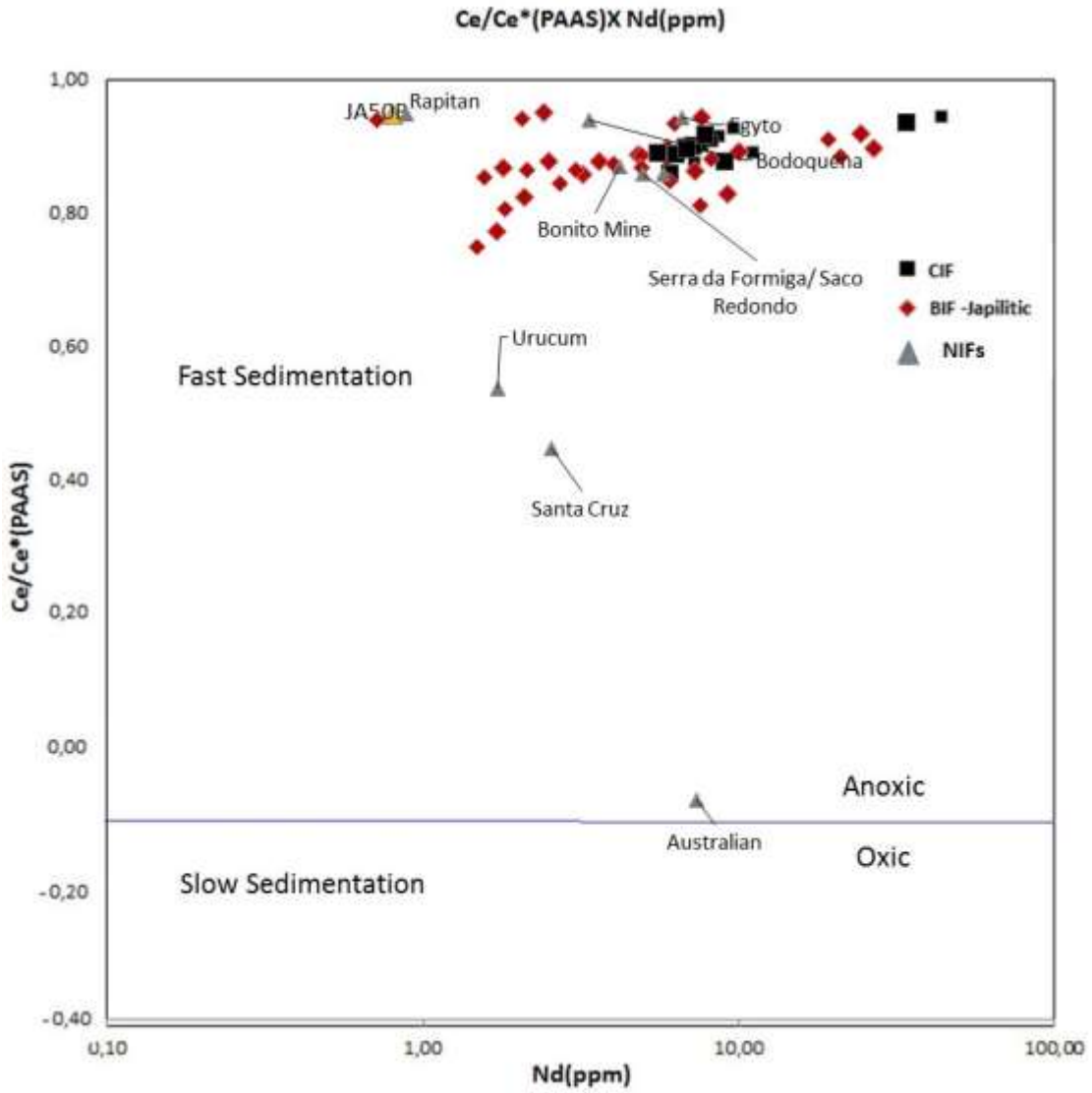

Figure 19. All of the samples are plotted of the fast sedimentation field, in anoxic environment.

The CIF is conglomerates of a very fine matrix with millimetre clasts and represents the most distal facies of the diamictites of the Paraguay basin. The REEY geochemistry shows that the true negative Ce / Ce * (PAAS) anomalies (Figures 13 and 19) are much less negative than the Urucum and Santa Cruz deposits (Viehmann et al., 2016 and Angrerer et al., 2016).

The occurrence of barite clasts in the CIF, suggests that at some time before the deposition of the Iron formations, the deposition of sulfates was exposed and contributed to the filling of the basin and could be related to the opening phase of the basin or to the pre- Neoproterozoic basement. The occurrence of barite suggests that sulfate fill up the basin before the pre-deposition of the iron formations, and represent more oxygenated marine environments, in shallower waters, similar to modern seawater conditions. All evidence suggests that the hydrothermal fluids that generate the Iron Formations in the Serra do Crisytalino sequence are cold, related to white fumaroles in reduced atmospheric conditions (Husten et al., 2004).

The REEY data of Serra do Cristalino (normalized by PAAS) show similar REEY patterns for the BIF and CIF facies. The metallic fluids that gave rise to the IFs were well diluted and of low temperatures, expressed by the absence of a significant anomaly in the Eu / Eu * <0,8 ratios. The positive anomalies in Y suggest contribution of Iron sources from continental margin, being a likely mixture with distal hydrothermal fluids, similar to low white smoker, with <200 ° C estimate temperatures, very close to modern composition conditions and ocean temperatures (Michard et al., 1993; Basta et al., 2011).

The contribution of clastic sediments was not able to completely modify the REEY pattern in the CIF and BIF from Serra do Cristalino, and thus, they are similar to the iron formations described in the literature and represent the Neoproterozoic seawater worldwide. Despite the clastic contribution, the chemical sedimentation is predominantly in the formation of CIFs, being slightly more enriched in REEY than the BIFs. The clastic contribution is related to glacial influences (enrichment in P), which increased the energy of the environment, bringing some clasts and reworking the rocks of the basin itself, adding the ferruginous mud that was being deposited in the basin. Thus, the clastic iron formations of the Serra do Cristalino also represent the composition of the water of the Neoproterozoic Sea.

The enrichment in HREE of and positive anomalies Y in BIF Neoproterozoic are signs inherited from the sea surface water (Bau and Dulski, 1996e). The REEY Geochemical behavior presented to the deposit of Serra do Cristalino iron formations are similar to the Urucum Pure BIFs, described by Viehmann et al., 2016, has as sources of continental material proximal the basin, with no evidence of any entry of high-temperature hydrothermal fluids into the REEYs The presence of spherulites, is an

evidence bacterial activity during the basin deposition. Pseudomorphic carbonate crystals, substituted by hematite, are also observed in this unit, suggesting a slightly more oxygenated environment in relation to BIF, allowing carbonate precipitation and bacterial activity.

The BIFs expression to seawater covered by ice and the CIFs represents the composition of seawater after melting (high P contents), which generates resurgence currents and clasts, also provides chemical components for seawater, to slightly more enriched BIFs

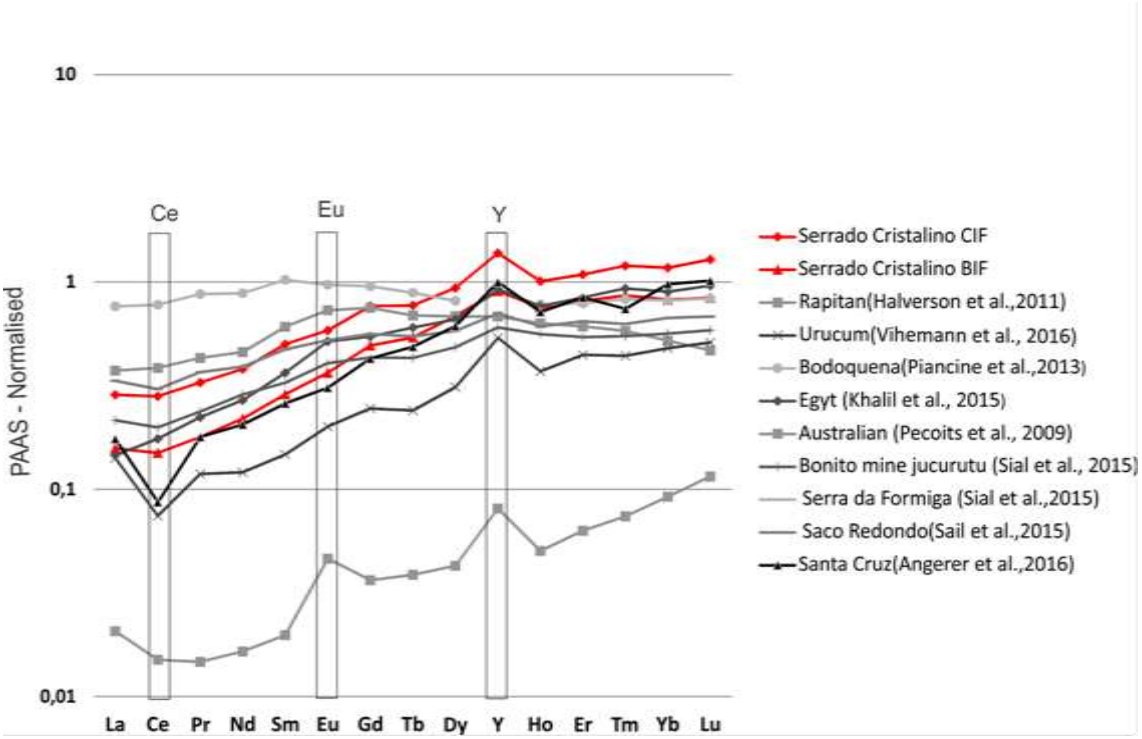

Figure 20. The geomorphic patterns of the PAAS normalized REEY (Mclennan et al., 1989) for the Serra do Cristalino Clastic Iron Formations in relation to the IF deposits of Neoproterozoic ages of the world. When we compare the Serra do Cristalino sequence with other deposit in the Paraguay belt, as Urucum (Viehmann et al., 2016) and Santa Cruz (Angerer et al., 2016), its clear that Serra do Cristalino has different origin. Their genesis reflect more anoxic, deep and distal environments in relation to their other Iron Formations deposited in the south of the Paraguay Belt. The petrographic and geochemical characteristics reflect the deeper, less oxygenated and more distal environment conditions of the Serra do Cristalino occurrence. It is also observed that they present patterns similar to those of other deposits of NIFs, such as Rapitan (Halverson et al., 2011), Bodoquena (Piecetini et al., 2013), Egito (Khalil et al., 2015), Bonito mine and Jucurutu (Sial et al., 2015).

Another point to discuss, is the presence of some pseudomorphic carbonate crystals in the Serra do Cristalino (Figure 6 -D and 8-D), and they are replaced by

hematite, which suggests that the environment of iron formation is not plataformal, but deeper, with low conditions of carbonate formation (Figura 13, 19 e 20).

7.3 Provenance, Stratigraphy and Depositional Evolution

The Banded Iron Formations of the Serra do Cristalino were deposited in a marine basin of passive margin at the edge of the Amazon craton, stratified-redox ocean, deeply, influenced by glaciogenic cycles of Sturtian age (<750 - 660Ma). Serra do Cristalino sequence make not part of Cuiabá Group, its older, and has the same stratigraphy of Noxa Xavantina sequence, 100 Km southward, and we suggest that both were deposited in the same basin, during the extensional phase related to the begging of passive margin formation of the Amazon Craton during the Rodinia break-up. Dantas et al. (2007) and Silva (2018) date volcanic rocks associated to BIFs and chert layers, in the Nova Xavantina sequence at 720 Ma, and interpreted as sin-depositional age of the basin. We suggest that the Serra do Cristalino could be correlate with Nova Xavantina rocks, and make part of the same basin. Therefore, the younger zircon founded in CIFs of the Serra do Cristalino, at around 700 Ma, could be considered as limits of maximum deposition of the Serra do Cristalino sequence. Thus, suggest that the BIFs were deposit sincronous to a Sturtian Glaciation global event.

Chemical - sedimentary succession of the Cuiabá Group as well as the Jacadigo Group, are in the same geotectonic and geochronological context of the passive margin of the Paraguay belt, but does not have or have not been found intercalated volcanic material to determine the age of precise deposition of the sequence (Viehmann et al., 2016). We also, suggest that the Serra do Cristalino it's a old sequence than Cuiba and Jacadigo Groups.

U-Pb and Sm-Nd isotopic data of CIF, allow us to suggest the age of the main sedimentary sources that contributed to the filling up the rifting phase of the north Paraguay Basin, shows provenance of sources dominantly Paleoproterozoic ages, derived mainly from the Amazon Craton. Similar conclusion was obtained by Viehmann et. al., 2015 that performed U-Pb dates on zircons in basement dropstones found in the BIFs of the Urucum deposit in the South Paraguay belt, which obtain ages around 1830 Ma, suggest that the crystalline basement is erode during the glacial period, and eventually deposited as dropstone. Similar situation could be applyied to the

diamictites of Serra do Cristalino that shows only old sources and which microglomerates represent a mixing of sedimentary clastic and chemical sediments, with intercalations of diamictites and BIF.

T_{DM} model ages from the jaspilitics and BIFs shows a short variation between 1.3 to 1.5 Ga and the E_{Nd} (t) values are close to zero. This suggest a derivation and proximity with metal sources. The CIF has a homogeneous E_{Nd} (t) values similar to the diamictites from the Glaciogenic unit that occur in the central part of Paraguay belt, described by Dantas et al. (2009) and interpreted as diluted in a large water mass influx.

The siliciclast sediments intercaled with the BIF tell us a different history. Layers of dated arenites shows multiple sources. The majority of detrital grains are Paleoproterozoic (2.2-1.7 Ga), but one Archean derivation (2.6-2.7Ga) and Mesoproterozoic ages peaks (1.5,1.2, 1.0 and 0.95 Ga) are evident. Mesoproterozoic ages around 900 Ma may be related to sources derived from the Aguapei Belt and younger granites from Rodonia, that occur far way southwestern for more 1500 Km. This suggest that arenites represent a new influx of material siliclastic in the Paraguay basin, after glaciogenic period, and detrital grains comes from a distal source. This is evident by the oldest T_{DM} model ages at around 2.2 Ga and strongly negative ENd (t) values.

8. CONCLUSIONS

The data of this work suggest that the occurrence of BIFs in the Serra do Cristalino region, northern of the Paraguay Belt, was preserved seawater conditions in neoproterozoic times and can be associated to the NOE's event. The new occurrence, now discovered, isn't related to the Cuiabá and Corumbá Groups, being correlated to an older basin in the Paraguay belt, similar to the Nova Xavantina volcanosedimentary sequence of early neoproterozoic age.

Our depositional model suggests that chemical sedimentary rocks was be deposited on the stratified-redox sub-basin in deep marine environment with influence on distal glacigenic sediments (CIFs) intercalated with jaspilitic BIFs. The jaspilitic BIFs facies shows that deposition, possibly, be associated to initial phase of deglaciation where the oceans met-covered by ice, isolated from the atmosphere making a anoxic environment, thus seawater enriched with metals. Under deglaciation

conditions, the iron was in solution, to establish contact with the atmosphere, reacts quickly and starts a new balance precipitating as jaspilitic BIFs. The CIFs represents distal debris flows from diamictites resulting the intermediate-to-final stages of the thaw which deposited predominantly in glaciogenic chemical sedimentation consider as relate the Sturtian Glaciation global age (~726-660 Ma) being observed by textural evidence on clastic rocks and a low chemical enrichment in Al_2O_3, P_2O_5, Zr, Na_2O and K_2O when we compare with to the Jaspilitic BIFs.

Chemically, the iron formations of the Serra do Cristalino are pure and, although there was a clastic contribution to the CIFs, they were not able to change the REEY patterns. These rocks were deposited in a cold water environment from low temperature hydrothermal sources evidenced by the absence of positive anomalies from Eu/Eu*. When compared these rocks to NIFs deposits in the world, we observed a similarity to the deposits of Rapitan (Halverson et al., 2011), Egypt (Khalil et al., 2015), Jucurutu (Sial et al., 2015) and different from Jacadigo's examples (Urucum deposit (Viehmam et al., 2016), Santa Cruz deposit (Angerer et al., 2016) which occur in the southern region of the Paraguay Belt. In relation to the other deposits of the belt, they present several differences: they are absence of Mn, few pseudomorphs from carbonates, all those minerals was be already replaced by hematite.

Subsequently, terrigenous sediments, sandstones and shales mark a siliciclastic environment, which can have deposited small layers of seasonal flows that increase the energy of the system by depositing sandy sediments from more distal sources. REEY patterns of the CIFs are similar although slightly higher than of the BIFs and reflect of the composition of the Neoproterozoic seawater in both sedimentary rocks, in an anoxic deep ocean dominated by low T hydrothermal input.

Nd isotopes and provenance studies based on U-Pb zircon geochronology suggest that the main sources of sediments that filled the basin, are of Paleoproterozoic to Mesoproterozoic ages and likely derived from the Amazonian Craton, which is consistent with a passive margin model for the Paraguay Belt. Also, the youngest zircon at around 720 Ma in the microdiamictites facies from the Serra do Cristalino occurrence, suggest that their glacial event could be related to Sturtian event, similar to Rapitan, and, thus to be associated to the global Neoproterozoic Oxygenation Event (NOE).

9. ACKNOWLEDGEMENTS

We thank all those who collaborated directly or indirectly for this study, and CNPq for the grants (Projects number 308312/2014-7 and 454272/2014-6) and the EDEM Company, for providing some data that supported the start of the research.

10. APPENDIX

Appendix 01: Synthesis of the U-Pb (LA-ICPMS) isotopic data on zircon grains of the JA 01 and JA 20, Clastic inron formation.

Sample Spot	Th/U	Isotopic ratios						Apparent age (Ma)					
		$^{207}Pb/^{206}Pb$	1σ%	$^{207}Pb/^{235}U$	1σ%	$^{206}Pb/^{238}U$	1σ%	$^{207}Pb/^{206}Pb$	2σ abs	$^{207}Pb/^{235}U$	2σ abs	$^{206}Pb/^{238}U$	2σ abs
035-ZR21	0.661	0.06365	1.37	1.038	2.05	0.1183	1.48	730	57	723	21	721	20
034-ZR20	0.404	0.08948	1.65	3.001	2.37	0.2433	1.66	1414	62	1408	36	1404	42
023-ZR14	1.463	0.11260	3.13	5.379	4.90	0.3464	3.76	1842	111	1881	82	1917	124
010-ZR5	0.463	0.11337	1.08	5.411	1.66	0.3461	1.20	1854	39	1887	28	1916	40
042-ZR26	0.791	0.11408	2.08	4.983	2.81	0.3168	1.85	1865	74	1816	47	1774	57
040-ZR24	0.699	0.11475	1.14	5.462	2.28	0.3452	1.94	1876	41	1895	39	1912	64
021-ZR12	1.524	0.11603	1.48	5.444	2.51	0.3403	1.99	1896	53	1892	43	1888	65
033-ZR19	0.891	0.11640	2.35	5.430	3.10	0.3383	1.98	1902	83	1890	52	1879	64
018-ZR11	1.296	0.11697	1.70	5.313	2.66	0.3294	2.02	1910	60	1871	45	1836	64
048-ZR30	0.709	0.11846	2.48	5.942	3.29	0.3638	2.12	1933	88	1967	56	2000	73
006-ZR3	0.847	0.11988	1.19	5.761	1.79	0.3485	1.28	1954	42	1941	31	1927	43
039-ZR23	0.570	0.12080	1.33	6.247	2.13	0.3750	1.62	1968	47	2011	37	2053	57
016-ZR9	0.438	0.12145	0.94	5.467	1.75	0.3265	1.43	1978	33	1895	30	1821	45
005-ZR2	0.232	0.12272	1.17	5.607	1.93	0.3314	1.50	1996	41	1917	33	1845	48
028-ZR16	0.455	0.12329	1.03	6.060	1.57	0.3565	1.13	2004	36	1985	27	1965	38
015-ZR8	0.719	0.12346	1.00	6.481	1.71	0.3807	1.33	2007	35	2043	30	2080	47
012-ZR7	0.476	0.12367	1.39	6.632	2.07	0.3889	1.48	2010	49	2064	36	2118	53
045-ZR27	0.545	0.12435	1.85	5.903	2.75	0.3442	2.00	2020	65	1962	47	1907	66
024-ZR15	0.271	0.12482	1.38	6.623	2.07	0.3848	1.50	2026	48	2062	36	2099	54
046-ZR28	0.894	0.12575	2.13	6.407	3.38	0.3695	2.60	2039	74	2033	58	2027	90
011-ZR6	0.126	0.12933	0.97	6.830	1.64	0.3830	1.27	2089	34	2090	29	2090	45
004-ZR1	0.286	0.12989	0.83	6.867	1.36	0.3834	1.01	2097	29	2094	24	2092	36
041-ZR25	0.423	0.13309	2.60	6.702	4.24	0.3652	3.33	2139	90	2073	74	2007	114
017-ZR10	0.300	0.13508	1.43	7.080	2.52	0.3801	2.05	2165	50	2121	44	2077	72
022-ZR13	1.067	0.20401	1.19	16.894	2.07	0.6006	1.65	2859	39	2929	39	3032	80
004-ZR1	0.011	0.07443	0.86	1.847	2.22	0.1800	2.02	1053	34	1062	29	1067	40
017-ZR10	0.549	0.09810	0.51	3.825	0.86	0.2828	0.59	1588	19	1598	14	1605	17
023-ZR14	0.892	0.11379	0.94	5.235	1.74	0.3336	1.42	1861	34	1858	30	1856	46
010-ZR5	0.717	0.12170	0.43	6.278	1.19	0.3741	1.04	1981	15	2015	21	2049	37
005-ZR2	0.362	0.12247	0.49	6.135	0.86	0.3633	0.59	1993	18	1995	15	1998	20
006-ZR3	0.429	0.12306	0.62	6.352	1.01	0.3744	0.71	2001	22	2026	18	2050	25
022-ZR13	0.593	0.12323	0.51	6.290	0.88	0.3702	0.61	2004	18	2017	15	2030	21
015-ZR8	0.748	0.13046	0.94	6.974	1.70	0.3877	1.36	2104	33	2108	30	2112	49
012-ZR7	1.137	0.18133	2.84	13.266	3.33	0.5305	1.70	2665	93	2699	62	2744	76
018-ZR11	0.175	0.19136	0.72	14.540	1.27	0.5510	0.98	2754	23	2786	24	2829	45
009-ZR4	0.621	0.12079	0.51	6.583	0.85	0.3953	0.57	1968	18	2057	15	2147	21
024-ZR15	0.416	0.16471	0.60	11.966	0.89	0.5268	0.53	2505	20	2602	17	2728	24
021-ZR12	0.065	0.14834	1.27	7.156	1.57	0.3498	0.84	2327	43	2131	28	1934	28
047-ZR29	0.910	0.11951	1.45	5.052	2.05	0.3066	1.41	1949	51	1828	35	1724	43
036-ZR22	0.480	0.12430	1.45	5.461	2.31	0.3186	1.76	2019	51	1894	39	1783	55
009-ZR4	0.675	0.11521	1.09	3.377	2.68	0.2126	2.42	1883	39	1499	42	1243	55

Appendix 02: Synthesis of the U-Pb (LA-ICPMS) isotopic data on zircon grains of the JA 06, Arenite.

Sample Spot	Th/U	Isotopic ratios						Apparent age (Ma)					
		$^{207}Pb/^{206}Pb$	1σ%	$^{207}Pb/^{235}U$	1σ%	$^{206}Pb/^{238}U$	1σ%	$^{207}Pb/^{206}Pb$	2σ abs	$^{207}Pb/^{235}U$	2σ abs	$^{206}Pb/^{238}U$	2σ abs
042-ZR26_COMP	0.066	0.18713	0.61	14.617	2.05	0.5665	1.93	2717	20	2893	89	2791	39
029-ZR15_COMP	0.707	0.13065	0.41	7.612	1.68	0.4225	1.59	2107	14	2272	61	2186	30
005-ZR2_COMP	0.912	0.12740	0.37	7.006	0.83	0.3988	0.65	2062	13	2164	24	2112	15
021-Zr14	0.439	0.13130	1.01	6.991	2.12	0.3861	1.83	2115	35	2105	65	2110	37
019-Zr12	0.399	0.13061	0.54	6.951	0.87	0.3860	0.57	2106	19	2104	21	2105	15
085-ZR58_COMP	0.598	0.12577	0.49	6.684	0.92	0.3854	0.68	2040	17	2102	25	2071	16
020-ZR10_COMP	0.084	0.12970	1.93	6.860	2.45	0.3836	1.46	2094	67	2093	52	2093	43
035-ZR19_COMP	0.594	0.12517	0.47	6.543	0.90	0.3791	0.68	2031	16	2072	24	2052	16
060-ZR39_COMP	0.639	0.12701	0.55	6.619	1.04	0.3779	0.80	2057	19	2067	28	2062	18
086-ZR59_COMP	0.232	0.11795	0.47	6.128	3.25	0.3768	3.19	1925	17	2061	112	1994	56
041-Zr30	0.389	0.12673	0.82	6.554	1.15	0.3750	0.71	2053	29	2053	25	2053	20
052-ZR34_COMP	0.908	0.12189	1.23	6.278	2.25	0.3735	1.85	1984	44	2046	65	2015	39
062-ZR41_COMP	0.328	0.12615	0.89	6.485	1.81	0.3728	1.53	2045	31	2043	54	2044	32
069-ZR46_COMP	0.366	0.11929	0.47	6.094	1.10	0.3705	0.92	1946	17	2032	32	1989	19
088-ZR61_COMP	0.490	0.12063	0.36	6.142	0.96	0.3693	0.81	1966	13	2026	28	1996	17
087-ZR60_COMP	0.807	0.11449	0.78	5.816	2.30	0.3684	2.13	1872	28	2022	74	1949	39
047-ZR29_COMP	0.682	0.12545	0.79	6.316	2.53	0.3651	2.38	2035	28	2006	82	2021	44
031-ZR17_COMP	1.636	0.11410	0.56	5.725	1.77	0.3639	1.64	1866	20	2001	56	1935	30
010-Zr5	0.398	0.11971	0.51	5.977	0.92	0.3621	0.67	1952	18	1992	23	1973	16
019-ZR9_COMP	0.707	0.11557	0.40	5.770	1.93	0.3621	1.85	1889	15	1992	63	1942	33
091-ZR64_COMP	0.791	0.11957	0.54	5.930	1.01	0.3597	0.77	1950	19	1981	26	1966	18
082-ZR57_COMP	0.399	0.11735	1.12	5.752	1.71	0.3555	1.24	1916	40	1961	42	1939	29
030-Zr21	0.433	0.12451	0.65	6.103	1.02	0.3554	0.69	2022	23	1961	23	1991	18
038-Zr27	0.452	0.12636	0.62	6.083	2.11	0.3491	1.98	2048	22	1930	66	1988	36
011-Zr6	1.140	0.12419	1.15	5.972	1.58	0.3487	1.01	2017	40	1928	34	1972	27
016-Zr9	0.230	0.11962	0.56	5.744	0.93	0.3482	0.65	1951	20	1926	21	1938	16
039-Zr28	0.583	0.12470	0.77	5.985	1.43	0.3481	1.15	2025	27	1925	38	1974	25
020-Zr13	0.348	0.12314	0.81	5.896	1.47	0.3472	1.17	2002	29	1921	39	1961	25
005-Zr2	0.172	0.11395	0.46	5.446	0.77	0.3466	0.49	1863	17	1918	16	1892	13
026-ZR14_COMP	0.472	0.12574	0.48	5.952	2.10	0.3433	2.01	2039	17	1903	66	1969	36
065-ZR42_COMP	0.468	0.11588	0.82	5.433	2.24	0.3400	2.05	1894	29	1887	67	1890	38
079-ZR54_COMP	1.516	0.11453	0.85	5.363	1.36	0.3396	1.00	1872	31	1885	33	1879	23
017-Zr10	0.338	0.12044	0.53	5.520	0.91	0.3323	0.64	1963	19	1850	20	1904	16
072-ZR49_COMP	1.515	0.11672	0.70	5.337	1.15	0.3316	0.84	1907	25	1846	27	1875	20
090-ZR63_COMP	1.171	0.11219	0.77	5.125	1.32	0.3313	1.01	1835	28	1845	32	1840	22
025-Zr16	0.469	0.11477	0.76	5.211	1.10	0.3292	0.70	1876	27	1835	22	1854	19
070-ZR47_COMP	2.045	0.11246	1.67	5.060	2.34	0.3263	1.59	1840	60	1820	50	1829	39
011-ZR6_COMP	0.476	0.11572	0.79	5.192	1.20	0.3254	0.83	1891	28	1816	26	1851	20
027-Zr18	0.585	0.11557	0.64	5.130	1.02	0.3219	0.70	1889	23	1799	22	1841	17
061-ZR40_COMP	0.869	0.11357	0.63	4.939	1.05	0.3154	0.76	1857	23	1767	23	1809	18
018-ZR8_COMP	0.292	0.09766	0.39	3.512	0.75	0.2608	0.52	1580	14	1494	14	1530	12
037-Zr26	0.373	0.06914	0.59	1.594	1.56	0.1672	1.40	903	24	997	26	968	19
067-ZR44_COMP	1.269	0.07091	2.15	1.633	3.23	0.1670	2.38	955	87	996	44	983	40
015-Zr8	0.106	0.07228	1.18	1.659	1.61	0.1665	1.03	994	47	993	19	993	20
025-ZR13_COMP	1.363	0.06991	1.14	1.575	1.80	0.1633	1.35	926	46	975	24	960	22

058-ZR37_COMP	1.139	0.06304	2.40	1.413	3.24	0.1625	2.14	710	100	971	39	894	38
038-ZR22_COMP	2.048	0.07022	2.36	1.566	3.11	0.1617	1.99	935	95	966	36	957	38
035-Zr24	1.324	0.07048	0.88	1.522	1.24	0.1566	0.79	942	36	938	14	939	15
071-ZR48_COMP	0.418	0.06849	0.83	1.474	1.33	0.1561	0.97	883	34	935	17	920	16
076-ZR51_COMP	1.890	0.06863	1.71	1.476	2.50	0.1560	1.79	888	70	935	31	921	30
028-Zr19	0.968	0.07090	0.74	1.522	1.12	0.1557	0.75	954	30	933	13	939	14
049-ZR31_COMP	2.025	0.07144	1.85	1.525	2.40	0.1548	1.48	970	75	928	25	940	29
036-Zr25	0.555	0.07037	0.86	1.501	1.25	0.1547	0.83	939	35	927	14	931	15
012-Zr7	1.524	0.06977	2.60	1.479	3.69	0.1538	2.60	922	105	922	45	922	44
032-Zr23	1.639	0.07110	0.92	1.504	1.31	0.1534	0.85	960	38	920	15	932	16
022-Zr15	1.670	0.06994	1.39	1.479	1.76	0.1533	1.02	927	56	920	18	922	21
068-ZR45_COMP	2.495	0.06987	0.86	1.475	1.31	0.1531	0.92	925	35	919	16	920	16
031-Zr22	1.887	0.06963	1.50	1.469	2.17	0.1530	1.53	917	61	918	26	918	26
006-Zr3	2.351	0.06977	1.36	1.468	1.96	0.1525	1.36	922	55	915	23	917	23
089-ZR62_COMP	1.987	0.06691	1.02	1.402	1.53	0.1520	1.08	835	42	912	18	890	18
075-ZR50_COMP	1.163	0.06800	1.19	1.419	1.54	0.1513	0.91	868	49	908	15	897	18
032-ZR18_COMP	2.632	0.07086	1.30	1.476	1.95	0.1510	1.41	953	53	907	24	921	24
004-Zr1	1.601	0.07133	0.59	1.482	1.19	0.1507	0.96	967	24	905	16	923	14
026-Zr17	2.099	0.07070	1.88	1.455	2.59	0.1492	1.74	949	76	897	29	912	31
040-Zr29	0.807	0.06313	0.88	0.993	1.33	0.1140	0.92	713	37	696	12	700	13

Appendix 03: Synthesis of the U-Pb (LA-ICPMS) isotopic data on zircon grains of the JA 53, Arenite.

Sample Spot	Th/U	Isotopic ratios						Apparent age (Ma)					
		$^{207}Pb/^{206}Pb$	1σ%	$^{207}Pb/^{235}U$	1σ%	$^{206}Pb/^{238}U$	1σ%	$^{207}Pb/^{206}Pb$	2σ abs	$^{207}Pb/^{235}U$	2σ abs	$^{206}Pb/^{238}U$	2σ abs
009-Z4	0.4552	0.0701	0.5933	1.4507	0.8819	0.1501	0.6525	931	12.2	910	5.30	901	5.5
040-Z24	0.4202	0.0715	1.3241	1.6212	2.3210	0.1644	1.9062	973	27.0	978	14.58	981	17.3
036-Z22	0.3015	0.0719	1.8849	1.6497	2.1295	0.1664	0.9909	983	38.4	989	13.46	992	9.1
041-Z25	0.2544	0.0782	0.8206	2.1961	1.3263	0.2038	1.0419	1151	16.3	1180	9.25	1196	11.4
017-Z10	0.4781	0.0810	0.5213	2.2948	0.9080	0.2055	0.7434	1221	10.2	1211	6.42	1205	8.2
053-Z33	0.3885	0.0933	0.5177	3.3377	0.8013	0.2593	0.6116	1495	9.8	1490	6.26	1486	8.1
023-Z14	0.6010	0.1083	0.4673	4.7556	0.7303	0.3183	0.5612	1772	8.5	1777	6.13	1782	8.7
024-Z15	0.4544	0.1210	0.8751	6.0149	1.0650	0.3605	0.6070	1971	15.6	1978	9.27	1985	10.4
030-Z18	0.7255	0.1291	0.7173	6.7832	0.9018	0.3809	0.5466	2086	12.6	2084	7.98	2081	9.7
047-Z29	0.3658	0.1341	0.5777	7.2696	0.9652	0.3931	0.7733	2152	10.1	2145	8.62	2137	14.1
015-Z8	0.6452	0.1336	0.4733	7.3358	0.7140	0.3982	0.5346	2146	8.3	2153	6.38	2161	9.8
045-Z27	0.7291	0.1365	0.6516	7.5013	0.8700	0.3987	0.5764	2183	11.3	2173	7.79	2163	10.6
006-Z3	0.3268	0.1744	0.5351	12.0745	0.7227	0.5022	0.4857	2600	8.9	2610	6.78	2623	10.5
048-Z30	0.4045	0.1759	0.8063	12.3282	1.0410	0.5083	0.6586	2615	13.4	2630	9.78	2649	14.3
012-Z7	0.3436	0.1756	0.5529	12.3256	0.7535	0.5092	0.5119	2611	9.2	2630	7.08	2653	11.1
040-Z25	0.4638	0.0740	1.3148	1.5733	1.8587	0.1542	1.3113	1041	26.3	960	11.47	925	11.3
028-Z17	0.2558	0.0731	0.5796	1.6019	1.0357	0.1589	0.8582	1017	11.7	971	6.45	951	7.6
039-Z24	0.4142	0.0807	0.5753	2.1299	0.9129	0.1914	0.7085	1215	11.3	1159	6.29	1129	7.3
046-Z29	0.3379	0.0832	0.5898	2.4468	1.0544	0.2134	0.8738	1273	11.5	1256	7.57	1247	9.9
042-Z27	0.5562	0.0937	0.8729	3.3894	1.2456	0.2624	0.8882	1502	16.4	1502	9.72	1502	11.9
010-Z05	0.2484	0.0940	0.4772	3.5158	0.9530	0.2714	0.8249	1507	9.0	1531	7.53	1548	11.3
005-Z02	0.4623	0.1083	0.4194	4.7986	0.9216	0.3212	0.8206	1772	7.7	1785	7.74	1796	12.9
036-Z23	0.1089	0.1304	0.6266	6.3133	1.1214	0.3510	0.9300	2104	11.0	2020	9.78	1940	15.6
035-Z22	0.2008	0.1315	0.4364	6.5649	1.0799	0.3621	0.9876	2118	7.6	2055	9.47	1992	16.9
033-Z20	0.3623	0.1244	0.5035	6.3540	0.8667	0.3705	0.7046	2020	8.9	2026	7.58	2032	12.3
034-Z21	0.3762	0.1302	0.4656	6.6731	1.1048	0.3717	1.0018	2101	8.2	2069	9.71	2037	17.5
018-Z11	0.2843	0.1280	0.4814	6.6563	0.8044	0.3771	0.6445	2071	8.5	2067	7.10	2063	11.4
023-Z14	0.7229	0.1285	0.3529	6.9066	1.2346	0.3898	1.1831	2078	6.2	2100	10.95	2122	21.4
045-Z28	0.6080	0.1320	0.5820	7.1022	1.0648	0.3903	0.8917	2125	10.2	2124	9.48	2124	16.1
011-Z06	0.7245	0.1281	0.3451	7.0300	0.8822	0.3979	0.8119	2072	6.1	2115	7.84	2159	14.9
024-Z15	0.3762	0.1295	0.6384	7.1278	1.1943	0.3993	1.0093	2091	11.2	2128	10.63	2166	18.6
029-Z18	0.2638	0.1296	0.4338	7.2039	0.8557	0.4031	0.7376	2093	7.6	2137	7.63	2183	13.7
012-Z07	0.2655	0.1289	0.5079	7.1912	1.1088	0.4047	0.9857	2082	8.9	2135	9.88	2191	18.3
006-Z36	0.3030	0.1345	0.8026	7.0746	1.0547	0.3816	0.6844	2157	14.0	2121	9.38	2084	12.2
005-Z35	0.3482	0.1835	0.3346	12.3570	0.7213	0.4883	0.6390	2685	5.5	2632	6.78	2564	13.5
009-Z37	0.4922	0.1858	0.3829	12.7004	0.8268	0.4959	0.7327	2705	6.3	2658	7.78	2596	15.7
010-Z38	0.3411	0.1787	0.4231	13.0852	0.7582	0.5310	0.6292	2641	7.0	2686	7.15	2746	14.1

11. REFERENCES

Albarède, F., Telouk, P., Blichert-Toft, J., Boyet, M.,, Agranier, A.,, Nelson, B., 2004. Precise and accurate isotopic measurements using multiple-collector ICPMS1. Chemical Geology, Volume 182, Issues 2–4, 15 February 2002, Pages 605–618.

Alexander, B.W., Bau, M., 2009. Distribution of high field strength elements (Y, Zr,REE, Hr, Ta, Th, U) in adjacent magnetite and chert bands in reference standardsFeR-3 and FeR-4 from the Temagami iron-formation, Canada, and the redox levelof the Neoarchean ocean. Precambrian Res. 174, 337–346.

Alexander, B.W., Bau, M., Andersson, P., Dulski, P., 2008. Continentally-derivedsolutes in shallow Archean seawater: rare earth element and Nd isotope evidence in iron formation from the 2.9 Ga Pongola Supergroup, South Africa.Geochim. Cosmochim. Acta 72 (2), 378–394.

Alibert, C., McCulloch, M.T., 1993. Rare earth element and neodymiumisotopic compositions of the banded iron-formations and associated shales from Hamersley, Western Australia. Geochim. Cosmochim. Acta 57,187–204.

Alibo, D.S., Nozaki, Y., 1999. Rare earth elements in seawater: particle association,shale-normalization, and Ce oxidation. Geochim. Cosmochim. Acta 63 (3–4),363–372.

Almeida, F.F.M., 1945. Geologia do sudoeste mato-grossense, vol. 116. Boletim da Divisão de Geologia e Mineralogia, Departamento Nacional de Produção Mineral, DNPM, pp. 1–118.

Almeida, F.F.M. (1964) Geologia do centro-oeste mato-grossense. Bol. Dep. Nac. Produ. Mineral. (D.N.P.M.), Div. Geol. Mineral.,Rio de Janeiro, Brasil 214, 137 pp.

Almeida, F.F.M. Glaciação Eocambriana em Mato Grosso. Notas Preliminares e Estudos da Divisão de Geologia e Mineralogia, Departamento Nacional de Produção Mineral DNPM, n.117, p.1-11, 1964b

Almeida, F.F.M 1965b. Geologia Já Serra da Bodoquena (Mato Grosso).Rio de Janeiro, DNPM/DGM. 96 p. (Boletim 219)

Almeida, F.F.M. Evolução Tectônica do Centro-Oeste brasileiro no Proterozóico Superior. Anais Acad. Bras. Ciências, n.40, p.285-295, 1968.

Almeida, F.F.M. (1984) Província Tocantins. Setor sudoeste. In O Precambriano do Brasil, Eds. De Almeida F.F.M. e Hasui Y., pp. 265-281. BlücherLtd. Publ., São Paulo, Brasil.

Alvarenga, C.J.S 1984. Dobramentos da Faixa Paraguai na borda sudeste do Cráton Amazônico. In: CONGR. BRÁS. GEOL., 33. Rio de Janeiro, 1984. Anais... Rio de Janeiro, SBG. v. 7, p. 3258-3271.

Alvarenga, C.J.S 1985. Evidências de íacies turbidíticas grosseiras no Grupo Cuiabá, MT. In: S1MP. GEOL. CENTRO-OESTE, 2. Goiânia, 1985. Atas... Goiânia, SBG. p. 256-266.

Alvarenga, C.J.S. 1988. Turbiditos e a glaciação do final do Proterozóico Superior no Cinturão Paraguai, Mato Grosso. Rev. Bras. Geoc., 18:323- 327.

Alvarenga, C.J.S., &Trompette, R. Glacial and turbidite Sedimentation of upper Proterozoic in Paraguay Belt, Mato Grosso, Brazil. INTERNATIONAL GEOLOGY CONGRESS, 28, 1989. Abstracts … Washington, 1989. v.1, p.374.

Alvarenga, C.J.S . 1990. Phénomènes sédimentaires, estructuraux et circulation de fluides developpes a la transition chaine-craton.Exemple de la chaime Paragaui d´age protérozoique supérieur, Mato Grosso, Brésil. 177p. Tese. (Doutorado) – Universithé d´Aix-Marseille II, Faculte des Sciences et Techniques de ST-JEROME, France, 1990. 177 p.

Alvarenga, C.J.S., &Trompette, R 1992. Glacially-influenced sedimentation in thelater Proterozoic of the Paraguay Belt (Mato Grosso Brazil). Palaeogeochim.Palaeoclimatol. Palaeoecol. 92, 85–105.

Alvarenga, C.J.S., &Trompette, R. 1994 .A Faixa Paraguai e sua compartimentação estratigráfica e tectônica. In.: CONGRESSO BRASILEIRO DEGEOLOGIA, 38, Camburiú, , Anais ...Camburiú, SBG, 1994. v.1, p.239-240.

Alvarenga, C.J.S. e Trompette, R. (1993) Evolução tectônica brasiliana da Faixa Paraguai: a estruturação da região de Cuiabá. Rev. Bras. Geociências. 23(1), 18-30.

Alvarenga, C.J.S et al. 2000. Paraguay and Araguaia Belts. In.: CORDANNI, U. G. et al. Tectonic Evolution of South América. Rio de Janeiro: INTERNATIONAL GEOLOGICAL CONGRESS, 31, p.183-193.

Alvarenga, C. J., Boggiani, P. C., Babinski, M., Dardenne, M. A., Figueiredo, M., Santos, R. V., Dantas, E. L. 2009. The Amazonian palaeocontinent. In: Gaucher, C., Sial, A.N., Halverson, G.P., Frimmel, H.E. (Eds): Neoproterozoic-Cambrian Tectonics, Global Change and Evolution: a focus on southwestern Gondwana. Developments in Precambrian Geology, 16, 15-28.

Alvarenga, C.J.S., Boggiani, P.C., Babinski, M., Dardenne, M.A., Figueiredo, M.F., Dantas, E.L., Uhlein, A., Santos, R.V., Sial, A.N., Trompette, R., 2011. Glaciallyinfluenced sed- imentation of the Puga Formation, Cuiabá Group and Jacadigo Group, and associated carbonates of the Araras and Corumbá groups, Paraguay Belt, Brazil. Geological Society of London. Memoirs 36, 487–497.

Angerer, T., Hagemann,S.G., Walde,D.H.G., Halverson, G. P. and Bovce, A. J., 2016. Multiple metal sources in the glaciomarine facies of the Neoproterozoic Jacadigo iron formation in the Santa Cruz Deposit, Corumbá, Brazil. Precambrian Research 275, 369-393.

Babinski, M., Trinidade, R.I.F., Alvarenga, C.J.S., Boggiani, P.C., Liu, D., Santos, R.V. and Brito Neves, B.B.de, 2006. Chronology of Neoproterozoic ice ages in Central Brazil. V South American Symposium on Isotope Geology, Short Papers, Punta del Este, pp. 223-226.

Babinski, M., et al., 2008. U–PB SHRIMP geochronology and isotope chemostratigraphy (C,O, Sr) of the Tamengo Formation, Southern Paraguay Belt, Brazil, VI South AmericanSymposium on Isotope Geology. Book of Abstracts.San Carlos de Bariloche 160.

Babinski, M., Boggiani, P.C., Trindade, R.I.F., Fanning, C.M., 2013. Detrital zircon agesand geochronological constraints on the Neoproterozoic Puga diamictites andassociated BIFs in the southern Paraguay Belt, Brazil. Gondwana Res. 23, 988–997.

Basta, F.F., Maurice, A.E., Fontboté, L., Favarger, P., 2011. Petrology and geochemistryof the banded iron formation (BIF) of Wadi Karim and Um Anab, Eastern Desert,Egypt: implications for the origin of Neoproterozoic BIF. Precambrian Res. 187,277–292.

Bau, M., 1993. Effects of syn- and post-depositional processes on the rare-earthelement distribution in Precambrian iron-formations. Eur. J. Mineral. 5, 257–267.

Bau, M., Dulski, P., 1996. Distribution of yttrium and rare-earth elements in the Pengeand Kuruman iron-formations, Transvaal Supergroup, South Africa. PrecambrianRes. 79 (1–2), 37–55.

Bau, M., Koschinsky, A., Dulski, P., Hein, J.R., 1996. Comparison of the partitioning behav-iours of yttrium, rare earth elements, and titanium between hydrogenetic marine fer-romanganese crusts and seawater. Geochim. Cosmochim. Acta 60 (10), 1709–1725.

Bau, M., Möller, P., Dulski, P., 1997. Yttrium and lanthanides in eastern Mediter-ranean seawater and their fractionation during redox-cycling. Mar. Chem. 56(1), 123–131.

Bau, M., Dulski, P., 1999. Comparing yttrium and rare earths in hydrothermal fluidsfrom the Mid-Atlantic Ridge: implications for Y and REE behaviour during near-vent mixing and for the Y/Ho ratio of Proterozoic seawater. Chem. Geol. 155(1–2), 77–90.

Beard, B.L., Johnson, C.M., 2004. Fe isotope variations in the modern and ancient Earth andother planetary bodies. Rev. Mineral. Geochem. 55 (1), 319–357.

Barros, A.M.; Silva, .H.; Cardoso, O.R.F.A.; Freire, F.A.; Sousa Júnior, J.J.; Rivetti, M.; Luz, D.S.; Palmeira, R.C.B.; Tassinari, C.C.G., 1982 Geologia In.: BRASIL. Departamento Nacional da Produção Mineral. Projeto Radambrasil. Folha SD.21 Cuiabá: geologia, geomorfologia, pedologia, vegetação e uso potencial da terra. (Levantamento de Recursos Naturais, 26) Rio de Janeiro,V.26. p.25-192,.

Bekker, A., Holland, H. D., Wang, P.-L, Rumble, D, Stein, H. J., Hannah, J. L., Coetzee, L. L., & Beukes, N. J., 2004. Dating the rise of atmospheric oxygen. Nature 427 (6970), 117–120

Bekker, A., et al. 2010 Iron formation: A sedimentary product of the complex interplay among mantle, tectonic, and biospheric processes. Society Economic Geology, 105,. p. 467-508.

Beukes, N. 2004. Biogeochemistry - Early options in photosynthesis. Nature, n.431(7008). p. 522–523

Bostrom, K., 1973. The origin and fate of ferromanganoan active ridge sediments. Stockh.Contrib. Geol. 27, 149–243.

Boyle, E., Jenkins, W.J., 2008. Hydrothermal iron in the deep western South Pacific.Geochim. Cosmochim. Acta A107.Breitkopf, J.H., 1988. Iron formations related to mafic volcanism and ensialic rifting in thesouthern margin zone of the Damara Orogen, Namibia. Precambrian Res. 38 (2),111–130.

Buck, K.N., Maeve, L.C., Berger, C.J.M., Bruland, K.W., 2007. Dissolved iron speciation intwo distinct river plumes and an estuary: implications for riverine iron supply.Limnol. Oceanogr. 52 (2), 843–855.

Bühn, B., Santos, R.V., Dardenne, M.A., Oliveira, C. G., 2009. Mass-dependent and mass-independent sulfur isotope fractionation (δ34S and δ33S) from Brazilian Archean and Proterozoic sulfide deposits by laser ablation multi-collector ICP-MSOriginal Research Article. Chemical Geology, Volumes 312–313, 18 June 2012, Pages 163-176

Canfield D.E., (2005) The early history of atmospheric oxygen: homage to Robert M. Garrels. Annu Rev Earth Planet Sci 33:1–36

Canfield, D. E., and Teske, A., 1996, Late Proterozoic rise in atmospheric oxygen concentration inferred from phylogenetic and sulphur-isotope studies: Nature, v. 382, p. 127–132.

Catling, D.C., Claire, M.W.,. 2005, How Earth's Atmosphere evolved to an oxic state: A status report. Earth and Planetary Science Letters. 237. 2005. pp: 1–20.

Condie, K.C., Aster, R.C., 2010. Episodic zircon age spectra of orogenic granitoids: thesupercontinent connection and continental growth. Precambrian Res. 180, 227–236.

Cox, G.M., Halverson,G. P, Minarik, W.G., Le Heron D. P., Macdonald, F. A., Bellefroid, E. J., Strauss, J.V., 2013. Neoproterozoic iron formation: an evaluation of its temporal,environmental and tectonic significance. Chem. Geol. 362, 232–249.

Dantas, E.L., Armstrong, R., Pimentel, M.M., Fuck, R.A., Martinelli, C., Silva, M.F., Laux, J.H., 2007. 800 Ma rifting in the Paraguay Belt, Central Brasil: U–Pb SHRIMP age determination, Rodinia break-up and implications for a connection with Avalonian peri-Godwana terranes. GSA Annual Meeting. Denver. Abstracts, CD ROM.

Dantas, E.L., De Alvarenga, C.J.S., Santos, R.V., Pimentel, M.M., 2009. Using Ndisotopes to understand the provenance of sedimentary rocks from a continentalmargin to a foreland basin in the Neoproterozoic Paraguay Belt, Central Brazil.Precambrian Res. 170, 1–12.

Dalstra H.J. & Guedes S. 2004. Giant hydrothermal hematite deposits with Mg-Fe metasomatism: a comparison of the Carajás, Hamersley, and other iron ores. Econ. Geo., 99: 1793- 1800.

Danielson ,A., Moller P., Dulski, P., 1992. The europium anomalies in banded iron formations and the thermal History of the oceanic crust. Chemical geology, vol.97, pp. 2965 -2977.

Dardenne, M., 1998. Modelo hidrotermal-exhalativo para os depósitos de Fe-Mn da região de Corumbá, Mato Grosso do Sul, 40. Congresso Brasileiro de Geologia, Anais, São Paulo (SBG).

DePoalo, D. J. A neodymium and strontium isotopic study of the Mesozoic calc-alkaline granitic batholithys of the Sierra Nevada and Peninsular Ranges, California. Journal of Geophysical Research, 1981, n. 86. p. 10470-10488.

Dymek, R.F., Klein, C., 1988. Chemistry, petrology and origin of banded iron-formation lithologies from the 3800 MA isua supracrustal belt, West Greenland.Precambrian Res. 39 (4), 247–302.

Douville, E., et al., 1999. Yttrium and rare earth elements in fluids from various deep-seahydrothermal systems. Geochim. Cosmochim. Acta 63 (5), 627–643.

Douville, E., Charlou, J.L., Oelkers, E.H., Bienvenu, P., Jove Colon, C.F., Donval, J.P.,Fouquet, Y., Prieur, D., Appriou, P., 2002. The rainbow vent fluids (36°140N,MAR): the influence of ultramafic rocks and phase separation on trace metalcontent in Mid-Atlantic Ridge hydrothermal fluids. Chem. Geol. 184, 37–48.http://dx.doi.org/10.1016/S0009-2541(01)00351-5.

Elderfield, H., Greaves, M.J., 1982. The rare-earth elements in seawater. Nature 296, 214–219

Eyles, N.; Januszczak, N. (2004). «'Zipper-rift': A tectonic model for Neoproterozoic glaciations during the breakup of Rodinia after 750 Ma» (PDF). Earth-Science Reviews [S.l.: s.n.] 65 (1-2): 1–73.

Freitas, B.T., Warren, L.V., Boggiani, P.C., De Almeida, R.P., Piacentini, T., 2011.Tectono-sedimentary evolution of the Neoproterozoic BIF-bearing JacadigoGroup, SW-Brazil. Sediment. Geol. 238, 48–70.

Frei, R., Polat, A.2007 Source heterogeneity for the major components of ~3.7 Ga banded iron formations (Isua Greenstone Belt,Western Greenland): Tracing the nature of interactingwatermasses in BIF formation. Earth and Planetary Science Letters, 2007, n.253, v.1–2, 266–281.

Frei, R., Dahl, P.S., Duke, E.F., Frei, K.M., Hansen, T.R., Frandsson, M.M. and Jensen, L.A. (2008) Trace Element and Isotopic Characterization of Neoarchean and Paleoproterozoic Iron Formations in the Black Hills (South Dakota USA): Assessment of Chemical Change during 2.9-1.9 Ga Deposition Bracketing the 2.4-2.2 Ga First Rise of Atmospheric Oxygen. Precambrian Research, 162, 441-474.

Frei, R., Gaucher, C., Poulton, S.W., Canfield, D.E., 2009. Fluctuations in Precambrian atmospheric oxygenation recorded by chromium isotopes. Nature, 461, 250–254.

Frei, R., Gaucher, C., Stolper, D., Canfield, D.E., 2013. Fluctuations in lateNeoproterozoic atmospheric oxidation—Cr isotope chemostratigraphy andiron speciation of the late Ediacaran lower Arroyo del Soldado Group(Uruguay). Gondwana Res. 23, 797–811..

Frei , R., Døssing, L.N., Gaucher, C., Boggiani, P.C., Frei, K.M., Bech Árting, T., Crowe, S.A., Freitas, B.T., 2017. Extensive oxidative weathering in the aftermath of a late Neoproterozoic glaciation – Evidence from trace element and chromium isotope records in the Urucum district (Jacadigo Group) and Puga iron formations (Mato Grosso do Sul, Brazil). Gondwana Research, 49, 1-20.

Fryer, B.J. Rare-earth elements in iron-formation (Part B). In: Trendall A.F., Morris R.C. (eds.), Iron Formation: Facts and Problems. Developments in Precambrian Geology. Amsterdam: Elsevier, 1993. p. 345-357.

Fryer, B.J., Fyfe, W.S., Kerrich, R., 1979. Archean volcanogenic oceans. Chem. Geol.24, 25–33.

Gross G. A. Stratiform iron. In: Geology of Canadiam Mineral Deposit Types. (eds) Eckstrand O.R., Sinclair W.D., Thorpe R.I. Geological Survey of Canada, Geology of Canada, 1996, n.8. p. 41-54.

Gaucher, C., Sial, A.N., Frei, R. 2015. Chemostratigraphy of Neoproterozoic banded iron formation (BIF): types, age and origin. In: Ramkumar, M. (Ed.)

Chemostratigraphy: concepts, techniques and applications. Elsevier, Amsterdam, pp. 433-449.

Graf, J.L., O'Connor, E.A., Van Leeuwen, P., 1994. Rare earth element evidence of origin and depositional environment of Late Proterozoic ironstone beds and manganese-oxide deposits, SW Brazil and SE Bolivia. Journal of South American Earth Sciences 7, 115–133.

Halverson, G.P., Poitrasson, F., Hoffman, P.F., Nédélec, A., Montel, J.M., Kirby, J., 2011.Fe isotope and trace element geochemistry of the Neoproterozoic syn-glacialRapitan iron formation. Earth Planet. Sci. Lett. 309, 100–112. http://dx.doi.org/10.1016/j.epsl.2011.06.021

Hoffman, P.F., Kaufman, A.J., Halverson, G.P., Schrag, D.P., 1998. A Neoproterozoicsnowball Earth. Science 281, 1342–1346.

Hoffman, P.F. & Schrag, D.P., 2002. The snowball Earth hypothesis: testing the limits of global change. Terra Nova 14, 129-155.

Holland, H.D., 2006. The oxygenation of the atmosphere and oceans. Phil. Trans. R. Soc. B 361, 903–915.

Huston, D.L, and Logan, G.A., 2004. Barite, BIFs and bugs: evidence for the evolution of the Earth's early hydrosphere. Earth and Planetary Science Letters 220 (2004) 41-55.

James, H.L. 1954. Sedimentary facies of iron formations. Econ. Geol. Lancaster: [s.n.], 1954, n.49, v.3. p. 235-293.

Kato,Y., Ohta, I., Tsunematsu,T., Watanabe,Y., Yukio Isozaki,Y., Maruyama S., Imai, N., 1998. Rare earth element variations in mid-Archean banded iron formations: implications for the chemistry of ocean and continent and plate tectonics.Geochimica et Cosmochimica Acta, V62, Issues 21-22 , P3475 -3497.

Kato, Y., Yamaguchi, K.E., Ohmoto, H., 2006. Rare earth elements in Precambrian banded iron formations: secular changes of Ce and Eu anomalies and evolution of atmospheric oxygen. In:

Kesler, S., Ohmoto, H. (Eds.), Evolution of the Atmosphere, Hydrosphere, and Biosphere on Early Earth: constraints from Ore Deposits. Geol. Soc. Am. Mem. 196, 269–289.

Khalil K. I., El-Shazly A.E., Lehmann B.,2015. Late Neoproterozoic banded iron formation(BIF) in the central Eastern desert of Egypt: mineralogical and geochemical implications fro the origin of the Gebel El Hadid iron ore deposit.Ore Geology Reviews 69 (2015) 380 – 399.

Keto, L.S., Jacobsen, S.B., 1988. Nd isotopic variations of Phanerozoic paleoceans.Earth Planet. Sci. Lett. 90, 395–410.

Klein, C., Beukes, N.J., 1993. Sedimentology and Geochemistry of the Glaciogenic Late Proterozoic Rapitan Iron-Formation in Canada. Econ. Geol. 88, 542–565.

Klein, C., Ladeira, E., 2004. Geochemistry and mineralogy of Neoproterozoic bandediron-formations and some selected, siliceous manganese formations from theUrucum District, Mato Grosso. Econ. Geol. 99, 1233–1244

Klein, C., 2005. Some Precambrian banded iron-formations (BIFs) from around the world:Their age, geologic setting, mineralogy, metamorphism, geochemistry, and origins.Am. Mineral. 90 (10), 1473–1499.

Košler., J.; Fonneland, H.; Sylvester ,P.; Tubrett, M.; & Pedersen, R., 2002 U–Pb dating of detrital zircons for sediment provenance studies—a comparison of laser ablation ICPMS and SIMS techniques Original Research Article. Chemical Geology, Volume 182, Issues 2–4, 15 February 2002, Pages 605-618.

Kröner, A., Hoffmann, J.E., Xie, H., Wu, F., Münker, C., Hegner, E., Wong, J., Wan, Y., Liu, D., 2013. Generation of early Archaean felsic greenstone volcanic rocks through crustal melting in the Kaapvaal, craton, southern Africa. Earth Planet. Sci. Lett. 381, 188–197.

Konhauser, K.O., Newman, D.K., Kappler, A., 2005. The potential significance of microbial Fe(III) reduction during deposition of Precambrian banded iron formations. Geobiology 3 (3), 167–177.

Lacerda Filho, J.W.; Brito, R.S.C.; Silva, M.G.; Oliveira, C.C. DE, Moreton, L.C., Martins, E.G., Lopes, R.C., Lims, T.M., Larizzatti, J.H. Valente, C.R. Geologia e Recursos Minerais do Estado de Mato Grosso do Sul. Programa Integração, Atualização e Difusão de Dados de Geologia do Brasil. Convênio CPRM/SICME-MS, MME. 121 p. 2006.

Lascelles, d.f. 2007. Black smokers and density currents: a uniformitarian model for the genesis of Banded iron – formations. Ore Geol. Rev 32, 381 411.

Lobato L.M., Hagemann S.G., Figueiredo e Silva R.C., Thorne W., Zucchetti M., Gutzmer J. 2008. Hypogene hydrothermal alteration associated with BIF-related iron ore mineralization. In: Hagemann, S.G., Rosière, C.A., Gutzmer, J., and Beukes, N.J., BIF-Related High-Grade Iron Mineralization. Reviews in Econ. Geo., 15: 107-128.

Luz, José da Luz. Projeto Fosfato de Bonito. Goiânia: CPRM, 1980. (Conv.Codesul / CPRM) LUZ, José da Luz; OLIVEIRA, Amóss de Melo; SOUIZA, João Olímpio; MOTTA, José Francisco Marciano; TANNO, Luiz Carlos; DOUZA, Nilson Batista de; ABREU FILHO, Waldemar. Projeto Coxipó. Relatório Final. Goiânia: CPRM, 1980. v.1, 136p.(Conv.DNPM / CPRM).

Ludwig, K.R., 2003. Mathematical-statistical treatment of data nd errors for Th-230/U geochronology. Uranium-Series Geochemistry, Reviews in Minerology and Geochemistry, 52: 631-656.

McGee, B., Halverson, G.P., Collins, A.S., 2012. Cryogenian rift-related magmatism and sed-imentation: South-western Congo Craton, Namibia. J. Afr. Earth Sci. 76, 34–49.

McGee, B., Collins, A. S., Trindade, R. I., Jourdan, F. 2015. Investigating mid-Ediacaran glaciation and final Gondwana amalgamation using coupled sedimentology and 40Ar/39Ar detrital muscovite provenance from the Paraguay Belt, Brazil. Sedimentology, 62(1), 130-154.

McGee, B., Collins, A. S., Trindade, R. I., Payne, J. 2015. Age and provenance of the Cryogenian to Cambrian passive margin to foreland basin sequence of the northern Paraguay Belt, Brazil. Geological Society of America Bulletin, 127(1-2), 76-86.

McLennan, S. M. (1989) Rare earth elements in sedimentary rocks: influence of provenance and sedimentary processes. Geochemistry and Mineralogy of Rare Earth Elements (Lipin, B. R. and McKay, G. A., eds.), Rev. Mineral. 21, 169–200

Michard, A., et al., 1993. Submarine thermal springs associated with young volca-noes: The Teahitia vents, Society Islands, Pacific Ocean. Geochim. Cosmochim.Acta 57 (21–22), 4977–4986.

Michard, A., Albarede, F., Michard, G., Minster, J. F., and Charlou, J. L., 1983. Rare-earth elements and uranium in high-temperature solutions from East Pacific Rise hydrothermal vent field (13°N. Nature, 303:795-797.

Michard A., and Albarede F., 1986. The REE content of some hydrothermal fluids. Chem. Geol., 55:51-60. Mitra, A., Elderfield, H., Greaves, M.J., 1994. Rare earth elements in submarine hydrothermal fluids and plumes fron the Mid-Atlantic Ridge. Marine Chemistry 46, 217 -235.

Morris, R.C., 1980. A textural and mineralogical study of the relationship of iron ore to banded iron formation in the Hamersley Iron Province of Western Australia. Geol. 75, !85 – 209.

Nogueira, A.C.R., Riccomini, C., Sial, A.N., Trindade, I.R., Faichild, T., 2007. Carbon and Strontium fluctuations and paleoceanographic changes in the late Neoproterozoic Araras carbonate platform, southern Amazon craton, Brazil. Chemical Geology, 237: 186-208

Pecoits, E., 2010. Ediacaran Iron Formations and Carbonates of Uruguay: Paleoceanographic, Palaeoclimatic and Palaeobiologic Implications. (Ph.D. thesis), University of Alberta (237 pp.).

Piacentini, T., Vasconcelos, P.M., Farley, K.A., 2013.40Ar/39Ar constraints on the ageand thermal history of the Urucum Neoproterozoic banded iron-formation,Brazil. Precambrian Res. 228, 48–62. http://dx.doi.org/10.1016/j.precamres.2013.01.002.

Pinho, F.E.C.; Ruiz, A.S.; Schmus, R.V.S., Figeirodo, M.; Godoy, A.M.,1990. Estudo Isotópico dos Granitos da Faixa de Dobramento Paraguai em Mato Grosso (dados inéditos).

Pinho F.E.C. 1990. Estudo das rochas encaixantes e veios mineralizados a ouro do Grupo Cuiabá, na região denominada "Garimpo dos Araés" Nova Xavantina, estado de Mato Grosso. Centro de Pesquisas em Geociências da Universidade Federal do Rio Grande do Sul, Porto Alegre, RS, Dissertação (Mestrado em Geoquímica), 114p.

Planavsky, N., Bekker, A., Rouxel, O.J., Kamber, B., Hofmann, A., Knudsen, A., Lyons, T.W., 2010. Rare Earth Element and yttrium compositions of Archean and Paleoproterozoic Fe formations revisited: new perspectives on the significance and mechanisms of deposition. Geochim. Cosmochim. Acta 74, 6387–6405.

Poulton, S.W., Raiswell, R., 2002. The low-temperature geochemical cycle of iron: fromcontinental fluxes to marine sediment deposition. Am. J. Sci. 302 (9), 774–805.

Remus, M. V. D.; Souza, R. S.; Cupertino, J. A.; De Ros, L. F.; Dani, N. & Lelarge, V. M. L. 2008. Proveniência sedimentar, métodos e técnicas analíticas aplicadas. Revista brasileira de geociência, 38, suplemento 2: 166-185.

Rosière C.A. & Rios F.J. 2004. The origin of hematite in high-grade iron ores based in infrared microscopy and fluid inclusion studies: the example of the Conceição Deposit, Quadrilátero Ferrífero, Brazil. Econ. Geol., 99: 611-624.

Rodrigues, R; Azevedo, R.L.M; Estrada, N.M.; Rehim, H.A.A; Sato, K.; Kawashita, K; Soliani Jr., Inferências cronoestratigráficas para carbonatos da Bacia dos Parecis, com base em dados da razão 87 SR / 86 Sr. In.: CONGRESSO BRASILEIRO DE GEOLOGIA, 38, 1994, Camboriu. 1994. Anais ... Camboriu: SBG, 1994. v.3, p.286-287.

Sahoo SK, Planavsky NJ, Kendall B, Wang X, Shi X, Scott C, Anbar AD, Lyons TW, Jiang G., 2012.Ocean oxygenation in the wake of the Marinoan glaciation. Nature 489 (7417), 546–549.

Schobbenhaus, C., Campos, D.A., Derze, G.R., Asmus, H.E., 1981. Mapa geológico do Brasil e da área oceânica adjacente incluindo depósitos minerais. Escala 1/2.500.000. Dep. Nac. Produc◦. Mineral (D.N.P.M.), Brasilia.

Shields-Zhou, G.A., Och, L.M. (2011). The case for a Neoproterozoic Oxygenation Event: geochemical evidence and biological consequences. GSA Today, 21 (3), 4-11. doi:10.1130/GSATG102A.1

Sial, A. N., Campos M. S., Gaucher C., Frei R., Ferreira V.P., Nascimento R.C., Pimentel M.M., Pereira N.S., Rodler A., 2015; Algoma-type Neoproterozoic BIFs and related marbles in tha Seridó Belt (NE Brazil): REE, C, O, Cr and Sr isotope evidence. Journal of South American Earth Sciences xx (2015) 1-20.

Silva, M. F. DA. 2007. Aerogeofísica, Litogeoquímica e Geologia na Caracterização do Rifte Intracontinental da Faixa Paraguai. Instituto de Geociências. Universidade de Brasília, Brasília, Dissertação de Mestrado, 1 v. 117 p.

Silva, M. F. DA. 2018. Evolução Tectônica de Rift para Margem Passiva da Faixa Paraguai-Mato Grosso, Brasil Central. Instituto de Geociências. Universidade de Brasília, Brasília, Tese de Doutorado N°144, 1 v. 198 p.

Spier, C. A. 2005 Geoquímica e Gênese das Formações Ferríferas Bandadas e do Minério de Ferro da Mina de Águas Claras, Quadrilátero Ferrífero, MG. [Tese Doutorado]. São Paulo: Instituto de Geociências; Universidade de São Paulo,. 298p.

Stern, R.J., Mukherjee, S.K., Miller, N.R., Ali, K., Johnson, P.R., 2013. 750 Ma bandediron formation from the Arabian-Nubian Shield—implications forunderstanding neoproterozoic tectonics, volcanism, and climate change.Precambrian Res. 239, 79–94. http://dx.doi.org/10.1016/j.precamres.2013.07.015.

Tagliabue, A., et al., 2010. Hydrothermal contribution to the oceanic dissolved iron inven-tory. Nat. Geosci. 3 (4), 252–256.

Trompette, R., Alvarenga, C.J.S. de, e Walde, D., (1998) Geological evolution of the Neoproterozoic Curumbá graben system (Brazil): Depositional context of the stratified Fe and Mn ores of the Jacadigo Group. Journal of South American Earth Science, v. 11, p. 587–597.

Viehmann, S., Bau, M., Bühn, B., Dantas, E.L., Walde, D.H.G. Geochemical characterisation of marine Neoproterozoic habitats: Evidence from HFSE, REY and Nd isotopes of the Cyrogenian Urucum Fe-Mn formation, Brazil. Precambrian Research, No prelo.

Walde, D.H.G., Hagemann, S.G.E. (2007) The Neoproterozoic Urucum/Mutún Fe and Mn deposits in W-Brazil/SE-Bolivia: assessment of ore deposit models. Zentralblattdt. Geologische Geowissenschaften 158 (1), 45–55.

Wang, X.L., Planavsky, N.J., Reinhard, C.T., Zou, H.J., Ague, J.J., Wu, Y.B., Gill, B.C., Schwarzenbach, E.M., Peucker-Ehrenbrink, B., 2016. Chromium isotope fractionation during subduction-related metamorphism, black shale weathering, and hydrothermal alteration. Chemical Geology 423, 19–33.

Urban, H., Stribrny, B., Lippolt, H.J., 1992. Iron and manganee deposits of the Urucum district, Mato-Grosse-do-Sul, Brazil. Economic Geology and the Bulletin of the Society of Economic Geologists 87, 1375–1392.

Xu, D.R., Wang, Z.L., Chen, H.Y., Hollings, P., Jansen, N.H., Zhang, Z.C., Wu, C.J., 2013b. Petrography and geochemistry of the Shilu Fe–Co–Cu ore district, South China: Implications for the origin of a Neoproterozoic BIF system. Ore Geology Reviews 57, 322–350.

Young, G.M., 1976. Iron-formation and glaciogenic rocks of the Rapitan Group, Northwest Territories, Canada. Precambrian Res. 3, 137–158.

Yeo, G.M., 1981. The Late Proterozoic Rapitan glaciation in the Northern Cordillera. In: Campbell, F. (Ed.), Proterozoic Basins of Canada: Geological Survey of Canada Paper81–10, pp. 25–46.

Zhang, Q.-R., Chu, X.-L., Feng, L.-J., 2011. Chapter 32 Neoproterozoic glacial records in the Yangtze Region, China. Geol. Soc., Lond., Mem. 36 (1), 357–366.

CAPÍTULO IV – REFERÊNCIAS BIBLIOGRÁFICAS

Albarède, F., Telouk, P., Blichert-Toft, J., Boyet, M.,, Agranier, A.,, Nelson, B., 2004. Precise and accurate isotopic measurements using multiple-collector ICPMS1. Chemical Geology, Volume 182, Issues 2–4, 15 February 2002, Pages 605–618.

Alexander, B.W., Bau, M., 2009. Distribution of high field strength elements (Y, Zr,REE, Hr, Ta, Th, U) in adjacent magnetite and chert bands in reference standardsFeR-3 and FeR-4 from the Temagami iron-formation, Canada, and the redox levelof the Neoarchean ocean. Precambrian Res. 174, 337–346.

Alexander, B.W., Bau, M., Andersson, P., Dulski, P., 2008. Continentally-derivedsolutes in shallow Archean seawater: rare earth element and Nd isotope evidence in iron formation from the 2.9 Ga Pongola Supergroup, South Africa.Geochim. Cosmochim. Acta 72 (2), 378–394.

Ali, K.A., Stern, R.J., Manton,W.I., Kimura, J.-I., Khamees, H.A., 2009. Geochemistry, Nd isotopes and U–Pb SHRIMP zircon dating of Neoproterozoic volcanic rocks fromthe Central Eastern Desert of Egypt: new insights into the ~750 Ma crust-forming event. Precambrian Research 171 (1–4), 1–22.

Alibert, C., McCulloch, M.T., 1993. Rare earth element and neodymiumisotopic compositions of the banded iron-formations and associated shales from Hamersley, Western Australia. Geochim. Cosmochim. Acta 57,187–204.

Alibo, D.S., Nozaki, Y., 1999. Rare earth elements in seawater: particle association,shale-normalization, and Ce oxidation. Geochim. Cosmochim. Acta 63 (3–4),363–372.

Almeida, F.F.M 1965b. Geologia Já Serra da Bodoquena (Mato Grosso).Rio de Janeiro, DNPM/DGM. 96 p. (Boletim 219)

Almeida, F.F.M. (1964) Geologia do centro-oeste mato-grossense. Bol. Dep. Nac. Produ. Mineral. (D.N.P.M.), Div. Geol. Mineral.,Rio de Janeiro, Brasil 214, 137 pp.

Almeida, F.F.M. (1984) Província Tocantins. Setor sudoeste. In O Precambriano do Brasil, Eds. De Almeida F.F.M. e Hasui Y., pp. 265-281. BlücherLtd. Publ., São Paulo, Brasil.

Almeida, F.F.M. Evolução Tectônica do Centro-Oeste brasileiro no Proterozóico Superior. Anais Acad. Bras. Ciências, n.40, p.285-295, 1968.

Almeida, F.F.M. Glaciação Eocambriana em Mato Grosso. Notas Preliminares e Estudos da Divisão de Geologia e Mineralogia, Departamento Nacional de Produção Mineral DNPM, n.117, p.1-11, 1964b

Almeida, F.F.M., 1945. Geologia do sudoeste mato-grossense, vol. 116. Boletim da Divisão de Geologia e Mineralogia, Departamento Nacional de Produção Mineral, DNPM, pp. 1–118.

Alvarenga, C. J., Boggiani, P. C., Babinski, M., Dardenne, M. A., Figueiredo, M., Santos, R. V., Dantas, E. L. 2009. The Amazonian palaeocontinent. In: Gaucher, C., Sial, A.N., Halverson, G.P., Frimmel, H.E. (Eds): Neoproterozoic-Cambrian Tectonics, Global Change and Evolution: a focus on southwestern Gondwana. Developments in Precambrian Geology, 16, 15-28.

Alvarenga, C.J.S . 1990. Phénomènes sédimentaires, estructuraux et circulation de fluides developpes a la transition chaine-craton.Exemple de la chaime Paragaui d´age protérozoique supérieur, Mato Grosso, Brésil. 177p. Tese. (Doutorado) – Universithé d´Aix-Marseille II, Faculte des Sciences et Techniques de ST-JEROME, France, 1990. 177 p.

Alvarenga, C.J.S 1984. Dobramentos da Faixa Paraguai na borda sudeste do Cráton Amazônico. In: CONGR. BRÁS. GEOL., 33. Rio de Janeiro, 1984. Anais... Rio de Janeiro, SBG. v. 7, p. 3258-3271.

Alvarenga, C.J.S 1985. Evidências de íacies turbidíticas grosseiras no Grupo Cuiabá, MT. In: S1MP. GEOL. CENTRO-OESTE, 2. Goiânia, 1985. Atas... Goiânia, SBG. p. 256-266.

Alvarenga, C.J.S et al. 2000. Paraguay and Araguaia Belts. In.: CORDANNI, U. G. et al. Tectonic Evolution of South América. Rio de Janeiro: INTERNATIONAL GEOLOGICAL CONGRESS, 31, p.183-193.

Alvarenga, C.J.S. 1988. Turbiditos e a glaciação do final do Proterozóico Superior no Cinturão Paraguai, Mato Grosso. Rev. Bras. Geoc., 18:323- 327.

Alvarenga, C.J.S. e Trompette, R. (1993) Evolução tectônica brasiliana da Faixa Paraguai: a estruturação da região de Cuiabá. Rev. Bras. Geociências. 23(1), 18-30.

Alvarenga, C.J.S., &Trompette, R 1992. Glacially-influenced sedimentation in thelater Proterozoic of the Paraguay Belt (Mato Grosso Brazil). Palaeogeochim.Palaeoclimatol. Palaeoecol. 92, 85–105.

Alvarenga, C.J.S., &Trompette, R. 1994 .A Faixa Paraguai e sua compartimentação estratigráfica e tectônica. In.: CONGRESSO BRASILEIRO DEGEOLOGIA, 38, Camburiú, , Anais ...Camburiú, SBG, 1994. v.1, p.239-240.

Alvarenga, C.J.S., &Trompette, R. Glacial and turbidite Sedimentation of upper Proterozoic in Paraguay Belt, Mato Grosso, Brazil. INTERNATIONAL GEOLOGY CONGRESS, 28, 1989. Abstracts … Washington, 1989. v.1, p.374.

Alvarenga, C.J.S., Boggiani, P.C., Babinski, M., Dardenne, M.A., Figueiredo, M.F., Dantas, E.L., Uhlein, A., Santos, R.V., Sial, A.N., Trompette, R., 2011. Glaciallyinfluenced sed- imentation of the Puga Formation, Cuiabá Group and Jacadigo Group, and associated carbonates of the Araras and Corumbá groups, Paraguay Belt, Brazil. Geological Society of London. Memoirs 36, 487–497.

Angerer, T., Hagemann,S.G., Walde,D.H.G., Halverson, G. P. and Bovce, A. J., 2016. Multiple metal sources in the glaciomarine facies of the Neoproterozoic Jacadigo iron formation in the Santa Cruz Deposit, Corumbá, Brazil. Precambrian Research 275, 369-393.

Babinski, M., Boggiani, P.C., Trindade, R.I.F., Fanning, C.M., 2013. Detrital zircon agesand geochronological constraints on the Neoproterozoic Puga diamictites andassociated BIFs in the southern Paraguay Belt, Brazil. Gondwana Res. 23, 988–997.

Babinski, M., et al., 2008. U–PB SHRIMP geochronology and isotope chemostratigraphy (C,O, Sr) of the Tamengo Formation, Southern Paraguay Belt, Brazil, VI South AmericanSymposium on Isotope Geology. Book of Abstracts.San Carlos de Bariloche 160.

Babinski, M., Pedrosa-Soares, A.C., Trindade, R.I.F., Martins, M., Noce, C.M., Liu, D., 2012. Neoproterozoic glacial deposits from the Araçuaí orogen, Brazil: Age, provenance and correlations with the São Francisco Craton and West Congo belt. Gondwana Research 21, 451–465, http://dx.doi.org/10.1016/j.gr.2011.04.008.

Babinski, M., Trinidade, R.I.F., Alvarenga, C.J.S., Boggiani, P.C., Liu, D., Santos, R.V. and Brito Neves, B.B.de, 2006. Chronology of Neoproterozoic ice ages in Central Brazil. V South American Symposium on Isotope Geology, Short Papers, Punta del Este, pp. 223-226.

Baldwin, G.J., Nägler, T.F., Greber, N.D., Turner, E.C., Kamber, B.S., 2013. Mo isotopic composition of the mid-Neoproterozoic ocean: an iron formation perspective. Precambrian Research 230, 168–178.

Baldwin, G.J., Turner, E.C., Kamber, B.S., 2012. A new depositional model for glaciogenic Neoproterozoic iron formation: insights from the chemostratigraphy and basin configuration of the Rapitan iron formation. Canadian Journal of Earth Sciences 49, 455–476.

Barrett, T.J., Jarvis, I., 1988. Rare-earth element geochemistry of metalliferous sediments from DSDP Leg 92: the East Pacific Rise transect. Chem. Geol. 67 (3–4), 243–259.

Barros, A.M.; Silva, .H.; Cardoso, O.R.F.A.; Freire, F.A.; Sousa Júnior, J.J.; Rivetti, M.; Luz, D.S.; Palmeira, R.C.B.; Tassinari, C.C.G., 1982 Geologia In.: BRASIL. Departamento Nacional da Produção Mineral. Projeto Radambrasil. Folha SD.21 Cuiabá: geologia, geomorfologia, pedologia, vegetação e uso potencial da terra. (Levantamento de Recursos Naturais, 26) Rio de Janeiro,V.26. p.25-192,.

Basta, F.F., Maurice, A.E., Fontboté, L., Favarger, P., 2011. Petrology and geochemistryof the banded iron formation (BIF) of Wadi Karim and Um Anab, Eastern Desert,Egypt: implications for the origin of Neoproterozoic BIF. Precambrian Res. 187,277–292.

Bau, M., 1993. Effects of syn- and post-depositional processes on the rare-earthelement distribution in Precambrian iron-formations. Eur. J. Mineral. 5, 257–267.

Bau, M., Dulski, P., 1996. Distribution of yttrium and rare-earth elements in the Pengeand Kuruman iron-formations, Transvaal Supergroup, South Africa. PrecambrianRes. 79 (1–2), 37–55.

Bau, M., Dulski, P., 1999. Comparing yttrium and rare earths in hydrothermal fluidsfrom the Mid-Atlantic Ridge: implications for Y and REE behaviour during near-vent mixing and for the Y/Ho ratio of Proterozoic seawater. Chem. Geol. 155 (1–2), 77–90.

Bau, M., Koschinsky, A., Dulski, P., Hein, J.R., 1996. Comparison of the partitioning behav-iours of yttrium, rare earth elements, and titanium between hydrogenetic marine fer-romanganese crusts and seawater. Geochim. Cosmochim. Acta 60 (10), 1709–1725.

Bau, M., Möller, P., Dulski, P., 1997. Yttrium and lanthanides in eastern Mediter-ranean seawater and their fractionation during redox-cycling. Mar. Chem. 56(1), 123–131.

Beard, B.L., Johnson, C.M., 2004. Fe isotope variations in the modern and ancient Earth andother planetary bodies. Rev. Mineral. Geochem. 55 (1), 319–357.

Bekker, A., et al. 2010 Iron formation: A sedimentary product of the complex interplay among mantle, tectonic, and biospheric processes. Society Economic Geology, 105,. p. 467-508.

Bekker, A., Holland, H. D., Wang, P.-L, Rumble, D, Stein, H. J., Hannah, J. L., Coetzee, L. L., & Beukes, N. J., 2004. Dating the rise of atmospheric oxygen. Nature 427 (6970), 117–120

Beukes, N. 2004. Biogeochemistry - Early options in photosynthesis. Nature, n. 431(7008). p. 522–523

Beukes, N.J., 1973. Precambrian iron-formation of Southern Africa. Econ. Geol. 68, 960–1004.

Bostrom, K., 1973. The origin and fate of ferromanganoan active ridge sediments. Stockh.Contrib. Geol. 27, 149–243.

Boyle, E., Jenkins, W.J., 2008. Hydrothermal iron in the deep western South Pacific.Geochim. Cosmochim. Acta A107.Breitkopf, J.H., 1988. Iron formations related to mafic volcanism and ensialic rifting in thesouthern margin zone of the Damara Orogen, Namibia. Precambrian Res. 38 (2),111–130.

Buck, K.N., Maeve, L.C., Berger, C.J.M., Bruland, K.W., 2007. Dissolved iron speciation intwo distinct river plumes and an estuary: implications for riverine iron supply.Limnol. Oceanogr. 52 (2), 843–855.

Bühn, B., Santos, R.V., Dardenne, M.A., Oliveira, C. G., 2009. Mass-dependent and mass-independent sulfur isotope fractionation (δ34S and δ33S) from Brazilian Archean and Proterozoic sulfide deposits by laser ablation multi-collector ICP-MSOriginal Research Article. Chemical Geology, Volumes 312–313, 18 June 2012, Pages 163-176

Bühn, B., Stanistreet, I.G., Okrusch, M., 1982. Late Proterozoic outer shelf manganese andiron deposits at Otjosondu (Namibia) related to the Damaran oceanic opening. Econ. Geol. 87, 1393–1411.

Canfield D.E., (2005) The early history of atmospheric oxygen: homage to Robert M. Garrels. Annu Rev Earth Planet Sci 33:1–36

Canfield, D. E., and Teske, A., 1996, Late Proterozoic rise in atmospheric oxygen concentration inferred from phylogenetic and sulphur-isotope studies: Nature, v. 382, p. 127–132.

Catling, D.C., Claire, M.W.,. 2005, How Earth's Atmosphere evolved to an oxic state: A status report. Earth and Planetary Science Letters. 237. 2005. pp: 1–20.

Condie, K.C., Aster, R.C., 2010. Episodic zircon age spectra of orogenic granitoids: thesupercontinent connection and continental growth. Precambrian Res. 180, 227–236.

Cox, G.M., Halverson,G. P, Minarik, W.G., Le Heron D. P., Macdonald, F. A., Bellefroid, E. J., Strauss, J.V., 2013. Neoproterozoic iron formation: an evaluation of its temporal,environmental and tectonic significance. Chem. Geol. 362, 232–249.

Dalstra H.J. & Guedes S. 2004. Giant hydrothermal hematite deposits with Mg-Fe metasomatism: a comparison of the Carajás, Hamersley, and other iron ores. Econ. Geo., 99: 1793- 1800.

Danielson ,A., Moller P., Dulski, P., 1992. The europium anomalies in banded iron formations and the thermal History of the oceanic crust. Chemical geology, vol.97, pp. 2965 -2977.

Dantas, E.L., Armstrong, R., Pimentel, M.M., Fuck, R.A., Martinelli, C., Silva, M.F., Laux, J.H., 2007. 800 Ma rifting in the Paraguay Belt, Central Brasil: U–Pb SHRIMP

age determination, Rodinia break-up and implications for a connection with Avalonian peri-Godwana terranes. GSA Annual Meeting. Denver. Abstracts, CD ROM.

Dantas, E.L., De Alvarenga, C.J.S., Santos, R.V., Pimentel, M.M., 2009. Using Ndisotopes to understand the provenance of sedimentary rocks from a continentalmargin to a foreland basin in the Neoproterozoic Paraguay Belt, Central Brazil.Precambrian Res. 170, 1–12.

Dardenne, M., 1998. Modelo hidrotermal-exhalativo para os depósitos de Fe-Mn da região de Corumbá, Mato Grosso do Sul, 40. Congresso Brasileiro de Geologia, Anais, São Paulo (SBG).

DePoalo, D. J. A neodymium and strontium isotopic study of the Mesozoic calc-alkaline granitic batholithys of the Sierra Nevada and Peninsular Ranges, California. Journal of Geophysical Research, 1981, n. 86. p. 10470-10488.

Derry, L.A., Jacobsen, S.B., 1990. The chemical evolution of Precambrian seawater: Evidence from REEs in banded iron formations. Geochim. Cosmochim. Acta 54, 2965–2977.

Dorr, J.V.N. 1945. Manganese and iron deposits of Morro do Urucum, Mato Grosso, Brazil. Bull. U.S. Geol. Survey 946A, 1–47. Dorr, J.V.N., 1973. Iron-formation in South America. Econ. Geol. 68, 1005–1022.

Douville, E., Charlou, J.L., Oelkers, E.H., Bienvenu, P., Jove Colon, C.F., Donval, J.P.,Fouquet, Y., Prieur, D., Appriou, P., 2002. The rainbow vent fluids (36°140N,MAR): the influence of ultramafic rocks and phase separation on trace metalcontent in Mid-Atlantic Ridge hydrothermal fluids. Chem. Geol. 184, 37–48.http://dx.doi.org/10.1016/S0009-2541(01)00351-5.

Douville, E., et al., 1999. Yttrium and rare earth elements in fluids from various deep-seahydrothermal systems. Geochim. Cosmochim. Acta 63 (5), 627–643.

Dymek, R.F., Klein, C., 1988. Chemistry, petrology and origin of banded iron-formation lithologies from the 3800 MA isua supracrustal belt, West Greenland.Precambrian Res. 39 (4), 247–302.

Eisbacher, G.H., 1981. Sedimentary tectonics and glacial record in the indermere Super-group, Mackenzie Mountains, northwestern Canada. Geological Survey of Canada Paper 80–27.

Elderfield, H., Greaves, M.J., 1982. The rare-earth elements in seawater. Nature 296, 214–219.

Eyles, N.; Januszczak, N. (2004). «'Zipper-rift': A tectonic model for Neoproterozoic glaciations during the breakup of Rodinia after 750 Ma» (PDF). Earth-Science Reviews [S.l.: s.n.] 65 (1-2): 1–73.

Fairchild, I.J., Kennedy, M.J., 2007. Neoproterozoic glaciation in the Earth system. Journal of the Geological Society of London 164, 895–921.

Frei , R., Døssing, L.N., Gaucher, C., Boggiani, P.C., Frei, K.M., Bech Árting, T., Crowe, S.A., Freitas, B.T., 2017. Extensive oxidative weathering in the aftermath of a late Neoproterozoic glaciation – Evidence from trace element and chromium isotope records in the Urucum district (Jacadigo Group) and Puga iron formations (Mato Grosso do Sul, Brazil). Gondwana Research, 49, 1-20.

Frei, R., Dahl, P.S., Duke, E.F., Frei, K.M., Hansen, T.R., Frandsson, M.M. and Jensen, L.A. (2008) Trace Element and Isotopic Characterization of Neoarchean and Paleoproterozoic Iron Formations in the Black Hills (South Dakota USA): Assessment of Chemical Change during 2.9-1.9 Ga Deposition Bracketing the 2.4-2.2 Ga First Rise of Atmospheric Oxygen. Precambrian Research, 162, 441-474.

Frei, R., Gaucher, C., Poulton, S.W., Canfield, D.E., 2009. Fluctuations in Precambrian atmospheric oxygenation recorded by chromium isotopes. Nature, 461, 250–254.

Frei, R., Gaucher, C., Stolper, D., Canfield, D.E., 2013. Fluctuations in lateNeoproterozoic atmospheric oxidation—Cr isotope chemostratigraphy andiron speciation of the late Ediacaran lower Arroyo del Soldado Group(Uruguay). Gondwana Res. 23, 797–811.

Frei, R., Polat, A.2007 Source heterogeneity for the major components of ~3.7 Ga banded iron formations (Isua Greenstone Belt,Western Greenland): Tracing the nature of interactingwatermasses in BIF formation. Earth and Planetary Science Letters, 2007, n.253, v.1–2, 266–281.

Freitas, B.T., Warren, L.V., Boggiani, P.C., De Almeida, R.P., Piacentini, T., 2011.Tectono-sedimentary evolution of the Neoproterozoic BIF-bearing JacadigoGroup, SW-Brazil. Sediment. Geol. 238, 48–70.

Frimmel, H.E., 2011. The Kaigas and Numees formations, Port Nolloth Group, in South Africa and Namibia. In: Arnaud, E., Halverson, G.P., Shields-Zhou, G. (Eds.), The Geological Record of Neoproterozoic Glaciations, Memoir, 36. The Geological Society, London, pp. 223–232.

Fryer, B.J. Rare-earth elements in iron-formation (Part B). In: Trendall A.F., Morris R.C. (eds.), Iron Formation: Facts and Problems. Developments in Precambrian Geology. Amsterdam: Elsevier, 1993. p. 345-357.

Fryer, B.J., 1977. Trace element geochemistry of the Sokoman iron formation. Can. J. Earth Sci. 14, 1598–1610.

Fryer, B.J., Fyfe, W.S., Kerrich, R., 1979. Archean volcanogenic oceans. Chem. Geol.24, 25–33.

Gaucher, C., Chiglino, L., Pecoits, E., 2004. Southernmost exposures of the Arroyo de Soldado Group (Vendian to Cambrian, Uruguay): paleogeographic implications for the amalgamation of W-Gondwana. Gondwana Research 7, 701–714.

Gaucher, C., Sial, A.N., Frei, R. 2015. Chemostratigraphy of Neoproterozoic banded iron formation (BIF): types, age and origin. In: Ramkumar, M. (Ed.) Chemostratigraphy: concepts, techniques and applications. Elsevier, Amsterdam, pp. 433-449.

Graf, J.L., O'Connor, E.A., Van Leeuwen, P., 1994. Rare earth element evidence of origin and depositional environment of Late Proterozoic ironstone beds and manganese-oxide deposits, SW Brazil and SE Bolivia. Journal of South American Earth Sciences 7, 115–133.

Gross G. A. Stratiform iron. In: Geology of Canadiam Mineral Deposit Types. (eds) Eckstrand O.R., Sinclair W.D., Thorpe R.I. Geological Survey of Canada, Geology of Canada, 1996, n.8. p. 41-54.

Halverson, G.P., Poitrasson, F., Hoffman, P.F., Nédélec, A., Montel, J.M., Kirby, J., 2011.Fe isotope and trace element geochemistry of the Neoproterozoic syn-glacialRapitan iron formation. Earth Planet. Sci. Lett. 309, 100–112. http://dx.doi.org/10.1016/j.epsl.2011.06.021

Hoffman, P.F. & Schrag, D.P., 2002. The snowball Earth hypothesis: testing the limits of global change. Terra Nova 14, 129-155.

Hoffman, P.F., Kaufman, A.J., Halverson, G.P., Schrag, D.P., 1998. A Neoproterozoicsnowball Earth. Science 281, 1342–1346.

Hofmann, A., 2005, The geochemistry of sedimentary rocks from the Fig Tree Group, Barberton greenstone belt: Implications for tectonic, hydrothermal and surface processes during mid-Archaean times: Precambrian Research, v. 143, p. 23−49.

Holland, H.D., 2006. The oxygenation of the atmosphere and oceans. Phil. Trans. R. Soc. B 361, 903–915.

Huston, D.L, and Logan, G.A., 2004. Barite, BIFs and bugs: evidence for the evolution of the Earth's early hydrosphere. Earth and Planetary Science Letters 220 (2004) 41-55.

James, H.L. 1954. Sedimentary facies of iron formations. Econ. Geol. Lancaster: [s.n.], 1954, n.49, v.3. p. 235-293.

Kato, Y., Yamaguchi, K.E., Ohmoto, H., 2006. Rare earth elements in Precambrian banded iron formations: secular changes of Ce and Eu anomalies and evolution of atmospheric oxygen. In:

Kato,Y., Ohta, I., Tsunematsu,T., Watanabe,Y., Yukio Isozaki,Y., Maruyama S., Imai, N., 1998. Rare earth element variations in mid-Archean banded iron formations:

implications for the chemistry of ocean and continent and plate tectonics.Geochimica et Cosmochimica Acta, V62, Issues 21-22 , P3475 -3497.

Kesler, S., Ohmoto, H. (Eds.), Evolution of the Atmosphere, Hydrosphere, and Biosphere on Early Earth: constraints from Ore Deposits. Geol. Soc. Am. Mem. 196, 269–289.

Keto, L.S., Jacobsen, S.B., 1988. Nd isotopic variations of Phanerozoic paleoceans.Earth Planet. Sci. Lett. 90, 395–410.

Khalil K. I., El-Shazly A.E., Lehmann B.,2015. Late Neoproterozoic banded iron formation(BIF) in the central Eastern desert of Egypt: mineralogical and geochemical implications fro the origin of the Gebel El Hadid iron ore deposit.Ore Geology Reviews 69 (2015) 380 – 399.

Klein, C., 2005. Some Precambrian banded iron-formations (BIFs) from around the world:Their age, geologic setting, mineralogy, metamorphism, geochemistry, and origins.Am. Mineral. 90 (10), 1473–1499.

Klein, C., Beukes, N.J., 1993. Sedimentology and Geochemistry of the Glaciogenic Late Proterozoic Rapitan Iron-Formation in Canada. Econ. Geol. 88, 542–565.

Klein, C., Ladeira, E., 2004. Geochemistry and mineralogy of Neoproterozoic bandediron-formations and some selected, siliceous manganese formations from theUrucum District, Mato Grosso. Econ. Geol. 99, 1233–1244

Klinkhammer, G., Elderfield, H., Hudson, A., 1983. Rare earth elements in seawater near hydrothermal vents. Nature 305, 185–188.

Konhauser, K.O., Newman, D.K., Kappler, A., 2005. The potential significance of microbial Fe(III) reduction during deposition of Precambrian banded iron formations. Geobiology 3 (3), 167–177.

Košler., J.; Fonneland, H.; Sylvester ,P.; Tubrett, M.; & Pedersen, R., 2002 U–Pb dating of detrital zircons for sediment provenance studies—a comparison of laser ablation ICPMS and SIMS techniques Original Research Article. Chemical Geology, Volume 182, Issues 2–4, 15 February 2002, Pages 605-618.

Kröner, A., Hoffmann, J.E., Xie, H., Wu, F., Münker, C., Hegner, E., Wong, J., Wan, Y., Liu, D., 2013. Generation of early Archaean felsic greenstone volcanic rocks through crustal melting in the Kaapvaal, craton, southern Africa. Earth Planet. Sci. Lett. 381, 188–197.

Lacerda Filho, J.W.; Brito, R.S.C.; Silva, M.G.; Oliveira, C.C. DE, Moreton, L.C., Martins, E.G., Lopes, R.C., Lims, T.M., Larizzatti, J.H. Valente, C.R. Geologia e Recursos Minerais do Estado de Mato Grosso do Sul. Programa Integração, Atualização e Difusão de Dados de Geologia do Brasil. Convênio CPRM/SICME-MS, MME. 121 p. 2006.

Lascelles, d.f. 2007. Black smokers and density currents: a uniformitarian model for the genesis of Banded iron – formations. Ore Geol. Rev 32, 381 411.

Le Heron, D.P., Cox, G., Trundley, A., Collins, A.S., 2011b. Two Cryogenian glacial successions compared: Aspects of the Sturt and Elatina sediment records of South Australia. Precambrian Research 186 (1–4), 147–168.

Lobato L.M., Hagemann S.G., Figueiredo e Silva R.C., Thorne W., Zucchetti M., Gutzmer J. 2008. Hypogene hydrothermal alteration associated with BIF-related iron ore mineralization. In: Hagemann, S.G., Rosière, C.A., Gutzmer, J., and Beukes, N.J., BIF-Related High-Grade Iron Mineralization. Reviews in Econ. Geo., 15: 107-128.

Ludwig, K.R., 2003. Mathematical-statistical treatment of data nd errors for Th-230/U geochronology. Uranium-Series Geochemistry, Reviews in Minerology and Geochemistry, 52: 631-656.

Luz, José da Luz. Projeto Fosfato de Bonito. Goiânia: CPRM, 1980. (Conv.Codesul / CPRM) LUZ, José da Luz; OLIVEIRA, Amóss de Melo; SOUIZA, João Olímpio; MOTTA, José Francisco Marciano; TANNO, Luiz Carlos; DOUZA, Nilson Batista de; ABREU FILHO, Waldemar. Projeto Coxipó. Relatório Final. Goiânia: CPRM, 1980. v.1, 136p.(Conv.DNPM / CPRM).

Lyons T.W., Reinhard C. T., Planavsky N.J., 2014, The rise of oxygen in Earth's early ocean and atmosphere. Rev. NATURE n°20, VOL 506, 307-315.

Lyons, T.W., Reinhard, C.T., 2009. Early Earth: oxygen for heavy-metal fans. Nature 461(7261), 179–181.

McGee, B., Collins, A. S., Trindade, R. I., Jourdan, F. 2015. Investigating mid-Ediacaran glaciation and final Gondwana amalgamation using coupled sedimentology and 40Ar/39Ar detrital muscovite provenance from the Paraguay Belt, Brazil. Sedimentology, 62(1), 130-154.

McGee, B., Collins, A. S., Trindade, R. I., Payne, J. 2015. Age and provenance of the Cryogenian to Cambrian passive margin to foreland basin sequence of the northern Paraguay Belt, Brazil. Geological Society of America Bulletin, 127(1-2), 76-86.

McGee, B., Halverson, G.P., Collins, A.S., 2012. Cryogenian rift-related magmatism and sed-imentation: South-western Congo Craton, Namibia. J. Afr. Earth Sci. 76, 34–49.

McLennan, S. M. (1989) Rare earth elements in sedimentary rocks: influence of provenance and sedimentary processes. Geochemistry and Mineralogy of Rare Earth Elements (Lipin, B. R. and McKay, G. A., eds.), Rev. Mineral. 21, 169–200

Michard A., and Albarede F., 1986. The REE content of some hydrothermal fluids. Chem. Geol., 55:51-60. Mitra, A., Elderfield, H., Greaves, M.J., 1994. Rare earth

elements in submarine hydrothermal fluids and plumes fron the Mid-Atlantic Ridge. Marine Chemistry 46, 217 -235.

Michard, A., Albarede, F., Michard, G., Minster, J. F., and Charlou, J. L., 1983. Rare-earth elements and uranium in high-temperature solutions from East Pacific Rise hydrothermal vent field (13°N. Nature, 303:795-797.

Michard, A., et al., 1993. Submarine thermal springs associated with young volca-noes: The Teahitia vents, Society Islands, Pacific Ocean. Geochim. Cosmochim.Acta 57 (21–22), 4977–4986.

Morris, R.C., 1980. A textural and mineralogical study of the relationship of iron ore to banded iron formation in the Hamersley Iron Province of Western Australia. Geol. 75, !85 – 209.

Mukherjee, S.K., 2008. Petrography, age (U-Pb zircon), geochemical and isotopic studies of the Sawawin banded iron-formation (BIF), northwestern Saudi Arabia: implications for understanding Neoproterozoic climate change. Ph.D. dissertation, University of Texas at Dallas, 137 p.

Nascimento, R.S.C., Sial, A.N., Pimentel, M.M., 2007. C- and Sr-isotope systematics applied to Neoproterozoic marbles of the Seridó belt, northeastern Brazil. Chemical Geology 237, 209–228.

Nogueira, A.C.R., Riccomini, C., Sial, A.N., Trindade, I.R., Faichild, T., 2007. Carbon and Strontium fluctuations and paleoceanographic changes in the late Neoproterozoic Araras carbonate platform, southern Amazon craton, Brazil. Chemical Geology, 237: 186-208

Pecoits, E., 2010. Ediacaran Iron Formations and Carbonates of Uruguay: Paleoceanographic, Palaeoclimatic and Palaeobiologic Implications. (Ph.D. thesis), University of Alberta (237 pp.).

Peter, J.M., 2003, Ancient iron formations: Their genesis and use in the exploration for stratiform base metal sulphide deposits, with examples from the Bathurst mining camp: Geological Association of Canada, GEOTEXT 4, p. 145−176.

Piacentini, T., Vasconcelos, P.M., Farley, K.A., 2013. 40Ar/39Ar constraints on the ageand thermal history of the Urucum Neoproterozoic banded iron-formation,Brazil. Precambrian Res. 228, 48–62. http://dx.doi.org/10.1016/j.precamres.2013.01.002.

Pinho F.E.C. 1990. Estudo das rochas encaixantes e veios mineralizados a ouro do Grupo Cuiabá, na região denominada “Garimpo dos Araés” Nova Xavantina, estado de Mato Grosso. Centro de Pesquisas em Geociências da Universidade Federal do Rio Grande do Sul, Porto Alegre, RS, Dissertação (Mestrado em Geoquímica), 114p.

Pinho, F.E.C.; Ruiz, A.S.; Schmus, R.V.S., Figeirodo, M.; Godoy, A.M.,1990. Estudo Isotópico dos Granitos da Faixa de Dobramento Paraguai em Mato Grosso (dados inéditos).

Planavsky, N., Bekker, A., Rouxel, O.J., Kamber, B., Hofmann, A., Knudsen, A., Lyons, T.W., 2010. Rare Earth Element and yttrium compositions of Archean and Paleoproterozoic Fe formations revisited: new perspectives on the significance and mechanisms of deposition. Geochim. Cosmochim. Acta 74, 6387–6405.

Poulton, S.W., Raiswell, R., 2002. The low-temperature geochemical cycle of iron: fromcontinental fluxes to marine sediment deposition. Am. J. Sci. 302 (9), 774–805.

Preiss, W.V. 2000. The Adelaide Geosyncline of South Australia and its significance in Neoproterozoic continental reconstruction. Precambrian Res. 100 (1), 21–63.

Preiss, W.V., Forbes, B.G., 1981. Stratigraphy, correlation and sedimentary history of Adelaidean (late Proterozoic) basins in Australia. Precambrian Res. 15 (3–4), 255–304.

Remus, M. V. D.; Souza, R. S.; Cupertino, J. A.; De Ros, L. F.; Dani, N. & Lelarge, V. M. L. 2008. Proveniência sedimentar, métodos e técnicas analíticas aplicadas. Revista brasileira de geociência, 38, suplemento 2: 166-185.

Rodrigues, R; Azevedo, R.L.M; Estrada, N.M.; Rehim, H.A.A; Sato, K.; Kawashita, K; Soliani Jr., Inferências cronoestratigráficas para carbonatos da Bacia dos Parecis, com base em dados da razão 87 SR / 86 Sr. In.: CONGRESSO BRASILEIRO DE GEOLOGIA, 38, 1994, Camboriu. 1994. Anais ... Camboriu: SBG, 1994. v.3, p.286-287.

Rosière C.A. & Rios F.J. 2004. The origin of hematite in high-grade iron ores based in infrared microscopy and fluid inclusion studies: the example of the Conceição Deposit, Quadrilátero Ferrífero, Brazil. Econ. Geol., 99: 611-624.

Sahoo SK, Planavsky NJ, Kendall B, Wang X, Shi X, Scott C, Anbar AD, Lyons TW, Jiang G., 2012.Ocean oxygenation in the wake of the Marinoan glaciation. Nature 489 (7417), 546–549.

Schobbenhaus, C., Campos, D.A., Derze, G.R., Asmus, H.E., 1981. Mapa geológico do Brasil e da área oceânica adjacente incluindo depósitos minerais. Escala 1/2.500.000. Dep. Nac. Produc◦. Mineral (D.N.P.M.), Brasilia.

Shields-Zhou, G.A., Och, L.M. (2011). The case for a Neoproterozoic Oxygenation Event: geochemical evidence and biological consequences. GSA Today, 21 (3), 4-11. doi:10.1130/GSATG102A.1

Sial, A. N., Campos M. S., Gaucher C., Frei R., Ferreira V.P., Nascimento R.C., Pimentel M.M., Pereira N.S., Rodler A., 2015; Algoma-type Neoproterozoic BIFs and related marbles in tha Seridó Belt (NE Brazil): REE, C, O, Cr and Sr isotope evidence. Journal of South American Earth Sciences xx (2015) 1-20.

Silva, M. F. DA. 2007. Aerogeofísica, Litogeoquímica e Geologia na Caracterização do Rifte Intracontinental da Faixa Paraguai. Instituto de Geociências. Universidade de Brasília, Brasília, Dissertação de Mestrado, 1 v. 117 p.

Silva, M. F. DA. 2018. Evolução Tectônica de Rift para Margem Passiva da Faixa Paraguai-Mato Grosso, Brasil Central. Instituto de Geociências. Universidade de Brasília, Brasília, Tese de Doutorado N°144, 1 v. 198 p.

Spier C. A. 2005 Geoquímica e Gênese das Formações Ferríferas Bandadas e do Minério de Ferro da Mina de Águas Claras, Quadrilátero Ferrífero, MG. [Tese Doutorado]. São Paulo: Instituto de Geociências; Universidade de São Paulo,. 298p.

Stern, R.J., Avigad, D.,Miller, N.R., Beyth,M., 2006. Evidence for snowball earth hypothesis in the Arabian–Nubian Shield and the East African orogen. Journal of African Earth Sciences 44, 1–20.

Stern, R.J., Mukherjee, S.K., Miller, N.R., Ali, K., Johnson, P.R., 2013. 750 Ma bandediron formation from the Arabian-Nubian Shield—implications forunderstanding neoproterozoic tectonics, volcanism, and climate change.Precambrian Res. 239, 79–94. http://dx.doi.org/10.1016/j.precamres.2013.07.015.

Stern, R.J., Mukherjee, S.K., Miller, N.R., Ali, K., Johnson, P.R., 2013. 750 Ma bandediron formation from the Arabian-Nubian Shield—implications forunderstanding neoproterozoic tectonics, volcanism, and climate change.Precambrian Res. 239, 79–94.

Swanson-Hysell, N.L., et al., 2010. Cryogenian glaciation and the onset of carbon isotope decoupling. Science 328 (5978), 608–611.

Tagliabue, A., et al., 2010. Hydrothermal contribution to the oceanic dissolved iron inven-tory. Nat. Geosci. 3 (4), 252–256.

Tang, J., Fu, H., Yu, Z., 1987. Stratigraphy, type and formation conditions of the late pre-cambrian banded iron ores in south China. Chin. J. Geochem. 6 (4), 331–341.

Trendall, A.F., 1973, Varve cycles in the Weeli Wolli Formation of the Precambrian Hamersley Group, Western Australia: ECONOMIC GEOLOGY, v. 68, p. 1089−1097.

Trompette, R., Alvarenga, C.J.S. de, e Walde, D., (1998) Geological evolution of the Neoproterozoic Curumbá graben system (Brazil): Depositional context of the stratified Fe and Mn ores of the Jacadigo Group. Journal of South American Earth Science, v. 11, p. 587–597.

Urban, H., Stribrny, B., Lippolt, H.J., 1992. Iron and manganee deposits of the Urucum district, Mato-Grosse-do-Sul, Brazil. Economic Geology and the Bulletin of the Society of Economic Geologists 87, 1375–1392.

Viehmann, S., Bau, M., Bühn, B., Dantas, E.L., Walde, D.H.G. Geochemical characterisation of marine Neoproterozoic habitats: Evidence from HFSE, REY and Nd

isotopes of the Cyrogenian Urucum Fe-Mn formation, Brazil. Precambrian Research, No prelo.

Walde, D.H.G., Hagemann, S.G.E. (2007) The Neoproterozoic Urucum/Mutún Fe and Mn deposits in W-Brazil/SE-Bolivia: assessment of ore deposit models. Zentralblattdt. Geologische Geowissenschaften 158 (1), 45–55.

Wang, X.L., Planavsky, N.J., Reinhard, C.T., Zou, H.J., Ague, J.J., Wu, Y.B., Gill, B.C., Schwarzenbach, E.M., Peucker-Ehrenbrink, B., 2016. Chromium isotope fractionation during subduction-related metamorphism, black shale weathering, and hydrothermal alteration. Chemical Geology 423, 19–33.

Xu, D.R., Wang, Z.L., Chen, H.Y., Hollings, P., Jansen, N.H., Zhang, Z.C., Wu, C.J., 2013b. Petrography and geochemistry of the Shilu Fe–Co–Cu ore district, South China: Implications for the origin of a Neoproterozoic BIF system. Ore Geology Reviews 57, 322–350.

Yeo, G.M., 1981. The Late Proterozoic Rapitan glaciation in the Northern Cordillera. In: Campbell, F. (Ed.), Proterozoic Basins of Canada: Geological Survey of Canada Paper81–10, pp. 25–46.

Young, G.M., 1976. Iron-formation and glaciogenic rocks of the Rapitan Group, Northwest Territories, Canada. Precambrian Res. 3, 137–158.

Zhang, Q.-R., Chu, X.-L., Feng, L.-J., 2011. Chapter 32 Neoproterozoic glacial records in the Yangtze Region, China. Geol. Soc., Lond., Mem. 36 (1), 357–366.